THE MECHANICAL RESPONSE OF MACROMOLECULES IN AND OUT OF EQUILIBRIUM

by

Felix Hanke

SUBMITTED IN PARTIAL FULFILLMENT OF THE
REQUIREMENTS FOR THE DEGREE OF
DOCTOR OF PHILOSOPHY

AT

DALHOUSIE UNIVERSITY
HALIFAX, NOVA SCOTIA
DECEMBER 2006

© Copyright by Felix Hanke, 2006

Library and Archives Canada

Published Heritage Branch

395 Wellington Street
Ottawa ON K1A 0N4
Canada

Bibliothèque et Archives Canada

Direction du Patrimoine de l'édition

395, rue Wellington
Ottawa ON K1A 0N4
Canada

Your file Votre référence
ISBN: 978-0-494-27196-4
Our file Notre référence
ISBN: 978-0-494-27196-4

NOTICE:
The author has granted a non-exclusive license allowing Library and Archives Canada to reproduce, publish, archive, preserve, conserve, communicate to the public by telecommunication or on the Internet, loan, distribute and sell theses worldwide, for commercial or non-commercial purposes, in microform, paper, electronic and/or any other formats.

The author retains copyright ownership and moral rights in this thesis. Neither the thesis nor substantial extracts from it may be printed or otherwise reproduced without the author's permission.

AVIS:
L'auteur a accordé une licence non exclusive permettant à la Bibliothèque et Archives Canada de reproduire, publier, archiver, sauvegarder, conserver, transmettre au public par télécommunication ou par l'Internet, prêter, distribuer et vendre des thèses partout dans le monde, à des fins commerciales ou autres, sur support microforme, papier, électronique et/ou autres formats.

L'auteur conserve la propriété du droit d'auteur et des droits moraux qui protège cette thèse. Ni la thèse ni des extraits substantiels de celle-ci ne doivent être imprimés ou autrement reproduits sans son autorisation.

In compliance with the Canadian Privacy Act some supporting forms may have been removed from this thesis.

While these forms may be included in the document page count, their removal does not represent any loss of content from the thesis.

Conformément à la loi canadienne sur la protection de la vie privée, quelques formulaires secondaires ont été enlevés de cette thèse.

Bien que ces formulaires aient inclus dans la pagination, il n'y aura aucun contenu manquant.

Canada

DALHOUSIE UNIVERSITY

To comply with the Canadian Privacy Act the National Library of Canada has requested that the following pages be removed from this copy of the thesis:

Preliminary Pages

Examiners Signature Page (pii)

Dalhousie Library Copyright Agreement (piii)

Appendices

Copyright Releases (if applicable)

Table of Contents

List of Tables

List of Figures

Abstract

This thesis develops theoretical aspects of stretching single polymer molecules using an Atomic Force Microscope. Particular emphasis is placed on the difference between controlled force and controlled position modes of the experiment, corresponding to the Gibbs and Helmholtz ensembles in statistical mechanics.

Initially, an analytic model for conformational transitions in thermodynamic equilibrium is developed and applied to Dextran. The observed force response is fitted, resulting in the two dominant conformers for Dextran, allowing a prediction of the proper thermal equation of state as well as a direct calculation of the observed thermal fluctuations.

A second part of the thesis deals with the fast stretching of polymer molecules. The results of Transfer Matrix calculations are used in a Master Equation approach to predict fast non-equilibrium effects in polymer stretching. The time scale is fixed by an expansion of the Master Equation, which can be fitted to relaxation time measurements on DNA. The predicted response of a molecule to fast stretching is qualitatively similar to the equilibrium force-extension curve, but occurs at much higher forces. This result is linked to memory effects in the thermal fluctuations of the molecule-cantilever system is much more pronounced in the Helmholtz (constant pulling velocity) regime. A calculation of non-equilibrium molecular relaxation is also presented in this work.

Following the discussions of polymers stretched in and out of thermodynamic equilibrium, the thesis considers the ultimate non-equilibrium process - breaking a single molecule. It is shown how the survival rate of a bond under the application of stress depends on the applied force. Moreover, the potential barrier is calculated analytically for the case of a Morse potential and is used to fit spectra obtained from breaking an ensemble of Terpyridine-Ru^{2+}-Terpyridine complexes. The theory allows the determination of three microscopic parameters: the depth V_0 of the unperturbed potential, the attempt frequency A and the width of the unperturbed potential γ. Finally, the necessity of using data at many different loading rates is discussed and it is shown that these loading rates need to vary at least two orders of magnitude to enable quantitative fitting.

List of Abbreviations and Symbols Used

A	attempt frequency for bond breaking theory
AFM	atomic force microscope
b	bond length
c	speed of pulse propagation along polymer backbone
C_N	characteristic ratio
D	AFM cantilever position
DFT	Density Functional Theory
f	force
FJC	Freely Joined Chain (polymer model)
FRC	Freely Rotating Chain (polymer model)
$\mathcal{G}$	Green function
G,g,ΔG	Gibbs free energy, Gibbs free energy difference
k	stiffness of bond potential
k_{B}	Boltzmann constant
k_c	AFM cantilever spring constant
K_S	bond stretch modulus
k^*_{off}	free dissociation rate in Evans-Ritchie model
ℓ	conformer length
L	polymer length
L_c	molecular contour length
L_K	Kuhn length
N	number of monomers in a molecule
N_c	number conformers accessible to a monomer
P	probability distribution
Q	average barrier between two molecular extension states
r	dimensionless loading rate
$\mathbf{r}$	spatial coordinate

RIS	Rotationally Isomeric States (polymer model)
T	temperature
$\mathcal{T}$	transfer operator
V_0	conformer potential minimum
ΔV	potential barrier in bond breaking theory
w_0	effective attempt frequency
Δx	barrier width in Evans-Ritchie model
Z	partition function in Helmholtz ensemble
α	force loading rate in bond breaking theory
α	thermal expansion coefficient
α_n	n^{th} moment of the transition rates in Gibbs regime
β	$1/(k_{\text{B}}T)$
Δ	transition width
Γ	partition function in Gibbs ensemble
Γ	coordinate in monomer configuration space
γ	bond angle in FRC model
γ	Morse potential width
ν	attempt frequency
θ	solvent condition in which molecule behaves like a phantom chain
σ	fluctuations of polymer end
τ	molecular relaxation time
ξ_n	n^{th} moment of the transition rates in Helmholtz regime
$\xi_{\parallel/\perp}$	longitudinal and transverse friction parameters

Acknowledgements

My time at Dalhousie University was very generously supported by the Killam Trusts through a Killam Scholarship. Other gratefully acknowledged sources of funding for my projects and Conference travels include the Dalhousie Faculty of Graduate studies and COMPINT. Most of the extensive numerical calculations for my projects were carried out on two High Performance Computing Centres: WestGrid Computing Resources and ACE-net, as well as on a computer in the group of Prof. Keith Louden, which was kindly arranged by Chris Leblanc.

A huge thank you goes out to my mentors and colleagues over the last few years. I believe it will be a while before I can fully appreciate the time and effort put in by my supervisor Hans Jürgen Kreuzer in teaching me the means and ways of exact statistical physics and many related subjects. Stephen Payne was always a good resource for theory and numerical issues, as well as proof reading manuscripts and making all kinds of important suggestions. Prof. Manfred Jericho helped a lot with the particulars of AFM experimentation. Andreas Serr and I had more than a few discussions about chemistry and polymer statistics, those were extremely helpful in many respects. I am further indebted to M. Azzouz (Laurentian University, Sudbury), R. R. Netz (Technische Universität München), and H. H. Rotermund (Fritz Haber Institut, Berlin/ Dalhousie University) for teaching and general guidance. Thanks also to a number of students who worked in Prof. Kreuzer's group or took classes that I was involved with. The most prominent suspects here are Doug Staple, Catherine Stevenson, Lisa Crystal, and most of the remainder of two thermodynamics classes who had to sit through the development and improvement of my teaching skills. Finally, K. A. Walther and J. M. Fernandez (both Columbia University) were so kind as to provide their original data on Dextran stretching.

There are too many friends to be mentioned here, but I will attempt a non-exclusive list anyway: Clare and the regular Pegasus crew, Stacy, Jeremy, Anne, Sofie, Dominique, Olaf, Rebekka (the whole local German community and its various visitors from abroad to be precise); Markus, Rafal, Denise, Matt, Ghislain, Fiona, and the three Smith kids; actually let's mention the entire Halifax climbing community. Not to be forgotten are Brad and Arielle (for introduction to the Dal Swing Society and otherwise), Mike J. and Tara, Kevin *K-man* W., and Mike F., Isaac and Angella for many late nights talking physics and other things. I definitely needed to get away from school once in a while and you guys were instrumental in getting out and about at all times of the year.

The last but not least thank you goes to all of my parents (Doris, Martin, Bettina, Klaus, Tom, and Michelle; roughly in order of occurrence), and grandparents, who have been just wonderful and extremely supportive (not only) over the last eight years, especially when I decided that I would not return from my exchange year.

Chapter 1

Introduction

In the 1920s it was discovered that certain materials consist of many chemically identical covalently bonded subunits. Ever since then macromolecules (or polymers) have been the subject of intense experimental and theoretical investigation in physics, chemistry, and biology. This thesis deals with the statistical mechanics of single polymers, whose equivalent subunits are adequately termed monomers. In particular, the theory of a special subclass of non-branched macromolecules is considered, in which each monomer is part of a central backbone. Important examples in this class include DNA, many starches, and most polyelectrolytes.

One of the theoretical challenges is that macromolecules have changing dominant characteristics depending the length scale considered. The primary structure of a polymer is the atomic arrangement on an Angstrom to nanometer scale. There are, generally, several possible local minima in a monomer's energy landscape, called conformers. A simple example is rotational isomerism in alkanes. The geometric and energetic details of this energy landscape can be investigated in great detail using Density Functional Theory (DFT) or *ab initio* methods.

A macromolecule contains a large number of monomers, typically of the order of 10^{2-4}. An immediate consequence is the availability of a huge number of possible molecular configurations: for N_C possible conformers one obtains around $(10^{2-4})^{N_C}$ possible arrangements, typically more than 10^{12}. This necessitates the use of configurational statistics for modeling the secondary structure of a coiled molecule. An added difficulty is that solvents often play an important role, as polymer-solvent interactions affect the conformational energy landscape. Moreover, a polymer chain cannot fold back onto itself. A lot of modeling is thus done using the concept of phantom chains, which have no excluded volume or solvent interactions.

There are solvents in which polymer chains behave exactly as if they were phantom chains at some well-defined temperature. Various analytic theories that attempt to

move away from ideal conditions (or θ-conditions) were developed several decades ago [1, 2]. These are based on simple chain models but include volume interactions. Part of the author's MSc work [3] dealt with modeling these excluded volume effects using a numeric mean-field theory, with the conclusion that an analytic theory for the accurate modeling of conformational statistics as well as the introduction of excluded volume interactions is not computationally feasible at present [3].

It remains to be noted that hydrogen and other bonds that involve monomers far apart along the backbone give rise to the tertiary structure which accounts for a lot of the observations in molecular biology. In particular, the three-dimensional structure and function of proteins is a result of the tertiary structure of these molecules. The explanation of protein functionality from first principles forms one of the current and future challenges in theoretical biological physics. Good introductions of polymer theory at different length scales are given by de Gennes [1], Doi and Edwards [2], Flory [4], and Grosberg and Khoklov [5].

Despite the deceptively simple concept of a single polymer chain, very few theories actually start from the fundamental principle of statistical mechanics: *A statistical system in thermodynamic equilibrium will sample all of its micro states with a probability of* $\exp(-\beta E_{\text{state}})$. As discussed above, accounting for the large number of available micro states even for one single molecule, is a daunting task that either requires extremely good methodology or extremely powerful computers. The Transfer Matrix (TM) method, developed recently by Prof. Kreuzer's group at Dalhousie University [3, 6–10] provides such a methodology, where the only approximation is that long-range volume effects (*i.e.* interactions that are more than two monomers apart) have to be neglected. However, this approximation is quite useful as soon as a force is applied between the two ends of a molecule.

An important aspect of the current work is to further develop the TM scheme as a universal tool, in particular to take it beyond its original use to obtain equilibrium properties of single molecules. This development is continued from previous advancements that explored the modeling of polymers in external potentials. Examples include potential tubes that mimic other molecules in a polymer brush [11, 12], or the modeling of an attractive surface via a Morse potential and the explanation of

polymer desorption experiments using equilibrium statistical mechanics [10]. A third application using a simple external potential that has not yet been implemented is a TM-based model for the movement of bacteria, which is generally thought to be due to the polymerization of Actine networks [13–15]. A short outline of the TM method is provided in Section 2.4. Detailed descriptions of the method are available in previously published theses at Dalhousie University [3, 6], as well as in the literature [7–9, 11].

The first application, presented in Chapter 2, revolves around the intricate interplay of a purely analytic theory of conformational transitions in polymer stretching with its TM method equivalent. Each of the two methods has its distinct advantages, and a complete understanding of relevant experiments can only be acquired with the use of both. The following three Chapters deal with polymers out of equilibrium. The possibility of calculating a thermodynamic partition function, as is being done using the TM method, is everything but a direct invitation to develop a Master equation approach to the out-of-equilibrium properties of polymer stretching, presented in Chapters 3 and 4. Most physically reasonable transition rates require the use of partition functions to obey detailed balance and allow for the proper approach to equilibrium. Finally, the concept of non-equilibrium polymer stretching is taken to the ultimate limit, with the development of a theory of molecular bond breaking.

1.1 Single Molecule Stretching: Experiment

The invention of the Atomic Force Microscope (AFM) in 1986 [16] enabled the measurement of the mechanical material properties extremely small length scales for the first time. The force applied to a micrometer-sized cantilever is measured by using the deflection of a laser off the cantilever tip (see Fig. 1.1(a)) and is essentially governed by Newton's and Hooke's Laws. Ideally, the cantilever tip is only a few nanometers in diameter and can be placed on a sample with Angstrom precision [17]. The AFM was originally used to investigate insulating surfaces as an alternative to Scanning Tunneling Microscopy [16], but a whole new field of physics called force spectroscopy has since been developed. While the underlying mechanical force laws are primarily classical in nature, AFM cantilevers are small enough to be susceptible to thermal

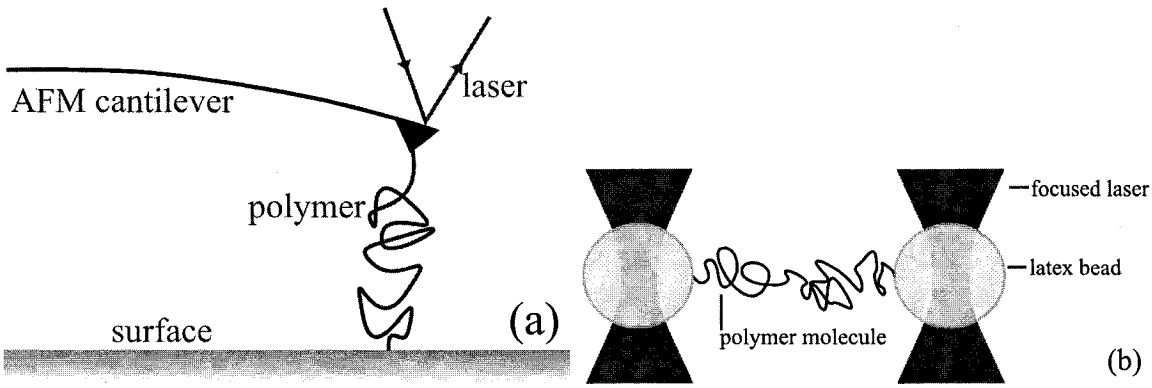

Figure 1.1: Comparison of the two most commonly used polymer stretching setups: (a) The Atomic Force Microscope (AFM) is based on stretching a molecule via a chemically attached cantilever whose extension is measured via laser deflection. (b) Two optical tweezers use one or two microscopic beads that are controlled via radiation pressure resulting from focused lasers. The force is measured from positions of the beads with respect to the centre of the laser.

fluctuations. In fact the careful measurement of thermal motion forms one of the most accurate methods to determine the all-important cantilever spring constant [18].

The AFM was first used for the stretching of single molecules in the 1990s [19,20]. The basic setup in this type of experiment is as follows: polymer molecules are chemically modified such that they will bond to a surface. An AFM tip is pushed into the surface such that the polymer can also bond to the tip, then it is retracted. A molecule attached to both the cantilever and the surface will be stretched as shown schematically in Fig. 1.1(a). The measured mechanical response is called the force-extension relation. Atomic Force microscopy has a vertical resolution of about 1 nm, while the force resolution is approximately 10 pN [21].

There are three main modes of AFM operation that are applicable to measuring single polymer molecules. The simplest and most common mode is to move the cantilever at a constant speed once the molecule is attached between AFM and substrate. If done sufficiently slowly, this type of experiment can be modeled using equilibrium statistical mechanics in the Helmholtz ensemble. A second possibility is to stretch the molecule with a controlled force, be it fixed (force-clamp spectroscopy) or linear in time (force-ramp spectroscopy). This would suggest using equilibrium theories in

the Gibbs or constant-force ensemble. However, recent measurements of the fluctuations in a force-ramp experiment have shown that this type of experiment cannot be done in thermodynamic equilibrium due to the update speed of the necessary feedback electronics [22]. Nevertheless, there can be important differences between the observed responses of all three experimental modes [23].

An alternative way of stretching single polymer molecules is based on using laser traps to manipulate small beads [24]. These optical tweezers can be used to stretch polymers if one end of the molecule is attached to the microscopic bead. The same experiment also allows insight into the dynamics of single molecules, in particular the relaxation behaviour of DNA molecules in solution [25, 26]. In the last few years the technique has been modified to use two separate lasers, each trapping one latex particle (see Fig. 1.1(b)). This most recent incarnation of optical tweezers was used for very accurate measurements of the relaxation behaviour of DNA via the position correlation of the two beads [27].

1.2 Single Molecule Stretching: Equilibrium Theory

Polymer molecules generally consist of a few hundreds to tens of thousands of monomers. Thus single macromolecules are small systems in the statistical mechanics sense which means that relative fluctuations of observables which scale with the inverse number of monomers cannot be neglected. The theory of fluctuations has been well known for decades,[1] but it was not applied to polymers until recently [32–34], when experimental advances such as the AFM described in the last Section allowed these theories to be tested. In the constant-speed AFM experiment, the fluctuations are dominated by the cantilever in the low-force regime, but are well suited for the extraction of microscopic data at higher forces [22]. On the other hand, the fluctuations are entirely governed by the molecule in constant force-loading rate experiments [32]. Some of the first direct numerical calculations of fluctuations are presented in Chapters 2 and 3.

The original models for polymer stretching were developed in the 1950's by Flory

[1] See Callen [28], Hill [29, 30], or Landau and Lifshitz [31] for introductions from various view points.

and coworkers [4, 35] using entropic elasticity. Flory's starting point was a phantom chain of randomly oriented rigid rods, termed the Freely Joined Chain (FJC). The Gibbs partition function for this system can be calculated exactly for any applied force and leads to the analytic force-extension response [4]:

$$L_{\mathrm{FJC}}(f) = Nb\left[\coth\left(\frac{fb}{k_{\mathrm{B}}T}\right) - \frac{k_{\mathrm{B}}T}{fb}\right]. \tag{1.1}$$

This expression gives the molecular length L for a model chain with N monomers of length b with an applied force f. With the advent of the experiments described in the last Section, models such as the Freely Joined Chain became more than a purely academic exercise and were used to fit experimental data [19, 20]. Numerous extensions of Flory's work were proposed to improve on the purely entropic response of the Langevin equation (1.1), see for example Abu-Lail and Camesano [36].

While Flory's model is based on discrete monomers, a path-integral calculation using as input only the bending stiffness of an otherwise continuous chain is also possible. This model is called the Worm-Like Chain and has also been used extensively to explain features and consequences of entropic elasticity [5, 37–39]. Unfortunately, it has so far been impossible to evaluate the path integral analytically and one has been restricted to use various analytic approximations [40].

Quite a number of investigated systems show a pronounced force-plateau in the response to stretching, which is the sign of a conformational transition, where one possible configuration of a monomer is forced to switch into a longer conformer that has a higher energy (see for example Bustamante *et al.* [41] for DNA experiments). Two simple extensions to Flory's FJC model were introduced in order to account for this behaviour. The monomer length in Eqn. (1.1) was calculated as a linear combination of a long and a short conformer that are separated by some force-dependent free energy difference $\Delta G(f) = \Delta G_0 - f(b_{\mathrm{long}} - b_{\mathrm{short}})$ [42], leading to a polymer version of the two-state model. The second equally important change to the original FJC concerns the molecular behaviour at high forces, where the Langevin relation (1.1) converges to a finite contour length. Experimental data shows that the molecular behaviour at these forces is spring-like, which was also incorporated into the FJC model by simply adding an additional extension that is linear in the force via the

monomer elasticity K_S [42],

$$L(f) = N\left(\frac{b_{\text{short}}}{1+\exp[\Delta G(f)/(k_{\text{B}}T)]} + \frac{b_{\text{long}}}{1+\exp[-\Delta G(f)/(k_{\text{B}}T)]}\right) \times \left[\coth\left(\frac{fL_K}{k_{\text{B}}T}\right) - \frac{k_{\text{B}}T}{fL_K}\right] + \frac{Nf}{K_S}. \quad (1.2)$$

The length L_K is the Kuhn length for the molecule in question. Equation (1.2) has often been used to model stretching data, first for polyethylene glycol (PEG) [42] and then for various polysaccharides [19, 21, 22, 43–49].

In order to make polymer models more realistic, the next obvious step is to restrict the bond angle γ between two monomers to one fixed value. The resulting model is the Freely Rotating Chain (FRC), for which only a few quantities can be calculated analytically [4]. The scaling estimate of its high-force limiting response as well as the numerical integration of its exact partition function was only carried out recently using Transfer Matrix (TM) techniques [6, 7]. An extended FRC theory termed QMFRC (for Quantum Mechanical Freely Rotating Chain), was developed a year ago using the FRC high-force response as well as a force and conformer dependent monomer length that was obtained from Density Functional calculations [50, 51].

While the FJC and FRC models were derived directly using statistical mechanics, the extensions to these models were obtained in a very non-rigorous fashion. The results are ad hoc fit-formulas and expressions that result in well-educated guesses of the physics behind single molecule stretching, but that could not be used in a complete statistical theory. One of the fundamental problems with both the two-state model and the QMFRC is that the monomer length depends only on the overall average of the applied force. The actual force acting on a single monomer is actually a projection of the overall force, which can be significantly smaller than the applied force. The result is a major theoretical inconsistency, particularly in the low-force regime, where entropic effects are the dominant contributions to the molecular response.

A second problem with these models is that the only predictable information is in fact the force-extension relation. In order to develop a self-consistent thermodynamic formalism it is necessary to construct appropriate free energies and a plausible thermal equation of state. This procedure is necessary to model experiments in the controlled position ensemble properly. Callen [28] outlines such a construction a postulated

equation of state. This procedure is straight forward, but highly non-trivial in the case of the FJC based two-state model and has not yet been attempted for the QMFRC.

Chapter 2 develops for the first time a rigorous analytic statistical mechanics model of an adapted version of the two-state model. The starting point is the original FJC model, but with a complete monomer-length dependent energy landscape and an additional integration over all monomer lengths. This procedure leads directly to a partition function in the Gibbs ensemble and is theoretically rigorous from the outset. There is also no necessity to add on a *monomer extensibility* as done in Eqn. 1.2, because the monomer extension comes for free with the use of an appropriate underlying potential.

Moreover, Chapter 2 discusses the possibility of measuring thermal effects, which turn out to be small but which should be experimentally accessible within a few years. This Chapter also provides a direct connection between the analytic theory and the Transfer Matrix method. The original formulation in the Gibbs ensemble can easily be used for fitting the experimental force response (*i.e.* the mechanical equation of state), but it can not be used directly to predict the observed molecular fluctuations.

In principle, it should be possible to obtain a Legendre Transform of the analytic Gibbs free energy in order to obtain Helmholtz free energy. Unfortunately, this procedure leads to numerous integrals that are intractable analytically and practically impossible to evaluate numerically with any reasonable accuracy. Transfer Matrix calculations are used at this point to overcome the issue. They require considerably more numerical effort, which makes the original fitting prohibitive, but they are very useful for the direct numerical imitation of actual experiments, as outlined in Section 2.4.

1.3 Polymers out of Equilibrium

For *slow* AFM pulling rates, the theories and developments described in the last Section and in Chapter 2 will eventually lead to a reasonably complete description of single molecule stretching. *Slow* in this context refers to the time scale for polymer

relaxation τ_{molecule}, which has to be small on the experimental time scale,

$$\tau_{\text{molecule}} \ll \tau_{\text{experiment}}. \tag{1.3}$$

The question of establishing thermodynamic equilibrium now reduces to a comparison of the relevant AFM pulling speeds and force-loading rates to molecular relaxation times.

Traditionally, the measurement of polymer extension has been done by first extending a molecule at some given loading rate and then retracting the AFM tip at the same rate. The observation of identical force responses was taken to be a sign of thermodynamic equilibrium [19,42]. This procedure was questioned recently by the measurement of the length fluctuations in a constant force-loading rate experiment [22]. Despite perfect agreement of the measured force-extension traces in the extension and contraction experiments, the observed length fluctuations did not match the the expected value, $\langle \sigma_l^2 \rangle = k_{\text{B}}T/(\partial f/\partial \langle L \rangle |_T)$, which suggest that the understanding of this experiment requires more than just equilibrium statistical mechanics. Moreover, there also existed significant force fluctuations, which can not be explained with a Gibbs ensemble framework.

The first model of polymer dynamics, proposed by Rouse in 1953 [52], solves the Newtonian equations of motion for a connected set of springs, each having zero equilibrium length. The springs play the role of monomers in this model. Owing to its simplicity, the Rouse model is often used as a testing ground for new theories, see for example Speck and Seifert [53]. A slightly more realistic model of a polymer molecule in solution was developed by Zimm[2] and includes the hydrodynamic effects of beads interacting with each other. These beads are still connected by springs with zero equilibrium length. The Zimm model cannot be integrated analytically, but it is specifically suitable for molecular dynamics calculations, as it is easy to write down the forces acting on each monomer and use molecular dynamics or Monte Carlo calculations [54–61].

A second way to approach fast polymer stretching is to analyze the tension propagating along the backbone of a polymer. In this case, one has to carefully account

[2]see de Gennes [1], Doi and Edwards [2], or Grosberg and Khoklov [5] for introductions to the Rouse and Zimm models

for the local structure of the polymer molecule, which is an unsolved problem at the present time. Scaling arguments and some simulations are possible only for semi-flexible molecules [62–66]. These are characterized by a contour length that is of the order of the correlation length and form an intermediate but important regime between the rigid rods and fully flexible molecules.

One of the classic approaches to non-equilibrium physics, the description of polymer stretching in terms of a Markov process, has not yet been implemented for the fast stretching of polymers. The approach presented in Chapters 3 and 4 uses molecular length L as a stochastic variable and is capable of obtaining the non-equilibrium length distribution functions $P(L,t)$ from very simple assumptions. This is done via a Master equation [67,68], which reads

$$\frac{\mathrm{d}P(L,t)}{\mathrm{d}t} = \int \mathrm{d}L'[W(L,L')P(L') - W(L',L)P(L)]. \tag{1.4}$$

Equation (1.4) has a very simple and intuitive interpretation: for the calculation of the rate of change of a probability distribution $P(L,t)$ one needs to take all the probabilities that increase P at length L and time t (this is the first term in the integral in equation (1.4)), and then subtract all those that decrease P (second term in (1.4)).

The main problem with using a Master equation is a good choice of the transition rates $W(L',L)$. While this choice is not exactly unique, there is a fundamental requirement on the transition rates: to avoid the possibility of perpetual motion, the rates into and out of a given length L have to cancel exactly in thermodynamic equilibrium,

$$W(L,L')P_{\mathrm{eqm}}(L') = W(L',L)P_{\mathrm{eqm}}(L). \tag{1.5}$$

The equilibrium probability distributions in the detailed balance equation (1.5) are best written in terms of partition functions, which is the primary result of Transfer Matrix calculations.

Chapters 3 and 4 develop such a Master Equation approach to the dynamics of polymer stretching. In addition to detailed balance, the simplest reasonable form for the dynamics of the molecule is used to obtain the stretching response out of equilibrium. Just as for the equilibrium considerations, it is necessary to distinguish

between the different stretching ensembles for the modeling of AFM experiments. Chapter 3 considers the constant force-loading and the constant velocity regimes.[3] The stretching response of a quickly stretched molecule is notably different in the Helmholtz and Gibbs regimes, in contrast to the equilibrium case where the difference occurs primarily in the fluctuations. Chapter 4 takes up the question of relaxation times, which was used as a criterion for the usefulness of equilibrium modeling in equation (1.3) at the beginning of this Section. This calculation in effect encompasses the force-clamp mode of AFM experimentation in detail.

Three different statistical mechanics regimes are considered, which are non equilibrium extensions of the Gibbs and Helmholtz ensembles. The constant force-loading (or force-ramp) and constant speed calculations are presented in Chapter 3, while the relaxation of molecules under the sudden application of stress is discussed in Chapter 4. The basis of the Master equation is to start from the fully developed equilibrium theory provided by the Transfer Matrix method and use reasonable rates for the transition between two extended states of a molecule. This allows the numerical solution of an integro-differential equation, leading to the stretching and relaxation response of a molecule close to equilibrium.

At present, the master equation approach neglects any long-range hydrodynamic interaction. Janovjak *et al.* [69] have shown that the drag due to the moving AFM support becomes important at pulling speeds of about 20μm/s and higher. This speed is well into the non-equilibrium regime for large macromolecules as predicted by the approach in this thesis, which means that the current theory should be applicable up to those pulling speeds.

Note that Seifert and Braun [70] developed a Master equation based model for polymer stretching concurrently to the one presented in this work. However, they look at the unfolding of globular polymer domains that are individually approximated by Worm-Like chains in the coil state, leading to a complicated two-state model where a molecular Section can either be in the coil state or in the globular state.

[3]Note the change in terminology: an ensemble requires thermodynamic equilibrium.

1.4 Breaking Molecular Bonds

In the preceding Sections, the ideas and experiments related to single molecule stretching with an AFM were reviewed. The ultimate end of such a single-molecule experiment is generally the rupture or unbinding of the polymer or some of its parts. Experimentally it is now possible to break a number of chemical complexes with an AFM by attaching polymer spacers such that the bond in question is the weakest link [71, 72]. *Dynamic Force Spectroscopy* (DFS) generally consists of repeating a breaking experiment many times over, preferably at different loading rates. The result is a spectrum of different breaking forces from which one hopes to be able to extract detailed information about the system under consideration [73–78].

Again, the availability of experimental data has spawned a lot of theoretical activity in this area and there is an ongoing debate as to what can actually be measured with DFS. [79–96]. The generally accepted starting point for the interpretation of such data is Kramer's rate theory (see the review by Hänggi *et al.* [97]). At zero force the bond is in a state near the free energy minimum, from which it could escape across some potential barrier via thermal excitation. The escape is facilitated by the application of an external force (hence the AFM), which leads to a lowering of the barrier. It is the detailed form of the free energy surface and the potential barrier that one seeks to measure with Dynamic Force Spectroscopy.

This procedure has been adopted for single bonds by Bell [80] and later by Evans and Ritchie [86], who were the first to point out the advantage of doing DFS using widely varying loading rates. The Evans-Ritchie model is based on an escape rate $k^*_{\text{off}} \exp(-\beta f \Delta x)$, which is increased upon the application of an external force f. The width of the potential barrier is taken to be Δx such that the free energy gained by crossing the barrier is $f\Delta x$. The Kramer's rate equation for the probability P that a bond is intact at time t is

$$\frac{\mathrm{d}P(t)}{\mathrm{d}t} = k^*_{\text{off}} \exp(-\beta f \Delta x) P(t). \tag{1.6}$$

Its integration is possible analytically for the case of a fixed force or a constant force-loading rate and can easily be done numerically for other external conditions [86, 89].

In recent years however, there has been an emerging consensus that this model is

incomplete and that much more can be done with the available data. Many groups agree that the underlying assumptions used in the Evans-Ritchie model (1.6) is much too simple to resemble realistic situations. Several avenues have been pursued to add physical realism to the situation. Rather than having a constant potential barrier somewhere in space, cubic reaction paths offer a much better interpolation of the underlying energy landscape [84]. Some authors include the effects of multiple reaction paths [79, 83] or the rebinding of molecular complexes [83, 94].

The theory is well developed and generally thought to be valid for several phenomena, such as the breaking of single bonds or the unfolding of proteins and DNA. However, recent investigations using force-clamp spectroscopy showed that at least the latter problem might be intractable with the conventional methods, as there are signs of a glassy transition that have yet to be predicted theoretically [73].

In the case of single bonds, there is some agreement that it is possible to measure three important physical parameters using DFS [85, 98]: the energy of thermal activation (or barrier height), the attempt frequency to cross this barrier, and the position of the transition state. Chapter 5 develops the theoretical framework to do these calculations from available data with the help of a simple spread sheet. This Chapter shows that a large spread of experimental loading rates is required in order to obtain meaningful results and discusses the uniqueness of fitting observed spectra.

The currently available literature takes little note of the important differences that are introduced with the varying modes of AFM operation, especially when polymer spacers are used to separate the complex under investigation and the substrate. The resulting difficulties in modeling experiments done at constant velocity are pointed out in Chapter 5.

Chapter 2

Conformational Transitions in Single Polymer Molecules Modeled with a Complete Energy Landscape: Continuous Two-state Model

This chapter has been submitted for publications to the European Journal of Physics E on Oct. 20, 2006. The authors are Felix Hanke and Hans Jürgen Kreuzer. The contribution of Felix Hanke consists of the idea to the approach, all numerical and analytic calculations and the manuscript and figure preparation.

Abstract

An extension of the two-state Freely Joined Chain model for the mechanical extension of polymer molecules is presented in which the discrete energies of the two conformers are replaced by continuous functions of the conformer length. The statistical mechanics is initially developed in the Gibbs ensemble and leads to a conformational multi-state model. This is used to fit the equilibrium force-extension curve for Dextran. The continuous model also allows the use of Transfer Matrix methods to calculate all statistical properties in the Helmholtz ensemble, including thermal fluctuations. The latter are obtained with near perfect agreement to experiment.

2.1 Introduction

Stretching a single polymer molecule in an atomic force microscope (AFM) or optical tweezer experiment allows one to measure the force-extension curve or the mechanical equation of state. For long polymer chains the low-force region is dominated by entropy, while bond angle and bond length deformations of only the longest conformer are important in the high-force regime. When the energy spectrum of the polymer, *i.e.* the conformational energy vs. length dependence is smooth, the force extension curve rises with a monotonically increasing slope. Simple descriptions of such situations are given by Freely Joined Chains, Freely Rotating Chains or the Worm Like Chain

model [4, 5]. An example of such a system is poly (ethylene-glycol) stretched in hexadecane [99]. On the other hand, if there are large steps in the energy landscape in the sense that the extended conformers are much higher in energy, one observes clear signs of a conformational transition in the force extension curve. Examples of such systems are poly(ethylene-glycol) stretched in water [99] and a large catalog of polysaccharides [19, 21, 22, 43–49]. The first AFM measurements on Dextran were carried out by Rief *et al.* [19] and showed signs of one conformational transition, which was later connected with α-linkages in the glucose rings [100]. A system with two of these transitions was also found by Marszalek *et al.* [45] in the stretching response of pectin.

Steered molecular dynamics calculations used with *ab initio* calculations have shown that the conformational change in polysaccharides is probably due to a chair-boat transition [101], although there exist claims that it might be a chair-inverted chair transition as well [102]. Recently, the careful analysis of force fluctuations suggested that there may be a third intermediate state between the chair and boat conformations in Dextran [22].

There are fitting formulas that are used to explain the experimental data. The most widely used one is a simple two state model [42, 99, 103], based on the Freely Joined Chain (FJC). A second more microscopic approach was developed recently based on a Freely Rotating Chain (FRC) frame work in conjunction with *ab initio* calculations [50, 51]. These models use either the analytically known force-extension relations of the FJC, or the high-force limit of the FRC model [7], but include a conformer and force dependent contour length.

In the FJC-based two-state model one assumes that a transition region the force-extension curve is dominated by just two conformers. These differ substantially not only in length but also in energy with a difference in the Gibbs free energy at zero force $\Delta G = G_{\text{long}} - G_{\text{short}} > 0$. The ratio of the monomer occupation probabilities at any given force f is then given by $p_{\text{short}}/p_{\text{long}} = \exp[\beta(\Delta G - f\Delta\ell)]$, where $\Delta\ell$ is the difference in the conformer length. The average conformer length is given by $\ell_{\text{conf}} = p_{\text{short}}\ell_{\text{short}} + p_{\text{long}}\ell_{\text{long}}$. This information is used in a Langevin function with

an added spring-like term to account for high-force extensibility:

$$\langle L(f)\rangle = N\ell_{\text{conf}}(f,\Delta G)\left(\cosh(\beta f L_K) - 1/(\beta f L_K)\right) + Nf/K_S. \tag{2.1}$$

Here, N is the monomer number, K_S is the segment extensibility, and L_K the Kuhn length. As long as one treats ΔG as a constant, the force-extension curve can not be regarded as the mechanical equation of state because its proper temperature dependence is lacking. The latter could of course be obtained by further measurements and fitting at different temperatures. A different aspect of this lack of knowledge was pointed out by Walther *et al.* [22], who were unable to reconcile the original two state model with the observed fluctuations in their measurements.

In this work, an extension of the FJC-based two-state model is presented that is complete and consistent with all thermodynamic requirements. This is achieved by setting up the proper statistical mechanics in the Gibbs ensemble, from which the correct mechanical and thermal equations of state and fluctuations follow directly. The new feature of the model is the replacement of the two conformer states with conformational potential energy curves. It will be demonstrated that this continuous two-state FJC model is especially useful for an easy specification of the statistically relevant conformers in a conformational transition. The next section presents the derivation of the extended FJC model, followed by an extensive example using data on Dextran.

2.2 Model

To set up the continuous multi-state FJC model, one starts from the Freely Joined Chain (FJC) model for a polymer with N monomers with a fixed length b that are joined together without restricting the bond angle. In the Gibbs Ensemble, the force f is fixed along the $\hat{\mathbf{z}}$ direction in a coordinate system. The Gibbs partition function Γ for a single monomer reads

$$\Gamma_{\text{FJC}}(f,T) = \frac{1}{v_0}\int d^3r\ \delta(|\mathbf{r}| - b)\exp(\beta\mathbf{f}\cdot\mathbf{r}). \tag{2.2}$$

The reference volume v_0 is required to ensure the proper dimensionality of the partition function, while $\beta = 1/(k_{\text{B}}T)$ contains the temperature dependence. From (2.2)

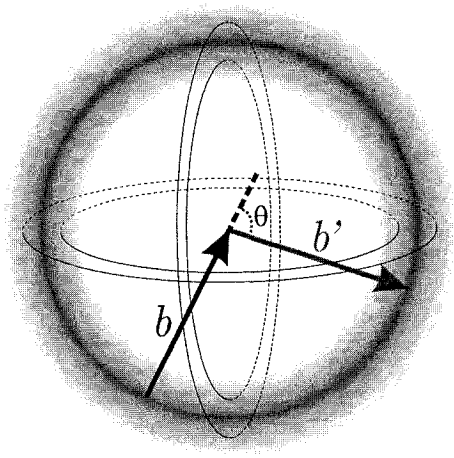

Figure 2.1: The Freely Joined Chain model with an external potential: Given the position of one monomer with length b, the following monomer can exist at some distance b' and a random angle θ with respect to the previous bond. Each distance b' is Boltzmann-weighed, where the darker regions in the figure correspond to lower potential.

one easily obtains the Langevin force-extension relation of a FJC chain, see for example Livadaru *et al.* [7] for details.

In the continuous two-state FJC model we replace the δ-function (ensuring a fixed bond length) in Eqn. (2.2) with the Boltzmann factor of some arbitrary potential $V(b)$ of the bond length b.

$$\Gamma(f,T,[V(b)]) = \frac{1}{v_0}\int d^3b\ \exp\left[\beta(\mathbf{f}\cdot\mathbf{b} - V(|\mathbf{b}|))\right] \tag{2.3}$$

$$= \frac{2\pi}{v_0}\int db\ \frac{b}{\beta f}\left\{\exp\left[\beta(fb - V(b))\right]\right. \\ \left. - \exp\left[-\beta(fb + V(b))\right]\right\} \tag{2.4}$$

The second step is the result of integrating out the angular degrees of freedom and making use of the fact that $\mathbf{f}\cdot\mathbf{b} = fb\cos\theta$ in a cylindrical polar coordinate system. Notice the functional dependence of the partition function on the potential $V(b)$, which demonstrates that Eqn. (2.4) is valid for any monomer potential. Fig. 2.1 gives a schematic view of the FJC model with a continuous potential $V(b)$.

For a polymer molecule with N non-interacting freely joined monomers, each of

which can be in any one of N_C conformers, the total Gibbs partition function reads

$$\begin{aligned}\Gamma_{\text{total}}(f,T) &= [\Gamma_{\text{monomer}}(f,T)]^N \\ &= \left[\sum_{i=1}^{N_C}\Gamma(f,T,[V^{(i)}(b)])\right]^N . \end{aligned} \tag{2.5}$$

Here $V^{(i)}(b)$ is the stretch potential of the i^{th} conformer which could, in principle, be different for each of the N monomers that make up the polymer. Restricting the number of different monomer potentials to two or three results in the continuous two-state or three-state FJC models respectively. From this partition function we obtain the Gibbs free energy $G(f,T) = -Nk_{\text{B}}T\ln\Gamma_{\text{monomer}}(f,T)$, from which the mechanical equation of state follows as

$$L(f,T) = -\left.\frac{\partial G}{\partial f}\right|_{T,N} = \frac{N}{\beta\Gamma_{\text{monomer}}}\left.\frac{\partial\Gamma_{\text{monomer}}}{\partial f}\right|_{T,N} . \tag{2.6}$$

Any other statistical properties such as the relative occupations of the conformers, entropy and fluctuations can also be obtained from Eqn. (2.5).

One possible way to proceed is to calculate the partition function (2.4) numerically for some given monomer potential $V(b)$. The latter can be obtained from quantum mechanical calculations as shown elsewhere [99, 104]. On the other hand, if we approximate this potential by a harmonic oscillator, *i.e.* expanding the potential to second order in the bond length

$$V(b) = \frac{k}{2}(b-b_0)^2 + V_0 + \mathcal{O}(b-b_0)^3; \qquad b_{\min} \le b \le b_{\max}, \tag{2.7}$$

it is straight forward albeit cumbersome to evaluate the partition function in Eqn.

(2.4):

$$\Gamma(f,T) = \frac{4\pi}{\beta^2 kf}\exp(-\beta V_0)\left[\exp\left(-\frac{\beta k}{2}(b_{\min}-b_0)^2\right)\sinh(\beta f b_{\min})\right.$$
$$\left.-\exp\left(-\frac{\beta k}{2}(b_{\max}-b_0)^2\right)\sinh(\beta f b_{\max})\right] + \frac{2\pi}{\beta f}\sqrt{\frac{\pi}{2\beta k}}$$
$$\times\left((b_0+\frac{f}{k})\exp(\beta f b_0)\left\{\mathrm{erf}\left[\sqrt{\frac{\beta k}{2}}\left(b_{\max}-b_0-\frac{f}{k}\right)\right]\right.\right.$$
$$\left.\left.-\mathrm{erf}\left[\sqrt{\frac{\beta k}{2}}\left(b_{\min}-b_0-\frac{f}{k}\right)\right]\right\} - (b_0-\frac{f}{k})\exp(-\beta f b_0)\right.$$
$$\left.\times\left\{\mathrm{erf}\left[\sqrt{\frac{\beta k}{2}}\left(b_{\max}-b_0+\frac{f}{k}\right)\right] - \mathrm{erf}\left[\sqrt{\frac{\beta k}{2}}\left(b_{\min}-b_0+\frac{f}{k}\right)\right]\right\}\right). \qquad (2.8)$$

For a given conformer, one can interpret the quantity k in Eqn. (2.7) as the conformer stiffness, while b_0 is the equilibrium length at zero force and V_0 is the conformer internal energy above some reference point. The approximation introduced with this potential is valid for relatively small extensions and compressions and agrees well with *ab initio* and density functional theory calculations for several systems [102, 104].

Equation (2.8) provides a tool to calculate all statistical properties of a single conformer in the Gibbs ensemble. A lot of single molecule conformational statistics can actually be modeled with a very small number of conformers. As an example, the mechanical response of poly (ethylene glycol) is well described with only a few appropriate potentials corresponding to an all-helical, one all-trans conformer as well as a few that exhibit gauche defects [99]. In fact, many systems exhibit conformational transitions which can be traced to the transition between two well-defined conformers [19, 42, 47, 101]. In the present case, summing Eqn. (2.8) for different conformers will adequately describe this situation: Once the partition function is calculated, it is trivial to do the remaining thermodynamics in the present formalism.

2.3 Application to the Stretching Response of Dextran

In contrast to models based on a modified form of the Langevin formula, the descriptions of polymer statistics in terms of Eqn. (2.5) allows one to integrate the energy landscape of a monomer directly. In this section we will use the parabolic form of

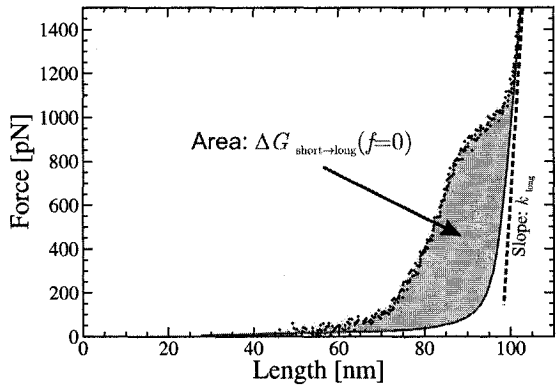

Figure 2.2: AFM data for Dextran [22] (×) and the force-extension curve for a hypothetical molecule which only contains the longer conformer.

the potential (2.7) to fit the force response of a specific polysaccharide, Dextran, for which a conformational transition is generally linked to a chair-boat transition [22].

Experimental data and the fitting procedure for the continuous two-state model are shown in Fig. 2.2. In the high-force regime, all monomers are in the most extended conformer. It is generally assumed to be a boat configuration with a length of $b_{0,\text{long}}$ =5.70Å [44]. The mechanical response for the highest forces is thus due to over-stretching of the molecule, *i.e.* bond angle deformations and bond stretching. This region can be described asymptotically by Hooke's law, $f = k_{\text{long}}(L - Nb_{0,\text{long}})/N$ in the parabolic potential approximation (2.7). The stiffness of the high energy conformer k_{long} can be obtained from a linear fit to the high force data, as shown in Fig. 2.2.

There are three parameters remaining in the continuous two-state model, the length and stiffness of the short conformer as well as the potential energy difference between short and long conformer. All three can be determined by a constrained fit to the experimental data. Armed with the knowledge of k_1 and $b_{0(1)}$, one can imagine a molecule that consists only of the longest conformer. Its force response can be derived from Eqn. (2.5) with $N_C = 1$. The result is the bottom curve in Fig. 2.2. Most importantly, the area between this hypothetical force-extension curve and the measured data is exactly equal to the difference in the Gibbs free energy

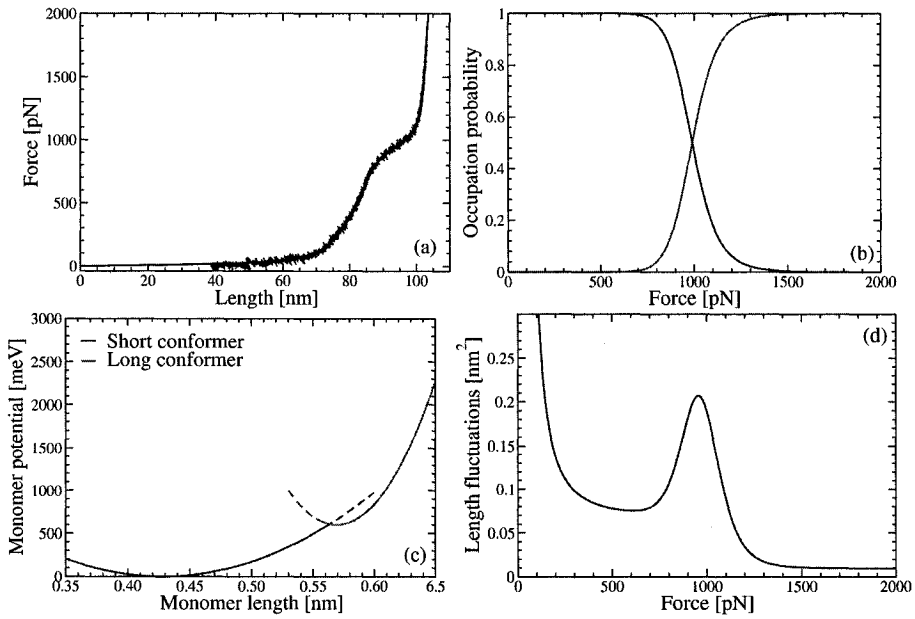

Figure 2.3: Results for Dextran with parameters $b_{0,\mathrm{short}} = 0.442 \pm 0.12$ nm, $b_{0,\mathrm{long}} = 0.570$ nm [44], $V_{0,\mathrm{long}} - V_{0,\mathrm{short}} = 543 \pm 54$ meV, $k_{\mathrm{short}} = 1.31 \pm 0.22 \times 10^4$ pN/nm, and $k_{\mathrm{long}} = 8.29 \pm 0.04 \times 10^5$ pN/nm. (a) force extension relation, (b) relative occupation probabilities of the two conformers, (c) monomer potential, and (d) length fluctuations in the Gibbs ensemble.

$\Delta G_{\mathrm{short}\to\mathrm{long}}(f)$ between the short and long conformers at zero force.

$$\begin{aligned} \Delta G_{\mathrm{short}\to\mathrm{long}}(0) &= \int_0^\infty [l_{\mathrm{long}}(f) - l_{\mathrm{exp}}(f)]df \\ &= [G_{\mathrm{long}}(\infty) - G_{\mathrm{long}}(0)] - [G_{\mathrm{exp}}(\infty) - G_{\mathrm{exp}}(0)] \\ &= G_{\mathrm{short}}(0) - G_{\mathrm{long}}(0). \end{aligned} \tag{2.9}$$

The last step is possible because the molecule is entirely in the short conformer at zero force, leading to $G_{\mathrm{exp}}(0) = G_{\mathrm{short}}(0)$. Moreover, the extended configuration is prevalent for very large forces, hence one has $G_{\mathrm{exp}}(\infty) = G_{\mathrm{long}}(\infty)$. For the purpose of fitting the missing microscopic parameters, equation (2.9) forms a constraint that reduces the number of free parameters by one. Fig. 2.3 shows the results calculated for the data from Ref. [22], *i.e.* the force-extension curve, the probability of finding any monomer within a given conformer, and the underlying monomer potentials.

From the partition function (2.5) one can also calculate the length fluctuations in the Gibbs ensemble via $\langle(\delta L)^2\rangle_G = -k_{\mathrm{B}}T(\partial^2 G/\partial f^2|_T)$, see Fig. 2.3(d). Such

fluctuations were discussed quite some time ago by Kreuzer and co-workers [32, 33] and by Keller *et al.* [34] but the corresponding experiments have only been done recently. The data presented in Fig. 2.3(d) shows a peak right at the transition region around $f = 950$pN, which is due to the additional entropy of having both conformers accessible simultaneously. The extended fluctuations of a completely free molecule at zero force are the reason for the low-force peak, whose magnitude is of the order of the mean-square radius of gyration.

Walther *et al.* [22] use a simple fluctuation model in the Helmholtz ensemble to show that the original two state model [42,103] for Dextran fails to describe the peak in fluctuation data in the transition regime of a Helmholtz ensemble experiment. This failure is due in part to the fact that the original two-state model, Eqn. (2.1), is not a proper mechanical equation of state in the thermodynamic equation of state, since it it was developed purely as a fit function.

Next, a discussion of thermal expansion is necessary. The thermal equation of state has received little if no attention to date, although there are some polymer systems for which it is very important [105]. The continuous two-state model allows one to determine this thermal equation of state. A measurable quantity is, in principle, the thermal expansion coefficient $\alpha = (1/L)(\partial L/\partial T|_f)$, which follows directly from Eqn. (2.6). Fig. 2.4 presents results for the force-dependence of α at three different temperatures. Shown in the lower panel is the change in monomer length with respect to room temperature.

In order to compare the Dextran results to the thermal expansion properties of a purely entropic system, the Langevin equation was used to calculate α at 293 K. A negative thermal expansion coefficient is one of the important signs of entropic elasticity, which makes it easy to link the negative peak in the top panel of Fig. 2.4 to the high entropy in the transition region. To accurately measure the effects of thermal expansion, it will be necessary to detect thermal changes in the molecular length of about 1%, As can be seen from the bottom panel in Fig. 2.4. The original two-state model allows for the calculation of limiting cases of the thermal expansion coefficient. These are given by the different possible forms of the free energy difference $\Delta G(0)$ in Eqn. (2.1): one is a purely entropic version, $\Delta G = -T\Delta S$ while the other

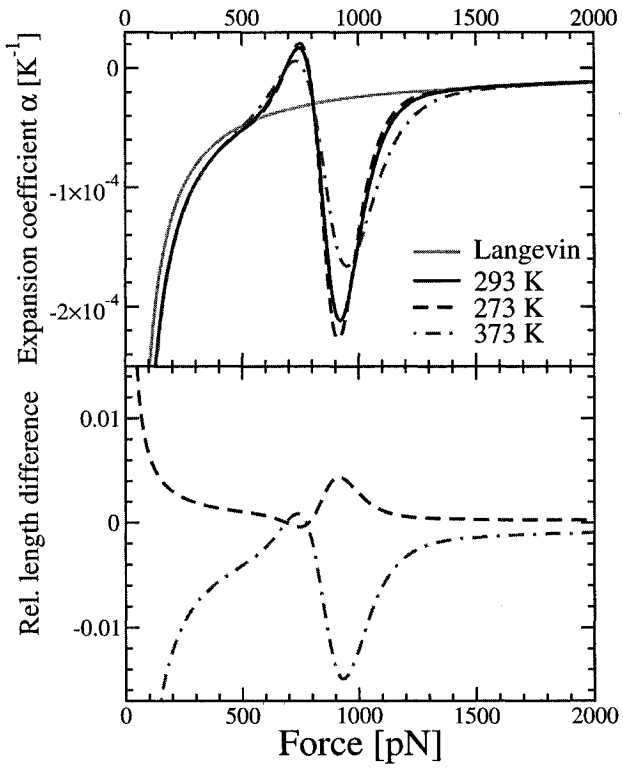

Figure 2.4: The thermal expansion coefficient for Dextran at three different temperatures (top), and the fractional length changes per monomer with respect to room temperature (bottom).

one us purely energetic, $\Delta G = \Delta U$. The result derived from the continuous two-state model is in between these two extreme cases.

2.4 Modeling of Position-Controlled AFM Experiments: Transfer Matrix Calculations

Up to this point the continuous multi-state model has been developed entirely in the Gibbs ensemble, where the force f is the controlled (or fixed) variable and the molecular length L is allowed to fluctuate. For the proper explanation of AFM experiments in which the position of a cantilever is controlled rather than the applied force, one has to calculate the molecular partition functions in the Helmholtz ensemble which can be done numerically with Transfer Matrix methods [7, 8, 11].

These calculations use the Green function formalism [2, 5], where the independent variable is chosen to be the distance L above the substrate. The Green function $\mathcal{G}_n(L, 0)$ of some monomer n is calculated with the Chapman Kolmogoroff equation

$$\mathcal{G}_n(L, 0) = \int dL' \mathcal{T}(L, L') \mathcal{G}_{n-1}(L', 0), \tag{2.10}$$

The transfer operator $\mathcal{T}$ specifies the possible position of a monomer n, given the state of monomer $n - 1$. For this model, $\mathcal{T}$ is given by

$$\mathcal{T}(L, L') = \sum_{i=1}^{N_C} \int_{-1}^{1} d\cos\theta \int_{b_{\min}^{(i)}}^{b_{\max}^{(i)}} db\ \delta(L - L' - b\cos\theta) \exp[-\beta V^{(i)}(b)], \tag{2.11}$$

with the same conventions as used for the monomer partition function (2.5) in the preceding sections. Notice that the transfer operator (2.11) is written for general monomer potentials. The continuous two-state model of the last sections is obtained by choosing $N_C = 2$ with parabolic conformer potentials $V^{(i)}(b)$. A molecule consisting of N monomers, is described by a Green function $\mathcal{G}_N(L, 0)$ that specifies the probability of finding the end of the molecule at a distance L above the substrate.

For the proper evaluation of observable properties such as length and force fluctuations, one still has to couple the polymer Green function G_N to one describing the AFM cantilever, treating the latter as a small statistical system. The conjugated Green function $\mathcal{G}^*(L_c, L)$ for a cantilever of length L_c and spring constant k_c is given by

$$\mathcal{G}^*(L_c, L) = \exp\left[-\frac{\beta k_c}{2}(L_c - L)^2\right], \tag{2.12}$$

from which we can calculate the probability density of finding the end of the molecule at some length L as

$$P(L) = \frac{\mathcal{G}^*(L_c, L)\mathcal{G}_N(L, 0)}{\int dL' \mathcal{G}^*(L_c, L')\mathcal{G}_N(L', 0)}. \tag{2.13}$$

Any quantity that is observable with the AFM can be calculated from the moments of this probability density, $\langle L^n \rangle = \int dL\ L^n P(L)$. In particular the average molecular length $\langle L \rangle$ is the first moment of (2.13), giving the force-extension curve in the Helmholtz ensemble as $\langle f \rangle(\langle L \rangle) = k_c(L_c - \langle L \rangle)$ for each value of the cantilever position L_c.

Notice that an infinitely stiff cantilever has $\mathcal{G}^*(L_c, L) = \delta(L_c - L)$, with the consequence that the Green function $\mathcal{G}_N$ is exactly equal to the Helmholtz partition function of an isolated molecule with a corresponding free energy $F(L) = -k_\mathrm{B}T \ln \mathcal{G}_N(L, 0)$; see Kreuzer *et al.* [32]. On the other hand, all of the Gibbs ensemble results of the previous sections can be obtained within this formalism if one observes that the conjugated Green function for the system *external force reservoir* is equal to $\mathcal{G}^*(f, L) = \exp(\beta f L)$. This property was used successfully to test the numerical method against the previous analytical calculations.

The calculation of the force extension curve in the Helmholtz ensemble yields the same result as presented in the previous section. In this formalism, the observed length fluctuations can be calculated directly as shown in Fig. 2.5. Note that the molecular parameters used for calculating these fluctuations are exactly those obtained by fitting the force extension curve of Fig. 2.3. The only additional information needed is the spring constant of the AFM cantilever used, $k_c = 50\mathrm{pN/nm}$ [22]. The near-perfect agreement of calculated and observed fluctuations at and around the transition region validates the continuous two-state model.

However, the data in Fig. 2.5 warrants further discussion as there are two more important regimes. The constant fluctuations in the region between 35 and 60nm are entirely governed by the AFM cantilever. They are given by the variance one would predict from Eqn. (2.12) for a simple cantilever, $\langle \sigma_c^2 \rangle = k_\mathrm{B}T/k_c = 0.08\mathrm{nm}^2$. For short length scales below about 35nm theory and experiment do not match. This is due to the influence of excluded volume and polymer-surface interactions, which limit the possible fluctuations.

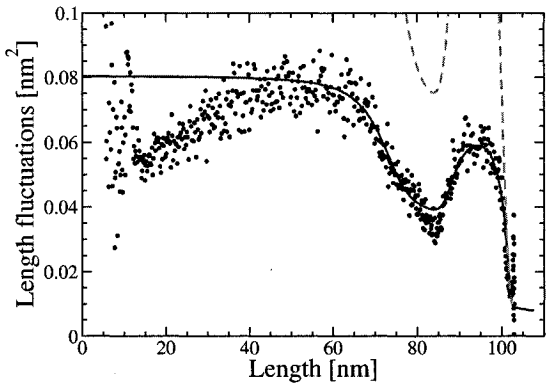

Figure 2.5: Length fluctuations for the data presented in Fig. 2.3. The predictions in the Helmholtz ensemble (solid line) are TM calculations using the parameters given earlier with the experimental cantilever spring constant $k_c = 50$pN/nm. Also shown to scale are the fluctuations predicted by the analytic theory in the Gibbs ensemble (dashed line).

One could model the interaction between polymer and substrate directly via an effective position-dependent external potential V_L in the Transfer operator [10] by adding a factor $\exp[-\beta V_L(L)]$ to the integral in Eqn. (2.11). Unfortunately, the nature of these surface interactions is too unspecific in most cases to yield reliable and reproducable results. The only case where this type of analysis is fruitful is for the pure desorption of molecules adsorbed on a substrate [10].

2.5 Discussion

This paper develops the exact statistical mechanics of an analytically integrable polymer model with a continuous energy landscape. This continuous multi-state model is applicable to the analysis of conformational properties of single polymer molecules. Since entropic elasticity is taken into account exactly as well as the underlying molecular energy landscape, the model will work particularly well for systems that have conformational transitions in the crossover regime between purely entropic and enthalpic stretching, which is generally around 300pN.

The stretching response of Dextran is studied extensively as an example. The parameters resulting from the force-extension fit are used to exactly reproduce the

thermal fluctuations observed experimentally. For this procedure to work, it is necessary to use the Transfer Matrix method, which is capable of exactly accounting for the coupling to an AFM cantilever in the Helmholtz ensemble.

The term *controlled position* (or *Helmholtz*) *ensemble* is used somewhat misleadingly in polymer physics and warrants further discussion. Generally, it describes systems with fixed length where the force is fluctuating. This is certainly the case for a coupled polymer-cantilever system in which the distance between cantilever and substrate is fixed. As discussed in the previous section, commonly used cantilevers are rather soft and show significant fluctuations themselves. Therefore one can not regard the polymer molecule itself to be in the Helmholtz ensemble, as it fluctuated in both the length and the force. From the definition of the fluctuations and Eqn. (2.13) it is easy to show that force and length fluctuations are related by the cantilever spring constant, $\langle \sigma_f^2(L_c) \rangle = k_c^2 \langle \sigma_L^2(L_c) \rangle$, as discussed in detail by Kreuzer *et al.* [32].

Nevertheless, experiments in the so-called force-ramp mode of the AFM show fluctuations which can not be explained by equilibrium statistical mechanics [22], which is due to the fact that the AFM response time is much slower than the molecular relaxation times. The availability of a partition function such as (2.8) will enable one to model this situation rigorously in a non-equilibrium theory based on the Master Equation [106], where the response of the force-ramp AFM itself can be included exactly.

Finally, it is worth noting that the description of a molecule in terms of a partition function automatically generates the proper thermodynamics, not only for the mechanical equation of state (as shown here) but also for the thermal equation of state.

Chapter 3

Non-Equilibrium Theory of Polymer Stretching Based on the Master Equation

This chapter has been published in Physical Review E (vol. **72**, Article Number 031804, 2005) as a regular article with the same title. The authors are Felix Hanke and Hans-Jürgen Kreuzer. The contribution of Felix Hanke to this manuscript consists of all numerical and analytic analysis and 90% of the manuscript preparation. Permission to use this work has been granted by the American Physical Society, a copy of the permission letter is attached to this thesis.

Abstract

We present a model for fast polymer-stretching experiments. We use the master equation and argue that the end-to-end extension of a polymer molecule can be used as a stochastic variable after appropriate coarse-graining. The main effect of increasing pulling speed or force loading rate is a marked hysteresis in the force-extension curve as well as an overall shift of the curve to higher forces when compared to the equilibrium curve. This can be understood in terms of the moments of the transition probability in the master equation. An analysis of the fluctuations and relaxation times is also given in the framework of our theory.

3.1 Introduction

A microscopic understanding of the mechanical properties of individual natural or synthetic polymer strands is required to model and predict their function in biological or technical processes, *e.g.* DNA replication, muscle contraction, or the rheological properties of polymers. Experimentally, single molecule force spectroscopy with the Atomic Force Microscope or with optical tweezers offers a versatile and powerful experimental tool to measure the extension of a single molecule as a function of applied force in different environments. The method allows to observe the binding

forces between different receptor-ligand systems [107,108] and the unfolding of protein domains [19, 23], or to measure the elastic properties of individual macromolecules [20, 42]. Likewise, the scanning force microscope, optical tweezers and near-field magnetic tweezers have been used to measure the elastic response of chromosomes [109], to study formation of DNA loops by an enzyme [110], and to investigate DNA-binding molecular motors (RNA polymerase, DNA polymerase, etc.) [111], to reveal the dynamics of these molecules during translocation, as well as the effect of external force loads on their performance.

The ultimate aim of polymer science must be the explanation of the macroscopic properties of a long repetitive chain molecule in terms of the structural properties of its subunits. To proceed from the microscopic details of the quantum chemistry of these subunits to a comprehensive description of the long chain a series of well-defined approximations must be invoked that at any stage can be subjected to rigorous scrutiny. Such a program of simplifications has been in place in polymer science for many years [4], but only recently has it become practical to implement this procedure from first principles [50, 99, 112].

Macroscopic properties of immediate interest are the force-extension curve and the corresponding fluctuations of force and length of the polymer molecule. To ensure that a measurement of the force-extension relation of a polymer molecule yields the equilibrium equation of state the rate of change of the external force must be slow on the time scale of the internal relaxation of the polymer chain, which is readily checked by a sufficient variation of this rate. If the rate of increase of the external force is such that equilibrium cannot be maintained internally, non-equilibrium effects are accessed which can be used to study the kinetics and, ultimately, the dynamics of the polymer chain. As long as one stays close to equilibrium relaxation effects can be studied. These same dynamics will then also manifest themselves far from equilibrium in the form of hysteresis and nonlinearities.

A simple approach to the dynamics of polymer chains is given by the Rouse model [1, 5], in which one derives a diffusion equation for the molecular motion to model the dynamics in terms of separate relaxation modes, *e.g.* of a linear chain of coupled harmonic oscillators. This model is appealingly simple, but it is incapable of taking

into account the hydrodynamic interactions between monomers. A first solution to this problem is provided by calculating hydrodynamic corrections to the Rouse modes within the framework of the Zimm model [5]. Monte Carlo methods and Molecular Dynamics Simulations provide another approach to the problem [60, 113, 114].

On the experimental side, the dynamics of polymer molecules have received a lot of attention in recent years [115]. DNA molecules in particular are long enough to be observed under flow stress via fluorescent labels [25, 116]. Quake and coworkers have developed a way of manipulating single DNA molecules with pairs of optical tweezers [26, 27]. These experiments provide a good way to study the relaxation dynamics of biopolymers under external forces. The process of molecular relaxation is an important issue in this work, because it is one of the few ways to access molecular relaxation times [27]. The latter are important in the interpretation of virtually all polymer experiments.

There are several different approaches to measure the mechanical properties of polymers in an AFM experiment. One is to control the spatial position and velocity of the cantilever, which suggests doing the analysis in the canonical ensemble for the equilibrium aspects. Alternatively, it is possible to control the force, f, and the force loading rate, $\mathrm{d}f/\mathrm{d}t$, by implementing an additional feed-back algorithm into the AFM control, which adjusts the position in such a way that only the force is controlled. Equilibrium situations of this type should be analyzed using the Gibbs ensemble. A third possibility is to use the same control to implement a force step, where f starts from a low value and is suddenly increased to some high value. All of these experiments have been done and have been shown to lead to spectacular differences, for example when looking at the unfolding of single titin domains [23]. The equilibrium theory of polymer stretching in the Gibbs and Helmholtz ensembles has been worked out by Kreuzer *et al.* [32, 33].

A first principles theory of non-equilibrium processes in polymer science would invariably have to start from the molecular energy landscape. Using the assumption that molecular stretching can be modeled as a Markov process, one can then derive a master equation. This approach has been pursued for short proteins and molecular clusters [117–119]. The energy landscape in those studies is obtained from quantum

chemical calculations. Following the work of Jarzynski [120, 121] it has recently become possible to measure the molecular free energy surface directly by averaging over finite sets of non-equilibrium data [122].

In this paper we will use a different approach to study the non-equilibrium dynamics of polymers. We will model conformational conversion in the stretching of a polymer as a Markov process. This presupposes that the dynamical time scale of conversion itself is fast compared with the macroscopic kinetics of the stretching process. We will show that the model can be simplified further by taking the molecular length itself as the stochastic variable. In the resulting master equation we will argue phenomenologically for a simple form of the transition probabilities that reproduces experimental equilibrium relaxation times. Because the transition rates in the master equation must satisfy detailed balance they will contain information about the equilibrium properties of the chain. For the calculation of the latter we will use two simple models, namely the Freely Jointed Chain (FJC) and the Freely Rotating Chain (FRC) models, although the generalization to more detailed polymer models is straightforward, albeit numerically more involved.

By using only the molecular length as our stochastic variable, we neglect some of the enthalpic effects observed for highly stretched and overstretched polymers. These effects have received a lot of attention in the recent literature [19, 23, 46, 50, 103] and can generally be explained with a two-state model that contains one type of short and long conformer. In this work, we will have a detailed look at the entropic regime and show some of the non-equilibrium effects one should expect to see there. We use the transfer matrix or Green function method [6,7,11] to obtain the equilibrium properties of these models. Our theory is presented explicitly in both the Gibbs and Helmholtz regimes. This will enable us to describe realistically the experimental situations of (*i*) constant force loading and (*ii*) constant velocity of the AFM cantilevers. The situations of instant stretching and release could in principle also be treated with our theory. However, this has already been done by several groups using scaling arguments for flexible and semiflexible chains [62, 66, 123–125]. A detailed comparison between the two approaches will be given elsewhere.

The paper is organized as follows: in the next section we derive the specific form

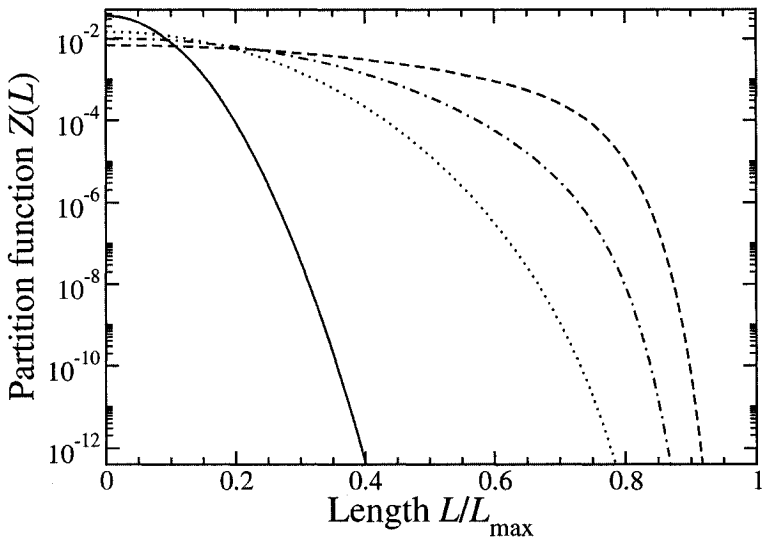

Figure 3.1: The partition functions $Z(L)$ for four representative chains with $N = 100$ monomers are shown on a log scale: FJC (solid line), and FRC with bond angles $\gamma = 30°, 45°, 60°$ (dashed, dot-dashed and dotted lines respectively). Notice the almost Gaussian dependence of the FJC partition function.

of the transition rates in the master equation and briefly comment on the numerical solution of the latter. We present a derivation of the macroscopic equations of motion that couple the time dependence of the average length of the polymer to the non-equilibrium evolution of the fluctuations. We then describe how to calculate the relaxation times and compare these to measured values for DNA molecules. This will enable us to estimate force loading rates and pulling velocities required to observe non-equilibrium effects. A discussion of the resulting force-extension curves as well as the fluctuations is given in section 3.3. An outline of a non-coarse-grained theory is given in appendix 3.5.

3.2 Theory

3.2.1 Equilibrium Polymer Properties

In order to discuss non-equilibrium polymer stretching, we first have to outline our approach to the equilibrium physics. As input for the theory in this paper, we will require the canonical partition function $Z(\mathbf{L}, N, T)$, which depends on the length $\mathbf{L}$, the number of monomers N, and the temperature T. This can be calculated exactly

from the Transfer Matrix method developed by our group [6, 7, 11]. We will use the freely jointed chain (FJC) and freely rotating chain (FRC) models, which are good approximations for flexible and semi-flexible polymers, respectively.

We would like to work in the large N limit, which means that the number of monomers must be much larger than the characteristic ratio: $N \gg C_N$. This ensures that the molecule consists of many Kuhn lengths, a, so that there are no directional correlations between the two ends. The FRC characteristic ratio is given by [4]

$$C_{FRC,N} = \frac{1+\cos\gamma}{1-\cos\gamma} - \frac{2\cos\gamma}{N}\frac{1-\cos^N\gamma}{(1-\cos\gamma)^2} \tag{3.1}$$

while for the Freely Jointed Chain we have $C_{\mathrm{FJC}} = 1$. The characteristic ratio for $\gamma = 30°$, appropriate for n-alkanes and $N = 100$ is about 13.

Fig. 3.1 shows the partition functions $Z(N, L, T)$ for some representative chains. For the FJC, our calculations can go up to $N = 150$ while $N = 100$ is the limit for the FRC. This means that our FRC modeling has to be restricted to the bond angle $\gamma = 60°$.

3.2.2 Master Equation

3.2.2.1 Gibbs Regime

Our study of non-equilibrium effects treats the stretching behavior of single polymer molecules as a Markov process that is represented with a master equation. If we take the index enumerating the conformers as the stochastic variable then the Markov process is defined by a function $P_i(\mathbf{f}, t)$ that gives the probability that under a force $\mathbf{f}$ the i^{th} conformer (of end-to-end length $\mathbf{L}_i$) is realized at time t. We then need as many equations of motion as there are conformers for the particular polymer. Such an approach is only feasible for *short* polymers and will be outlined in some detail in the appendix. Here, we present a more coarse-grained approach in which we treat the end-to-end length itself as the stochastic variable.

In this approach, the force can be controlled externally; in equilibrium this corresponds to using the Gibbs ensemble (see ref. [32] for a detailed discussion). We will refer to this mode as the Gibbs regime away from equilibrium.

We now introduce a function $P(\mathbf{L}, \mathbf{f}, t)$ that gives the probability that at time t

the end-to-end length $\mathbf{L}$ is realized under a force $\mathbf{f}$. Its value in equilibrium is given by

$$P_{\mathrm{eq}}(\mathbf{L},\mathbf{f}) = \frac{Z(N,\mathbf{L},T)\exp(\beta\mathbf{f}\cdot\mathbf{L})}{\exp[-\beta g(T,\mathbf{f})]}. \tag{3.2}$$

$g(T,\mathbf{f})$ is the free energy in the Gibbs ensemble. Away from equilibrium we postulate a master equation

$$\frac{\mathrm{d}}{\mathrm{d}t}P(\mathbf{L},\mathbf{f},t) = \frac{1}{b^3}\int \mathrm{d}^3L' \ \left[W(\mathbf{L},\mathbf{L}';\mathbf{f})P(\mathbf{L}',\mathbf{f},t) - W(\mathbf{L}',\mathbf{L};\mathbf{f})P(\mathbf{L},\mathbf{f},t)\right]. \tag{3.3}$$

The transition element $W(\mathbf{L}',\mathbf{L};\mathbf{f})$ gives the probability per unit time that the length of the polymer changes from $\mathbf{L}$ to $\mathbf{L}'$ under a force $\mathbf{f}$; the monomer length b being required for normalization purposes. These transition rates can in principle be calculated from the microscopic dynamics of the coupled polymer-solute system; this will be done elsewhere. Here we follow a phenomenological approach and postulate their form based on simple ideas. We argue that a small change in the force will result in, at most, a small length change over a time interval $\mathrm{d}t$ and write

$$W(\mathbf{L}',\mathbf{L};\mathbf{f}) \sim w_0 \exp\left[-\frac{\beta\Delta}{b^2}(\mathbf{L}'-\mathbf{L})^2\right]. \tag{3.4}$$

The parameter Δ controls the width of effective transitions. The prefactor

$$w_0 = \nu\exp(-Q/k_{\mathrm{B}}T) \tag{3.5}$$

consists of an attempt frequency ν and an energy barrier Q between two conformers. This will be discussed in detail at the end of this section. The quantity $\beta\Delta/b^2$ is typically of the order of a few inverse b^2 so that the Gaussian dependence of the transition probability W on $|\mathbf{L}'-\mathbf{L}|$ makes sure that the end of the molecule has to remain close to the starting point of a given jump. This also justifies to ignore any further dependence on $|\mathbf{L}'-\mathbf{L}|$ in Q. For longer distances, several transitions should be required.

We still need to ensure that detailed balance is satisfied for the master equation (3.3). Thermodynamic equilibrium not only requires that $\mathrm{d}P/\mathrm{d}t = 0$, but that all the terms on the right-hand side of equation (3.3) vanish individually, *i.e.*

$$W(\mathbf{L},\mathbf{L}';\mathbf{f})P_{\mathrm{eq}}(\mathbf{L}',\mathbf{f}) - W(\mathbf{L}',\mathbf{L};\mathbf{f})P_{\mathrm{eq}}(\mathbf{L},\mathbf{f}) = 0, \tag{3.6}$$

or

$$W(\mathbf{L},\mathbf{L}';\mathbf{f}) = W(\mathbf{L}',\mathbf{L};\mathbf{f})\frac{P_{\rm eq}(\mathbf{L},\mathbf{f})}{P_{\rm eq}(\mathbf{L}',\mathbf{f})}$$
$$= w_0 \exp\left[\beta\mathbf{f}\cdot(\mathbf{L}-\mathbf{L}') - \frac{\beta\Delta}{b^2}(\mathbf{L}'-\mathbf{L})^2\right]\frac{Z(N,\mathbf{L},T)}{Z(N,\mathbf{L}',T)}. \quad (3.7)$$

To ensure that the transitions $\mathbf{L}\rightarrow\mathbf{L}'$ and $\mathbf{L}'\rightarrow\mathbf{L}$ are symmetric we choose a form

$$W(\mathbf{L}',\mathbf{L};\mathbf{f}) = w_0 \exp\left[\frac{\beta}{2}\mathbf{f}\cdot(\mathbf{L}'-\mathbf{L}) - \frac{\beta\Delta}{b^2}(\mathbf{L}'-\mathbf{L})^2\right]\sqrt{\frac{Z(L',N,T)}{Z(L,N,T)}}. \quad (3.8)$$

The non-equilibrium force-extension relation is given by

$$\overline{\mathbf{L}}(\mathbf{f},t) = \frac{1}{b^3}\int \mathrm{d}^3L\ \mathbf{L}P(\mathbf{L},\mathbf{f},t) \quad (3.9)$$

and its equation of motion is obtained from (3.3)

$$\frac{\mathrm{d}\overline{\mathbf{L}}}{\mathrm{d}t} = \langle\alpha_1(\mathbf{L})\rangle. \quad (3.10)$$

We define the mean-square fluctuations of the molecular end-to-end distance as a second rank tensor

$$\left\langle\overleftrightarrow{\sigma^2}\right\rangle = \langle\mathbf{LL}\rangle - \langle\mathbf{L}\rangle\langle\mathbf{L}\rangle. \quad (3.11)$$

In a coordinate system where the force points along the z-axis, this tensor is diagonal. In this case, the equation of motion for an element is

$$\frac{\mathrm{d}\langle\sigma_{ii}^2\rangle}{\mathrm{d}t} = \langle\alpha_{2ii}\rangle + 2\langle L_i\alpha_{1i}\rangle - 2\langle L_i\rangle\langle\alpha_{1i}\rangle. \quad (3.12)$$

For equations (3.10) and (3.12) we have defined the $n^{\rm th}$ moment of the transition probabilities,

$$\overleftrightarrow{\alpha}_n(\mathbf{L},\mathbf{f}) = \frac{1}{b^3}\int \mathrm{d}^3L'\ (\mathbf{L}'-\mathbf{L})^n W(\mathbf{L}',\mathbf{L};\mathbf{f}) \quad (3.13)$$

as a tensor of rank n.

To solve the master equation one discretizes the space accessible to a given molecule into a manageable number of points so that the master equation (3.3) becomes a set of coupled differential equations, one per mesh point. Since this would lead to a rather large and intractable system in three dimensions, we will present numerical results

only for the polymer distribution along the force axis. This reduces the problem to one dimension and the transition probabilities have the form

$$W(L', L; f) = w_0 \exp\left[\beta\frac{f}{2}(L' - L) - \frac{\beta\Delta}{b^2}(L' - L)^2\right]\sqrt{\frac{Z(N, L', T)}{Z(N, L, T)}} \qquad (3.14)$$

This corresponds to the approximation that the additional two integrations in equation (3.3) have roughly the same effect for all times. We show in section 3.2.4 that this approximation corresponds to the limit of small length fluctuations $\sigma_{zz}^2 \ll L_{\max}^2$.

We now discuss the origin and meaning of the attempt frequency ν in the prefactor (3.5). The internal excitation modes that trigger the length changes are sound waves that travel along the backbone of the polymer chain. For the longest wave spanning the length of the molecule we can write $\nu = c_s/L_{\max}$. As an example, these modes are calculated in the Rouse model by assuming that the molecule is a chain of coupled harmonic oscillators. To get more realistic estimates we have used the vibrational spectrum previously calculated with density functional theory for short chains of (methoxy-terminated) ethylene glycol monomers, EG (O-CH_2-CH_2-) [104]. For $(EG)_3$ the frequencies of longitudinal vibrations along the backbone for the helical and planar conformers are 82 and 640 cm^{-1}, respectively, with a wavelength of 10.5Å (the contour length between the outermost O atoms). For helical $(EG)_4$ this frequency is 72 cm^{-1}, not quite down by a factor of 3/4 from the $(EG)_3$ value because of the presence of the two end-groups. Likewise, for transverse vibrations we find frequencies in the range from 18 to 30 wavenumbers for both conformers. Attaching several water molecules to $(EG)_3$ in order to mimic the presence of the solvent, we find that the longitudinal frequencies increase by 15 to 20 %.

For $(EG)_3$, we get for the speed of sound, $c_s = \nu\lambda$, about 2,000 m/s and 16,000 m/s for the helical and all-trans conformers, respectively. The reason why the speed, and thus the force constant, is so much larger for the all-trans conformer is the fact that for the helical conformer the vibration involves the deformation of the dihedral angle whereas for the all-trans conformer it is the harder deformation of the C-C and C-O bond angles. Similarly we get for a short alkane chain $c_s \simeq 4,500$ m/s. This leads us to identify the attempt frequency as $\nu = c_s/L_m$. The same first principle calculations for $(EG)_3$ also produced the energy landscape, i.e. potential energy curves,

depicted in Fig. 3.2. It shows explicitly how much the force constants differ between different conformers. In addition we get an estimate of the activation energies, Q in equation (3.5), for conformational conversion, namely up to 0.3 eV, particularly for the solvated polymer. One can also identify a very weak dependence on the length L. Needless to say that these energy landscapes include hydrodynamic effects.

So far we have only considered longitudinal sound waves along the polymer backbone as contributing in the stretching of the molecule. However, relaxation perpendicular to the direction of the force is also of importance and can be measured. This is triggered by transverse sound waves which can be accounted for by writing

$$w_0 = \gamma(\mathbf{c}\cdot\hat{\mathbf{f}})\exp[-\beta Q]/L_{\max} \tag{3.15}$$

where $\mathbf{c} = (c_{\parallel}, c_{\perp}, c_{\perp})$ and $\hat{\mathbf{f}}$ is a unit vector in the direction of the force. For completeness, we have also included an accommodation coefficient γ to account for the probability that not all attempts lead to a length change. It also incorporates hydrodynamic effects; this will be elaborated on in future work.

3.2.2.2 The Helmholtz Regime

The discussion above treats in detail the case of controlling the force on a molecule and changing it as a known function of time. However, AFM experiments are generally done by controlling the position of the cantilever D and measuring its resulting deflection, which gives the force on the molecule as well as its stretching length. Fig. 3.3(a) shows the schematic setup of the situation.

This approach corresponds to doing the equilibrium statistical mechanics in the Helmholtz regime. In order to do this properly, we need to take into account the exact effects of the cantilever. The approach is the same as in the Gibbs regime: we will use a master equation with the length as the stochastic variable. This problem will be solved entirely in one dimension, since the AFM experiments generally pull polymers vertically away from some surface. We will comment on the equivalence of the one and three dimensional cases in the section 3.2.4.

The transition probabilities still have the form $W(L', L) \sim \exp(-\beta\Delta(L'-L)^2/b^2)$,

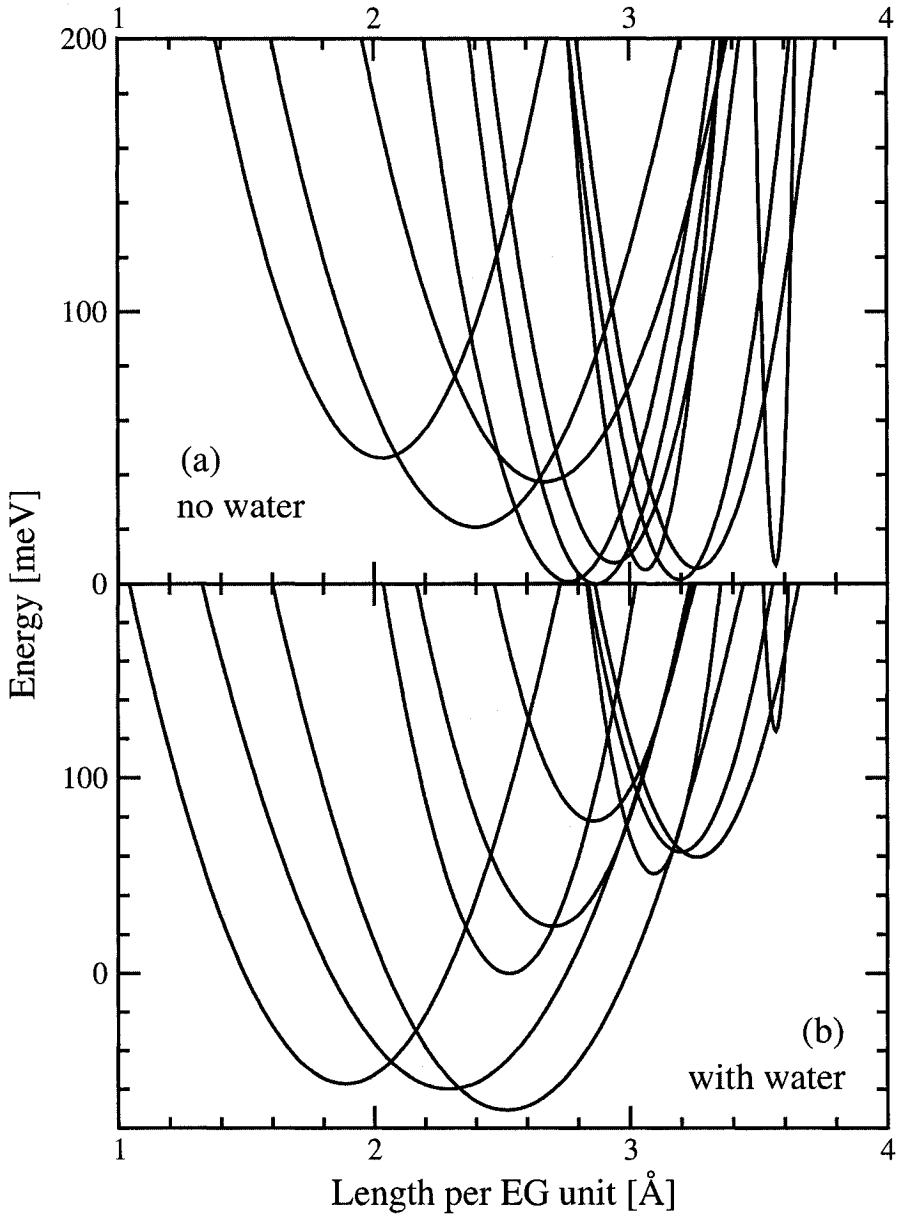

Figure 3.2: The calculated energy landscape for the ten energetically different conformers of $(EG)_3$ in vacuum and in water. These conformers are indexed by the state of the C-C bond, which can be either gauche-plus (g^+) gauche-minus (g^-) or trans (t). From left to right in plot (a) the minima belong to the conformers (g^+g^-t), ($g^+g^+g^-$), (g^+g^-t), (g^+g^+t), ($g^+g^+g^+$), (g^+tg^+), (g^+tg^-), (tg^+t), (ttg^+), and (ttt). When dissolved in water, the order of the minima is the same but for ($g^+g^+g^+$) and (g^+g^+t), which change their relative positions [99,104]. Most minima are within k_BT of each other at room temperature. These curves reproduce PEG stretching both in vacuum and in water [8]

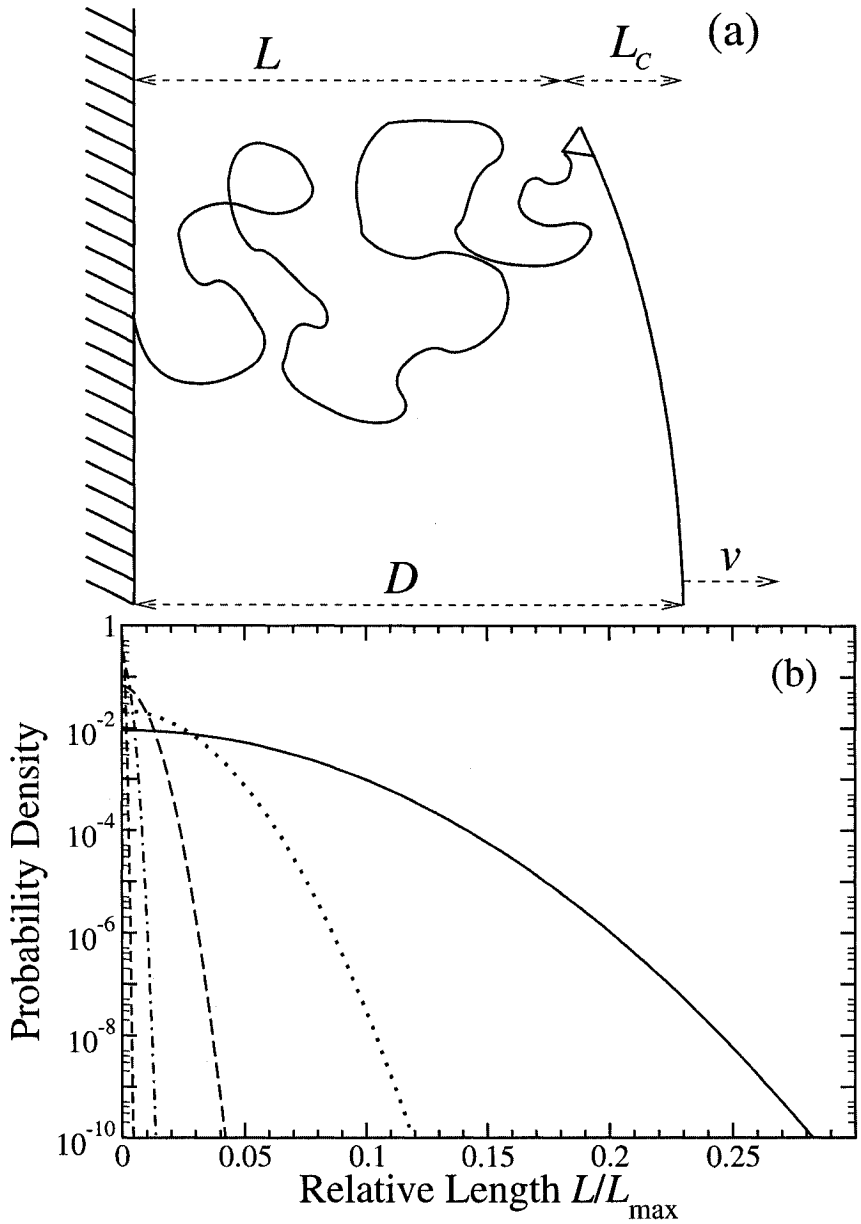

Figure 3.3: (a) The basic setup of an AFM experiment, where the position D of the cantilever is controlled and the actual length of the polymer L as well as the displacement of the cantilever L_C fluctuate. (b) The end-to-end distance distribution of polymer and cantilever for $D = 0$ calculated for a FJC ($N = 150$) and different spring constants. The solid line has no spring attached (for comparison) and the other lines have $k_c a^2/k_B t = 0.1$(dashed), 1(long dashed), 10(dot-dashed), 100(dotted line).

but now the equilibrium distribution for the system depends on both, L and D as [32]

$$P_{\mathrm{eq}}(L,D) = \frac{Z(L)\mathrm{e}^{-\beta k_c (D-L)^2/2}}{\int \mathrm{d}L\; Z(L)\mathrm{e}^{-\beta k_c (D-L)^2/2}}. \tag{3.16}$$

This probability density function for different values of the cantilever spring constant k_c is shown in Fig. 3.3(b). For simplicity, we chose $D = 0$ for those plots. One can see that the effect of a stiff cantilever is to narrow the axial end-to-end distance probability distribution of the polymer. We will discuss this point in detail below.

The introduction of a spring changes the overall transition probabilities considerably. By requiring detailed balance and with $W(L', L)$ symmetric, we find

$$W(L', L; D) = w_0 \exp\left(-\frac{\beta\Delta(L-L')^2}{b^2} + \frac{\beta k_c}{4}\left[(D-L)^2 - (D-L')^2\right]\right)\sqrt{\frac{Z(L')}{Z(L)}}. \tag{3.17}$$

We can use this form to integrate the master equation (3.3) directly. The cantilevers used in the experiments by Gaub *et al.* [42, 72] and other groups have spring constants around $k_c \sim 10^2 - 10^3 k_{\mathrm{B}}T/b^2$. When substituting these into the equilibrium distribution (3.16) or the transition probabilities and hence the master equation, we find that the Gaussian dependences are almost δ-functions. Taking the formal limit $k_c \to \infty$ we have, as in reference [32]

$$P(L,D) \sim \delta(D-L). \tag{3.18}$$

This is to be expected, as stiff cantilevers do not deform significantly over distances comparable to the molecular contour length. The same happens in the master equation where we find for some time-dependent cantilever position $D(t)$

$$\begin{aligned}\frac{1}{w_0}\frac{\mathrm{d}}{\mathrm{d}t}P(L) = &-\exp\left((-\frac{\beta\Delta}{b^2} + \frac{\beta k_c}{4})(D-L)^2\right)\sqrt{\frac{Z(D)}{Z(L)}}P(L) \\ &+\sqrt{\frac{4\pi}{\beta k_c}}\delta(D-L)\int \mathrm{d}L'\; \exp\left((-\frac{\beta\Delta}{b^2} + \frac{\beta k_c}{4})(D-L')^2\right)\sqrt{\frac{Z(D)}{Z(L')}}P(L').\end{aligned} \tag{3.19}$$

For a cantilever with a finite but large spring constant, the only appreciable thermodynamic fluctuations are in the force, with almost no length fluctuations at all. The subsequent lack in spatial spread of the probability distribution makes it rather

difficult to integrate the Master equation numerically. One tends to be constrained to spring constants less or equal to those used experimentally, *i.e.* $k_c \lesssim 10^2 k_B T/b^2$.

We now address the question of equilibrium in a pulling experiment with a stiff cantilever. For finite k_c we must consider the fluctuations in both force and length. Equilibrium is attained if the system can sample all its microstates over the time scale of the experiment. In particular this means that it has time to go through all of its fluctuations. Consider what happens when we pull the molecule so fast that the equilibrium position, after a system's relaxation time, is beyond the reach of the initial fluctuations. The system could not have got there by a quasi-static process and must be out of equilibrium. Next we take into account that in the limit $k_c \to \infty$ the (equilibrium) length fluctuations are very small; in fact they can be described by [32]

$$\frac{\delta L}{\overline{L}} = (D/\overline{L} - 1)\frac{\delta f}{f}. \tag{3.20}$$

We should expect that a necessary (but not sufficient) condition for a quasi-static process is

$$(v\tau)^2 \lesssim \overline{\sigma^2}, \tag{3.21}$$

where τ is the relaxation time of the whole system (molecule and cantilever) and $\overline{\sigma^2}$ is the mean square length fluctuation.

Similar to the Gibbs regime, we can define the moments of the transition probabilities in the Helmholtz regime as

$$\zeta_n(L, D) = \frac{1}{b}\int \mathrm{d}L' \; (L' - L)^n W(L', L; D) \tag{3.22}$$

Notice that we are now dealing with one-dimensional quantities so that there is no longer a tensor character. Analogous to the analysis in the Gibbs regime, we can then write the non-equilibrium force-extension relation as

$$\frac{\mathrm{d}\overline{L}}{\mathrm{d}t} = \langle \zeta_1(L, D) \rangle \,. \tag{3.23}$$

The spatial fluctuations are calculated from

$$\frac{\mathrm{d}\overline{\sigma^2}}{\mathrm{d}t} = \langle \zeta_2(L, D) \rangle + 2(\langle L\zeta_1(L, D) \rangle - \langle L \rangle \langle \zeta_1(L, D) \rangle). \tag{3.24}$$

Once we have obtained the spatial fluctuations of the molecular end, either from the complete time-dependent probability density function or the equation above, we can work out the mean square force fluctuations $\overline{\sigma_f^2}$ via [32]

$$\overline{\sigma_f^2} = k_c^2 \overline{\sigma^2}. \tag{3.25}$$

As we saw above the fluctuations in the length are almost negligible, but those in the force remain finite. In the pure Helmholtz regime the force is, in fact, the only quantity that can fluctuate.

3.2.3 Macroscopic Equations of Motion

To simplify the non-equilibrium force-extension relation we assume that the fluctuations and higher moments of the probability density are small. We can then expand the i^{th} component of the vector $\overrightarrow{\alpha_1}$ as

$$\langle \alpha_{1i}(\mathbf{L},\mathbf{f})\rangle \simeq \alpha_{1i}(\overline{\mathbf{L}},\mathbf{f}) + \frac{1}{2}\sum_{j=1}^{3} \overline{\sigma_{jj}^2}(\mathbf{L},\mathbf{f})\, \frac{\partial^2}{\partial \overline{L_j}^2} \alpha_{1i}(\overline{\mathbf{L}},\mathbf{f}) \Big|_{\mathbf{f}}, \tag{3.26}$$

with

$$\overline{\sigma_{jj}^2} = \overline{L_j^2} - \overline{L_j}^2. \tag{3.27}$$

A similar expansion is possible for the components of $\langle \overleftrightarrow{\alpha_2} \rangle$. The macroscopic equations of motion for the average length (3.10) and the fluctuations (3.12) now read

$$\frac{\mathrm{d}\overline{L_i}}{\mathrm{d}t} = \alpha_{1i} + \frac{1}{2}\sum_{j=1}^{3} \langle \sigma_{jj}^2 \rangle \frac{\partial^2 \alpha_{1i}}{\partial \overline{L_j}^2} \tag{3.28}$$

$$\frac{\mathrm{d}\langle \sigma_{ii}^2 \rangle}{\mathrm{d}t} = \alpha_{2ii} + 2\langle \sigma_{ii}^2 \rangle \frac{\partial \alpha_{1i}}{\partial \overline{L_j}} + \frac{1}{2}\sum_{j=1}^{3} \langle \sigma_{jj}^2 \rangle \left[\frac{\partial^2 \alpha_{2ii}}{\partial \overline{L_j}^2} + 2\overline{L_i} \frac{\partial^2 \alpha_{1i}}{\partial \overline{L_j}^2} \right]. \tag{3.29}$$

All the moments and their derivatives in (3.28) and (3.29) are evaluated at the average non-equilibrium length $\overline{\mathbf{L}}$ and the applied force $\mathbf{f}$.

We note that the first moment of the transition probability $\overrightarrow{\alpha}_1$ is zero along the equilibrium force-extension curve. This can be shown by expanding the integral (3.13) in terms of small $(\mathbf{f} - \mathbf{f}_{\text{eq}})$. The second derivatives of its components also turn out to be zero along the equilibrium force-extension curve, so that the right hand side of (3.28) is identically zero for equilibrium.

Knowing the equilibrium fluctuations at zero extension, one can integrate the system (3.28) and (3.29) directly. However, this approach is only valid close to equilibrium and the computational effort in calculating the moments $\overrightarrow{\alpha_1}$ and $\overleftrightarrow{\alpha_2}$ is similar to that in the direct integration of the full master equation. We will show later that the moments presented here yield a nice graphic interpretation of non-equilibrium stretching nevertheless.

The same analysis can be done for the Helmholtz regime, by expanding the average moments $\langle\zeta_2(L,D)\rangle$ and $\langle\zeta_2(L,D)\rangle$ as defined in equation (3.22). The resulting equations of motion are of course the one dimensional equivalents of (3.28) and (3.29), with all the α_i replaced by ζ_i:

$$\frac{\mathrm{d}\overline{L}}{\mathrm{d}t} = \zeta_1 + \frac{1}{2}\overline{\sigma^2}\frac{\partial^2\zeta_1}{\partial\overline{L}^2} \tag{3.30}$$

$$\frac{\mathrm{d}\overline{\sigma^2}}{\mathrm{d}t} = \zeta_2 + \overline{\sigma^2}\left[\frac{1}{2}\frac{\partial^2\zeta_2}{\partial\overline{L}^2} + 2\frac{\partial\zeta_1}{\partial\overline{L}}\right]. \tag{3.31}$$

3.2.4 Relaxation Times

The relaxation time τ for a system close to equilibrium can be extracted from the Gibbs equation of motion (3.28) by setting $\overline{\mathbf{L}} = \mathbf{L}_{\mathrm{eq}} + \overline{\delta\mathbf{L}}$ and expanding around $\mathbf{L}_{\mathrm{eq}}$ with $\overrightarrow{\alpha_1}(\mathbf{L}_{\mathrm{eq}},\mathbf{f}) = \mathbf{0}$ so that

$$\begin{aligned}\frac{\mathrm{d}\overline{\delta L_i}}{\mathrm{d}t} &= \left.\frac{\partial\alpha_{1i}(\mathbf{L}_{\mathrm{eq}},\mathbf{f})}{\partial\overline{L_i}}\right|_{\mathbf{f}}\overline{\delta L_i} \\ &= -\frac{1}{\tau_i}\overline{\delta L_i}.\end{aligned} \tag{3.32}$$

This defines two relaxation times $\tau_{\parallel}$ and $\tau_{\perp}$ in the directions parallel and perpendicular to the applied force. To evaluate the moments of the transition rates analytically we introduce $\mathbf{r} = \mathbf{L}' - \mathbf{L}$ and write

$$W(\mathbf{r},\mathbf{L};\mathbf{f}) = w_0 \exp\left[-\frac{\beta\Delta}{b^2}\mathbf{r}\cdot\mathbf{r} + \frac{1}{2}\beta\mathbf{f}\cdot\mathbf{r}\right]\sqrt{\frac{Z(N,\mathbf{L}+\mathbf{r},T)}{Z(N,\mathbf{L},T)}}. \tag{3.33}$$

The partition function can be expanded as

$$Z(N,\mathbf{L}+\mathbf{r},T) = Z(N,\mathbf{L},T)\left[1 + \mathbf{r}\cdot\frac{\nabla Z}{Z} + \frac{1}{2}\mathbf{r}\cdot\mathbf{r}\frac{\nabla^2 Z}{Z} + \cdots\right]. \tag{3.34}$$

Statistical mechanics dictates that the various derivatives of the partition function are related to the equilibrium force $\mathbf{f}_{\rm eq} = -k_{\rm B}T\nabla Z/Z$. Using these results, we find to leading order and for a uniaxial force $\mathbf{f} = f\hat{\mathbf{z}}$

$$W(\mathbf{r},\mathbf{L};\mathbf{f}) \simeq w_0 \left[1 - \beta\frac{\mathbf{r}\cdot\mathbf{r}}{4}\frac{\partial f_{\rm eq}}{\partial L}\exp\left[-\frac{\beta\Delta}{b^2}\mathbf{r}\cdot\mathbf{r} + \frac{1}{2}\beta(\mathbf{f}-\mathbf{f}_{\rm eq})\cdot\mathbf{r}\right]\right] \tag{3.35}$$

For long chains $f_{\rm eq}$ only depends on $\ell = L/L_{\rm max}$. Note that $f_{\rm eq}$ is not equal to the external force $\mathbf{f}$.

We can use the expression (3.35) to calculate the molecular relaxation time from the derivative of the first moment of W (see equation (3.32)). To leading order, we get the inverse transverse and longitudinal relaxation times as

$$\frac{1}{\tau_{\|}} = \xi_{\|}\frac{\partial f}{\partial \ell} \tag{3.36}$$

$$\frac{1}{\tau_{\perp}} = \xi_{\perp}\sqrt{\frac{f}{\ell}\frac{\partial f}{\partial \ell}}. \tag{3.37}$$

In our theory, the longitudinal and transverse friction parameters have the explicit form

$$\xi_{\|/\perp} = \frac{\pi^{\frac{3}{2}}}{4}\frac{c_{s\|/\perp}}{L_{\rm max}^2}e^{-\beta Q}\frac{b}{(\beta\Delta)^{\frac{5}{2}}}. \tag{3.38}$$

Notice that we need to differentiate between longitudinal and transverse pulse velocities due to the different nature of the two relaxation modes. Thus our master equation approach has recovered the well known result that the relaxation time is proportional to the square of the number of monomers. We also find rightly that the longitudinal relaxation time is inversely proportional to the derivative of the force-extension relation with the overall factor of proportionality given in terms of the phenomenological parameters in the transition rates. The transverse relaxation depends on the normalized force-extension relation $f(\ell)$ as well as its derivative. Hatfield and Quake [114] postulated a different form for this dependence, but they did not take into account that $f(\ell)$ is non-linear for large extensions. Indeed, the substitution $f(\ell) = k\ell$ into equation (3.37) recovers their result. By keeping further terms in the expansion (3.35) we can easily calculate the corrections needed as one studies relaxation further away from equilibrium.

We still have to discuss the conditions under which we are justified to reduce the master equation to one dimension only. We see from equation (3.35) that the effects

of the transverse spread in the probability functions are mainly contained within the Gaussian dependence of the transition rates. Higher order effects are smaller by at least one additional power of $1/L_{\max}$. Thus for small fluctuations $\langle \sigma_{zz}^2 \rangle \ll L_{\max}^2$, all the important phenomena happen on short length scales and higher order effects can be neglected. The difference between a full three-dimensional model and a one-dimensional equivalent is now a constant factor that stems from the integration of the master equation over the two transverse dimensions. We obtain a "one-dimensional" longitudinal relaxation time

$$\tau_{\|,1\mathrm{D}} \approx \frac{\pi}{\beta\Delta}\tau_{\|,3\mathrm{D}}. \tag{3.39}$$

The two formulations should be equivalent if $\tau_{\|,1\mathrm{D}}$ and $\tau_{\|,3\mathrm{D}}$ are approximately equal.This leads to the fact that Δ is about $\pi k_{\mathrm{B}}T$ or of that order.

3.3 Results

3.3.1 The Relaxation Times

The free parameters in our theory are w_0 and Δ. Although we gave estimates of their magnitude, we can use experimental relaxation times to determine their values for specific systems. These relaxation times have been measured for the case of λ-DNA by Meiners and Quake [27]. We need to use equations (3.36) and (3.37) as well as the knowledge of the partition function (and hence the force-extension relation) in order to extract the phenomenological friction coefficients (3.38) Once we have obtained a values for $\zeta_{\|}$, it is simple to calculate the input value for w_0 as well as the size of the barrier Q. One can also make estimates about the differences between $c_{s,\|}$ and $c_{s,\perp}$ for a given model.

We have fitted the FJC model ($N = 150$), as well as several FRC polymers with 100 monomers, to the data given in reference [27]. Equally good fits were obtained for the freely jointed chain and the freely rotating chain with a bond angle $\gamma = 60°$. These two models will hence be used for the rest of our analysis. Fig. 3.4 shows the fits to the DNA data obtained from the FJC model. The FRC fits are very similar and not shown here.

From our fitting, we obtain the parameters $\xi_{\|}^{-1} = 103$ ms and 61 ms as well as $\xi_{\perp}^{-1} = 522$ ms and 301 ms for the FJC and FRC chains respectively. As we can see

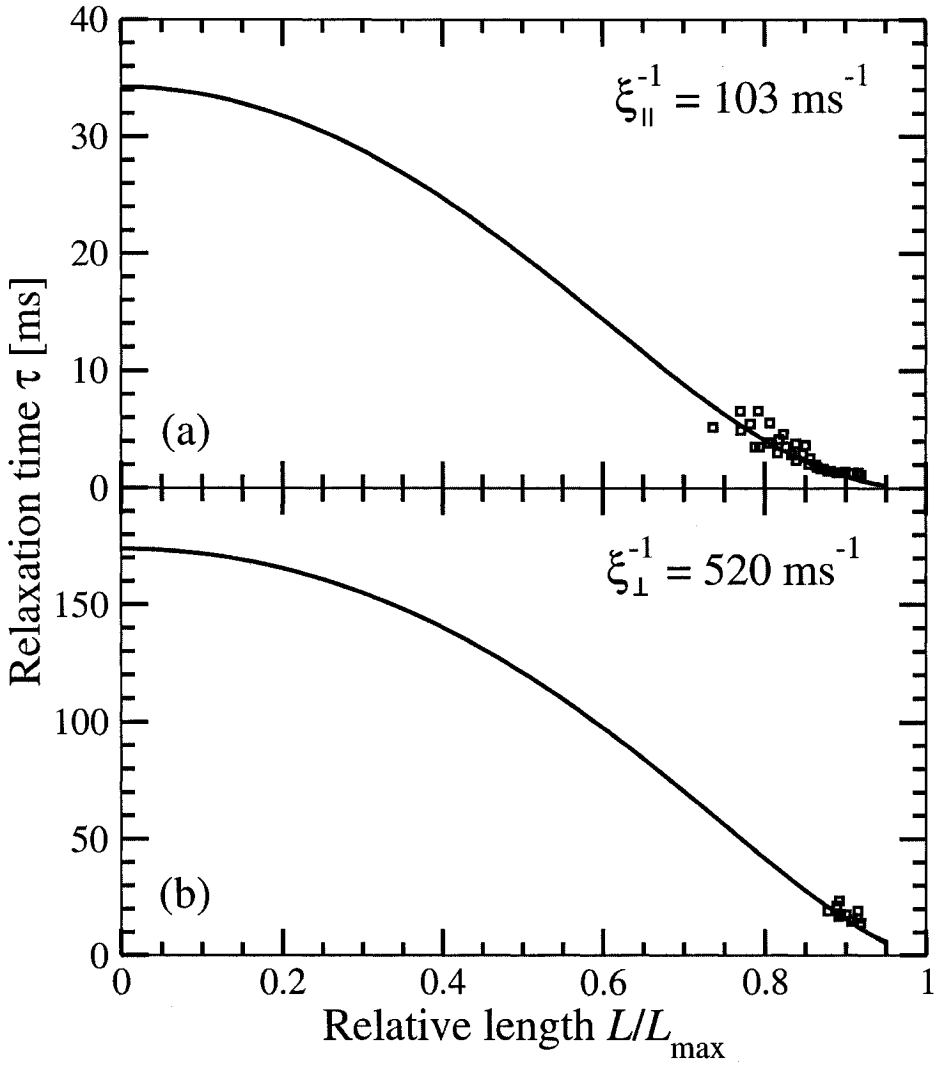

Figure 3.4: The FJC fits to experimental values of the longitudinal and transverse relaxation time of λ-DNA measured by Meiners and Quake [27]. In these fits, we used the Langevin relation to determine the force-extension relation and its derivatives.

from equation (3.38) the only real difference is in the parallel and perpendicular pulse velocities, which leads to the conclusion that they have to differ by a factor of about five. From the fitted data, we can obtain the values of w_0 to be used in the input of our theory. This will then be the basic unit of frequency for a given molecule. Along with the knowledge of the Kuhn length a (which takes the place of the monomer length b) and the thermal energy $k_{\mathrm{B}}T$ we then have a complete specification of the magnitude of all relevant quantities in our calculation. Using $\beta\Delta = \pi$, the contour length $L_{\max} = 16\ \mu$m and a Kuhn length of $a = 52$ nm [114], we find $w_{0,\mathrm{FJC}} = 3.8\times10^4$ s^{-1} and $w_{0,\mathrm{FRC}} = 6.3 \times 10^4$ s^{-1}. We can also use our order of magnitude estimate for the longitudinal pulse velocity from section 3.2.2 to obtain an estimate for the transition barrier, $Q \approx 0.2$ eV.

Notice that these results are only for DNA, where relaxation time data is readily available. However, the knowledge of the relevant parameters in equation (3.38) or some other phenomenological estimate of the ξ will enable the analysis for other polymers as well. In fact, for a rough estimate, one can simply apply the results presented here and scale w_0 using the appropriate contour and Kuhn lengths.

3.3.2 Non-Equilibrium Force-Extension Curves: Gibbs Regime

In its discrete form the master equation (3.3) is a system of coupled first order differential equations. In Fig. 3.5 we show non-equilibrium force-extension curves for the FJC and FRC models, varying the rate r of increase of the force. Starting at zero, we increase the force linearly in time up to $fb/k_{\mathrm{B}}T = 20$ and then decrease back to zero at the same rate. The force loading rate r, given here in units of $w_0 k_{\mathrm{B}}T/b$ is varied exponentially. For small r, we find results very close to the equilibrium force-extension relation for a given model, which can be calculated directly from the partition functions. As we increase r, the internal molecular relaxations are too slow to keep up with the increasing force, which means that the whole non-equilibrium force-extension relation is shifted upward.

When the force is decreased, the molecule remains at larger lengths than the equilibrium value for a given force f. In fact, for very fast force loading rates, the molecular length increases further despite the decreasing force. This results in an

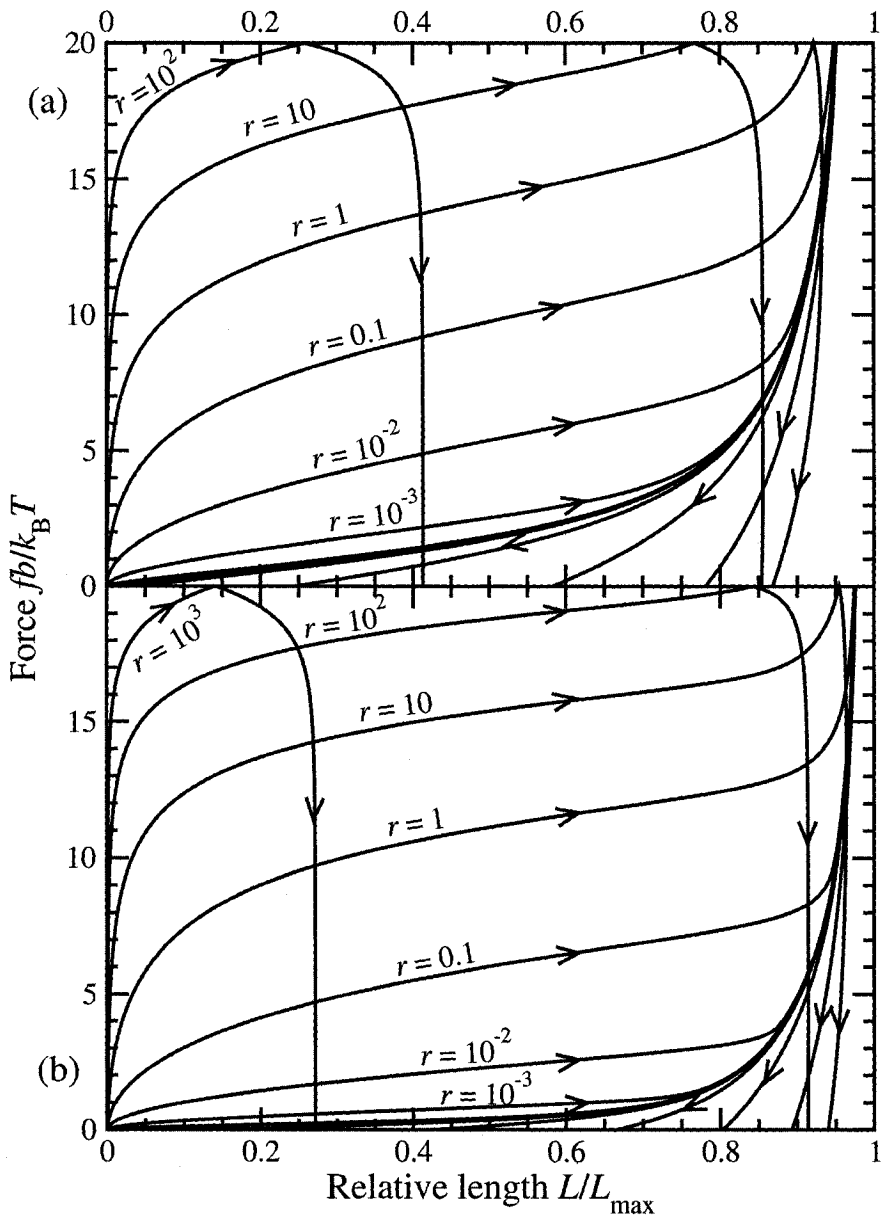

Figure 3.5: The non-equilibrium force-extension relations calculated from the master equation (3.3) (a) for the FJC model with 150 monomers and (b) for the FRC model with 100 monomers and a bond angle of 60°. The rates r are given in dimensionless units (see text) and are used as labels for the curves. Additional (unlabeled) curves that almost coincide with the equilibrium force-extension relations are for $r = 10^{-4}, 10^{-5}$ in plot (a) and for $r = 10^{-4}$ in plot (b). The force-loading rates r are given in units of $w_0 k_B T/b$.

overall hysteresis that is larger for a larger rate of increase of the force and which is the obvious signature of non-equilibrium.

More information is available about the non-equilibrium relaxation curves in Fig. 3.5 when we plot the relative length fluctuations $\overline{\sigma^2}/L_{\max}^2 = (\overline{L^2} - \overline{L}^2)/L_{\max}^2$. These are also available from the solution of the master equation. They also serve as a check for our theory, because the one-dimensional approximation to the three dimensional theory requires $\overline{\sigma^2}/L_{\max}^2$ to be small. Fig. 3.6 shows some representative traces of the fluctuations that correspond to the non-equilibrium force-extension curves.

First of all a note on the relative fluctuations in general is necessary. While the FJC polymer is almost purely Gaussian for small extensions, *i.e.* it can be modeled successfully with a classical random walk, the FRC is much stiffer which leads to larger fluctuations. This difference is observable in both the equilibrium properties as well as the hysteresis. Not surprisingly, the hysteresis in these higher moments of the molecular probability density function is much more pronounced than for the force-extension curves themselves. As indicated above, in order to be in equilibrium the fluctuations have to be the same for increasing as for decreasing forces. Fig. 3.6 shows that this is a much more restrictive criterion. In fact, when we look at the $r = 10^{-4}$ trace of the FRC model, we see that the force-extension relation practically coincides with the equilibrium relation. However, the fluctuations still show rather large deviations from equilibrium. Unfortunately, our numeric method does not allow calculations below this value for r; numerical precision plays a major role when integrating the master equation with $\dot{P}(L) \approx 0$. For that type of calculation, one simply has to use the equilibrium transfer matrix approach by itself.

Next we will discuss the rates r that have been used in these calculations. The time variable used in the solution of the master equation (3.3) is dimensionless and has the form $\tau = w_0 t$. We have also renormalized the force $\tilde{f} = fb/k_{\mathrm{B}}T$ for the purpose of our numerical analysis. We can use the quantities derived in section 3.3.1 to shed some light on the meaning of those transition rates. In terms of the variable

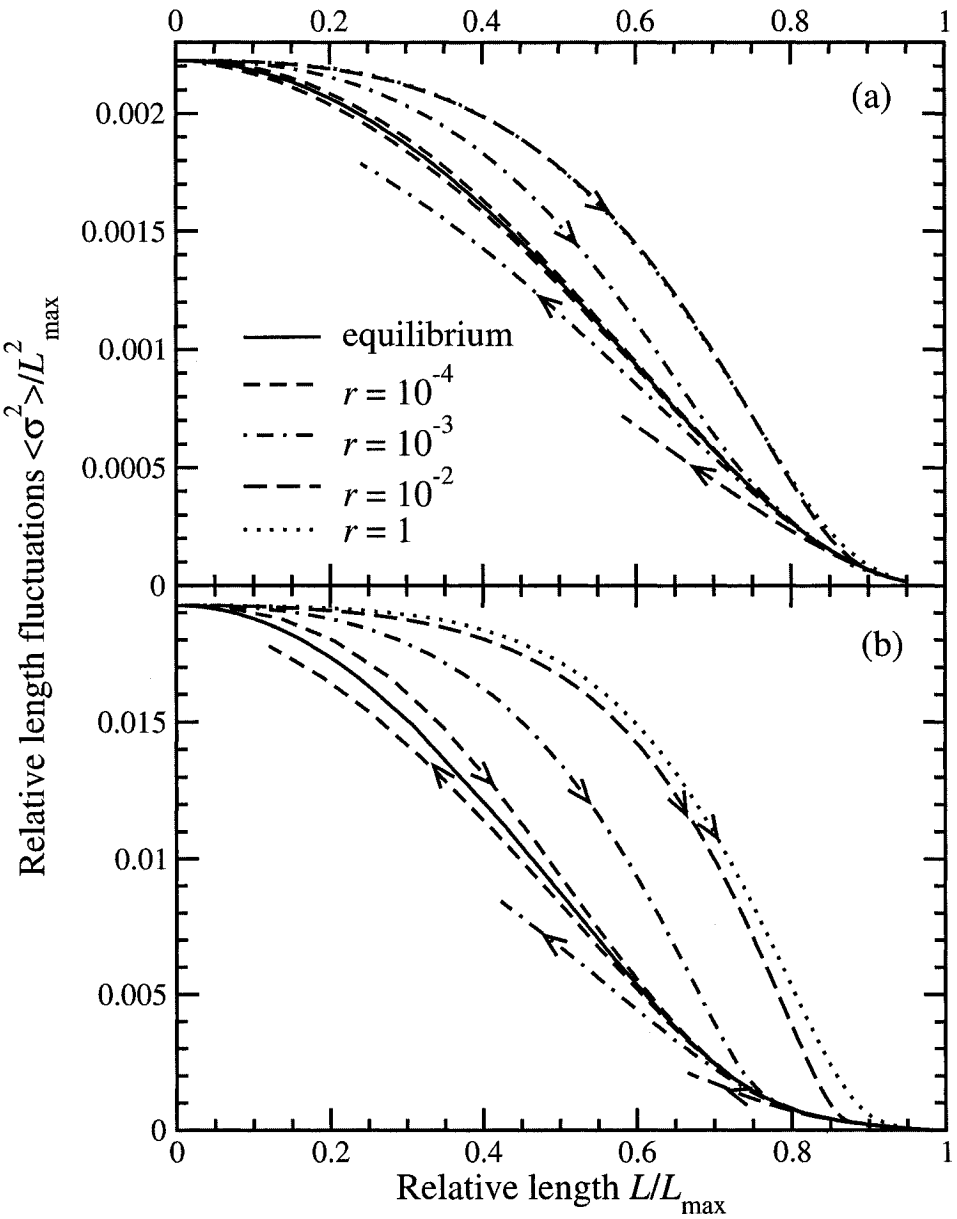

Figure 3.6: The length fluctuations corresponding to the non-equilibrium force-extension curves in Fig. 3.5 for representative traces of both (a) the FJC model and (b) the FRC chains. Note that the $r = 10^{-2}$ and $r = 1$ curves in plot (a) practically overlap.

r shown on the plots in Fig. 3.5, the force loading rates for the two models are

$$\frac{\mathrm{d}f}{\mathrm{d}t} = 3r \text{ nN/s} \quad \text{for the FJC model,} \tag{3.40}$$

$$\frac{\mathrm{d}f}{\mathrm{d}t} = 5r \text{ nN/s} \quad \text{for the FRC model.} \tag{3.41}$$

When comparing the dimensionless force loading rates between Figs. 3.5(a) and 3.5(b), one finds that the model dynamics of the FJC are roughly one order of magnitude faster than those of the FRC. This can be seen in the displacement of a given curve from its equilibrium value. However, the same order of magnitude can be found in the fits to the relaxation time of both models, as shown in equations (3.40) and (3.41). This enables us to work out a consistent picture of DNA stretching and determines when one should be using an explicitly non-equilibrium model to understand experiments. To within an order of magnitude in r, Fig. 3.5 and 3.6 show that non-equilibrium effects become important when $r \gtrsim 10^{-3}$. Using those values and the results from the last paragraph, this corresponds to a force loading rate of about 3-5 pN/s for DNA. We see that both models predict roughly the same magnitude of the non-equilibrium effects for a given force loading rate. This adds to the confidence in our results.

An interesting observation from Fig. 3.5 is that the curves resemble their equilibrium counterparts above a certain critical force, f_c, if one shifts the force axis appropriately. This can be explained quite well on the basis of the growth of fluctuations in the non-equilibrium stretching. As pointed out above, equilibrium conditions require that the AFM cantilever moves slow enough that it samples the molecular fluctuations available to it. When doing experiments and theory in the Gibbs regime, these spatial fluctuations are quite large, because (at least in theory) the cantilever has to respond to all of the molecular motions. As soon as one upsets this fluctuation envelope, one obtains a new kind of dynamic state where the fluctuations about the mean position are skewed. In order to establish this state, one needs to pull fast and at comparatively large forces. However, once this state is established at the end of the molecule, the system is governed by roughly the same entropic properties as in the equilibrium case.

Experimentally, the force and position origins are generally chosen by looking for

the point where the cantilever stops pushing on the surface. The shoulders observed in Fig. 3.5 look quite similar and we question this practice for high force-loading rates. While this effect is not very pronounced in the Helmholtz regime, our current results have a major impact on the interpretation of the low-force regime of the data acquired by Fernandez *et al.* [46]. These experiments were done with polysaccharide, rather than DNA, which means that the absolute force loading rates should be different. However, the soft shoulder that we calculated for the non-equilibrium curves is well visible. The force-loading rates in their experiments are between 1 and 3 nN/s, which is about the onset of the non-equilibrium regime in our theory.

3.3.3 Non-Equilibrium Force-Extension Curves: Helmholtz Regime

Next we have to discuss the Helmholtz regime, where we control the cantilever position rather than the force directly. Our calculations will proceed as follows. Initially, we increase the cantilever position D with a speed v_r (in units of bw_0), starting from zero. Once some specified maximum position is reached, we decrease it again with the same speed back to zero. If we encounter a negative force on the way, the calculation is stopped.

Unfortunately, we cannot calculate the molecular properties when a realistically stiff cantilever is used, because in this case the exponentials in the transition probability (3.17) become unacceptably large. We also attempted the integration of the master equation (3.19) in the $k_c \to \infty$ limit, but that also did not yield any useful results because the probability distribution $P(L)$ was much too sharp for our purposes. To avoid these numerical difficulties one can follow the approach outlined by Kreuzer *et al.* [32,99] and describe the effects of the cantilever entirely with an effective force $\overline{f} = k_c(D - \overline{L})$. The numerical analysis now has to be done in the Gibbs regime. This amounts to a mean-field theory and would allow us to model systems with much higher spring constants than in the exact approach. Our calculations show that fixing the force in such a manner leads to unacceptably large length fluctuations (*c.f.* Fig. 3.3(b)). The comparison between mean-field and exact calculations is not too promising.

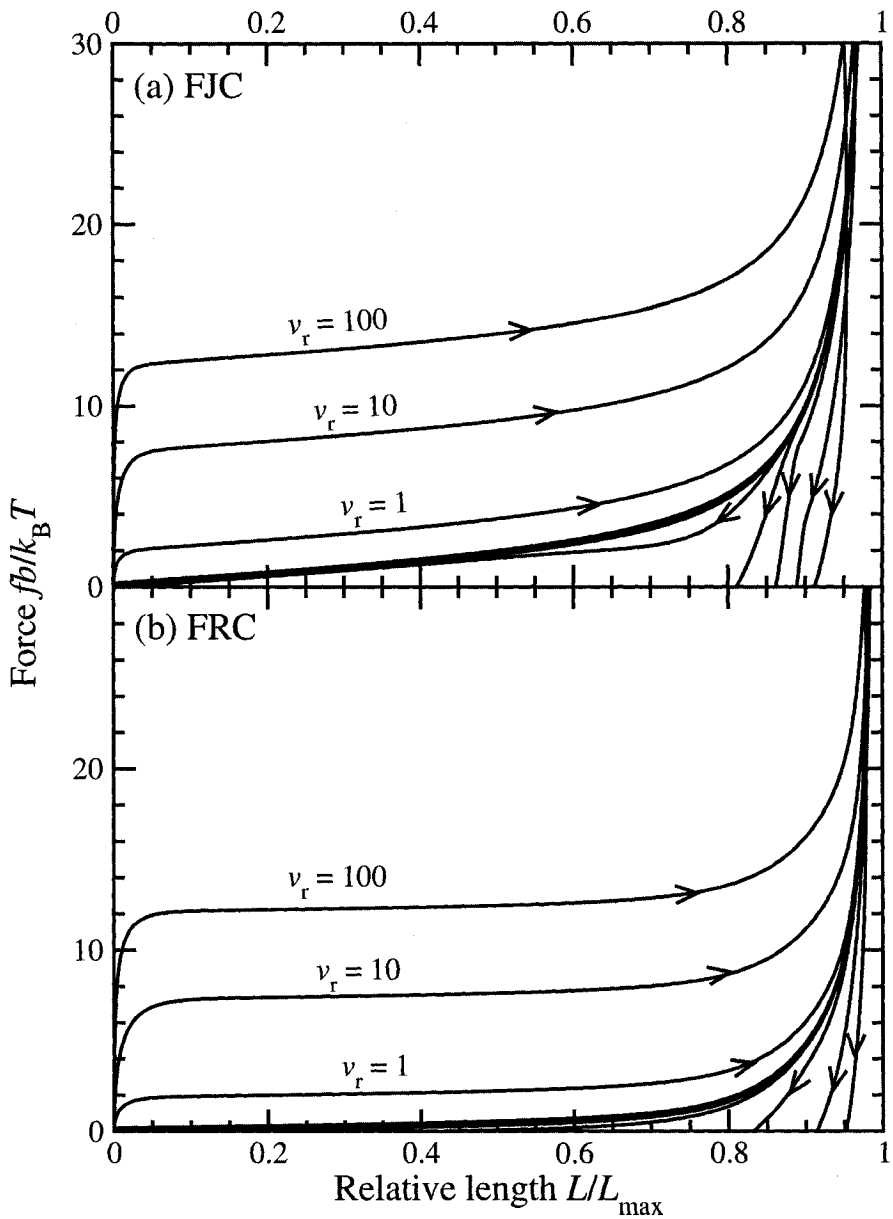

Figure 3.7: The force-extension curves for $k_c = k_B T/a^2$ for the FJC chains in panel (a) and the FRC chains in panel (b). The dimensionless velocities $v_r = v/aw_0$ are used to label the curves.

Fig. 3.7 shows the results obtained from the calculations with small spring constants. The natural units of velocity are given by $w_0 b$; we have these for DNA via our relaxation time fits. For the FJC model with N = 150, we find $w_{0,\mathrm{FJC}} b = 2$ mm/s, while the FRC fits result in $w_{0,\mathrm{FRC}} b = 3.3$ mm/s. This gives fairly consistent results when we compare with the plots in Fig. 3.7: One should expect to see conformational non-equilibrium effects when DNA molecules are pulled at speeds above $v_r = 0.1$ or $v \approx 200 - 300$ μm/s.

The comparison of Fig. 3.7 to experiments is again not quite straight forward, because we need to estimate the time scales for each experiment separately. This is based on the values of b, $L_{\max}$, a number for the transition barrier Q, as well as the backbone pulse velocity c_s.

For the simple polymer poly(ethylene-glycol) (PEG) these are known quite well (see Fig. 3.2), so we will use it as an example. In their original work, Oesterhelt *et al.* [42] used PEG with a contour length of around 400 nm and a Kuhn length of $a = 7$Å. The barrier between a helical and a trans conformer is about $Q = 50$meV and $c_s \approx 4500$m/s [8, 104]. In the framework of our theory, this leads to $w_0 = 1.6 \times 10^6 \mathrm{s}^{-1}$. The onset of the non-equilibrium effects at $v_r = 0.1$ in Fig. 3.7 would then correspond to a pulling velocity of $v \approx 0.1$m/s. This is well within the range of the experimental values. If one were to do experiments in the Gibbs regime, force-loading rates corresponding to $r = 10^{-3}$ are about 10μN/s. Both of these are well above the current limits of AFM spectroscopy, which means that it is a safe assumption to treat PEG molecules as equilibrium systems, as has been done in experiments by Kudera *et al.* [72].

A rather nice demonstration of the difference between the Helmholtz and Gibbs regime is the plot of the force fluctuations (Fig. 3.8) corresponding to the force-extension curves presented above. These are the important fluctuations in the Helmholtz regime. Since our theory has the length as stochastic variable, we have to calculate the force fluctuations from equation (3.25). The qualitative difference to the Gibbs regime fluctuations in Fig. 3.6 is striking. First of all note that there is hardly any hysteresis and that the curves almost completely superimpose. The plateau for the low-extension region is due to the cantilever, which limits the overall fluctuations of

the system. In this regime, the term $\exp(-\beta k_c(D-L)^2/2)$ dominates not only the equilibrium probability density (3.16), but also the transition rates (3.17) and hence the whole master equation. In fact, one can show that the classical fluctuations of a single cantilever that is maintained at some finite extension l_c is always equal to $\langle \sigma_f^2 \rangle = k_c k_B T$ [30]. The high-extension regime of the fluctuations is controlled by the polymer, which provides the limiting factor in the system in this region.

By controlling the force in the calculation for the Gibbs regime, this effect is not present at all. The effects of the polymer on the overall fluctuations of the system only come into play once the molecule is stretched far enough such that its fluctuations become the limiting factor. From the equilibrium trace in Fig. 3.6 we can tell that this becomes the case around $L/L_{\max} \approx 0.8 - 0.9$, which is indeed where the fluctuations in the Gibbs and Helmholtz regimes are the same.

We would also like to point out the slight increase of $\overline{\sigma_f^2}$ at the beginning of some curves. This corresponds to the high velocity (topmost) traces in Fig. 3.7. This effect naturally appears when the molecule is taken far out of equilibrium and it can not reach all its natural equilibrium fluctuations fast enough. The fluctuation envelope lags behind and this leads to a broadening of the instantaneous molecular probability distribution $P(L,t)$.

In order to shed light on the properties of stiffer cantilevers we can solve the master equation for short times only and investigate what happens at short extensions. Fig. 3.9 shows such results for the FJC chains only. These traces have been calculated for a velocity $v = bw_0$, because that way the probability density functions change quickly so that the numerical algorithm does not quite break down for the short times considered here. The conclusion from these calculations is quite obvious. The effect of a stiffer cantilever is a more extreme increase of the force at short length scales. This is very interesting as the cantilevers considered here are still much softer than those used for typical experiments.

To conclude this section, we want to discuss the feasibility of observing non-equilibrium effects. The force loading rates currently achieved in single protein pulling experiments are about 3 nN/s [46], which is well into the non-equilibrium range for DNA, but not necessarily for other systems. Theory suggests that pulling speeds of

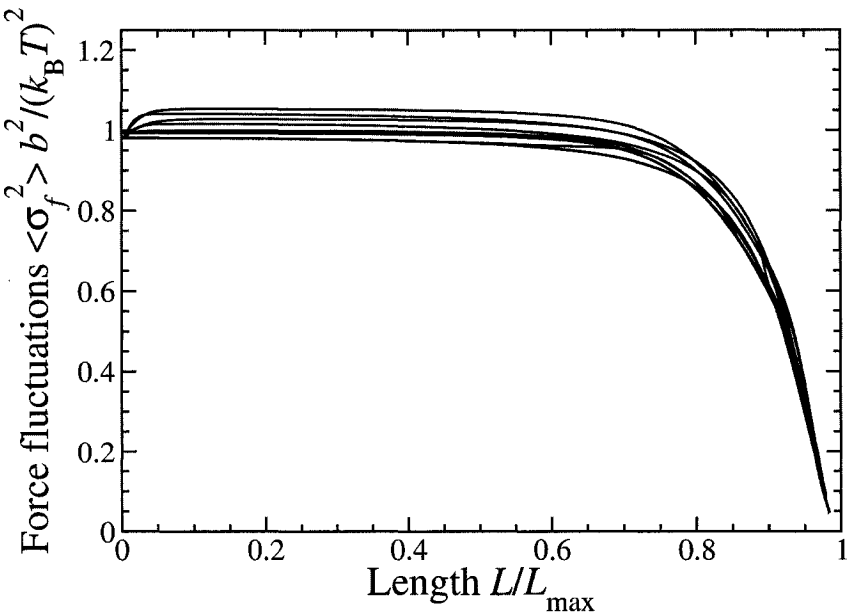

Figure 3.8: The force fluctuations that correspond to all of the force-extension curves in the Helmholtz regime given in Fig. 3.7. There is hardly any hysteresis in these curves, because they are almost completely dominated by the properties of the cantilever, which has a spring constant of $k_c = k_B T/b^2$.

the order of 10 mm/s should be possible. This figure is based on a cantilever resonance frequency of tens of kHz and a z range of a few microns. Anything faster would be prevented by the cantilever resonance.

3.3.4 The Moments of the Transition Probabilities

In this section, we will discuss the moments of the transition probabilities as they occur in the macroscopic equations of motion, Eqns. (3.28) to (3.31), for the one-dimensional version of our model. In Figs. 3.10 and 3.11 we show the first and second moments, as a function of relative extension, for our FJC and FRC models.

From equations (3.28) and (3.30) we see that the first moment in each regime essentially corresponds to a velocity. In fact, this velocity term is the greatest influence in the region near equilibrium where α_2 and ζ_2 are constant. The contours of the canonical moments of the transition probabilities correspond almost exactly to the non equilibrium force-extension curves presented above, since the velocity is the controlling parameter in the corresponding calculations. In this case, the fluctuations

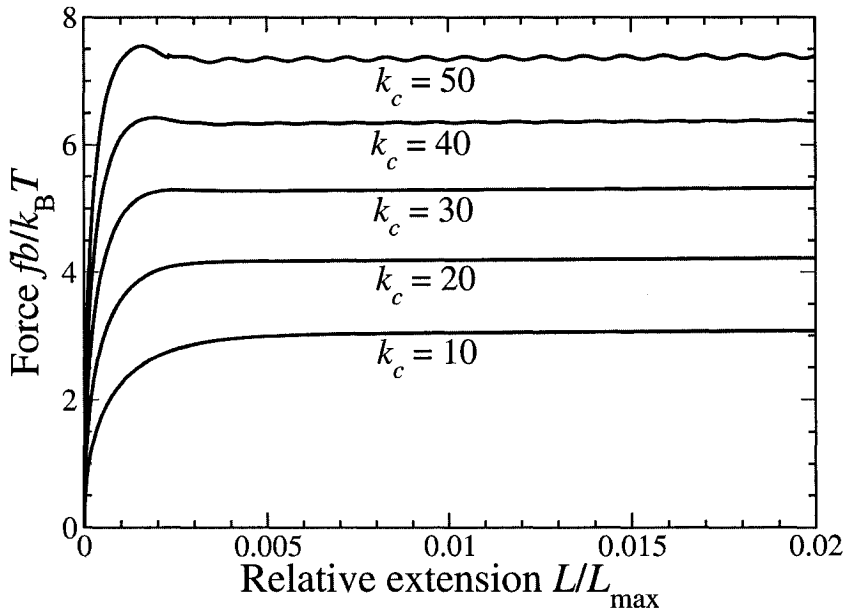

Figure 3.9: The initial stages of constant velocity FJC ($N = 150$) force-extension traces for stiffer cantilevers. The pulling velocity in all cases was $v_r = 1$. The spring constants k_c are in the natural units of k_BT/b^2. For comparison, cantilevers that are typically used in experiments start at around $k_c \approx 100k_BT/b^2$ at room temperature.

and corrections from the gradients of ζ_2 only have a small effect. This becomes especially clear when we remember that the magnitude of the fluctuations is controlled by the cantilever (see last section).

Notice that the ζ's contain the key to the rapid force increase in some of the plots in Fig. 3.9. The key is in the approximate relation $v \approx \zeta_1$. If we regard a pulling experiment as moving through the $f(\ell)$ plane in Fig. 3.10, the molecule has to reach a given ζ_1 contour as fast as possible. The fastest way to do so from the origin is to move vertically upward, that is at constant $L = 0$. Once the curve has been reached, it can be traced throughout the rest of the experiment and we see exactly what has been shown in the previous section.

The situation changes for the Gibbs regime. There is no longer a one-to-one correspondence between the force-extension curves and the contours in Fig. 3.11, although equations (3.28) and (3.29) can still be solved if we know $\alpha_1(L, f)$ and $\alpha_2(L, f)$. In the Gibbs regime we control the applied force with some force-loading rate r. At each point in time, some cantilever velocity v_c is required to maintain the

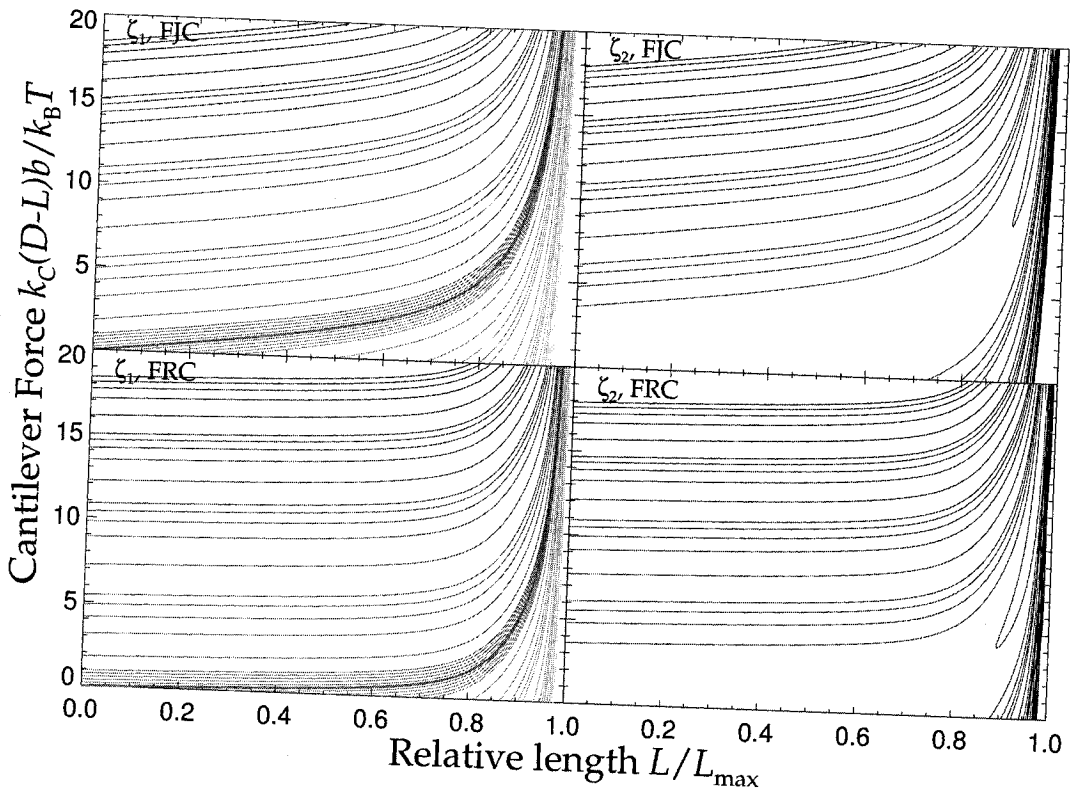

Figure 3.10: Contour plots for the moments ζ_1 and ζ_2. The contours vary from values of -1000 to 1000 in levels of $\pm n \times 10^m$, where $n = \{1, 2, 4, 6, 8\}$ and $m = \{-2, -1, 0, 1, 2\}$. The heaviest line corresponds to $\xi = 1000$, while the lightest ones are for the negative ζ_1. The $\zeta = 0$ contour is a little wider.

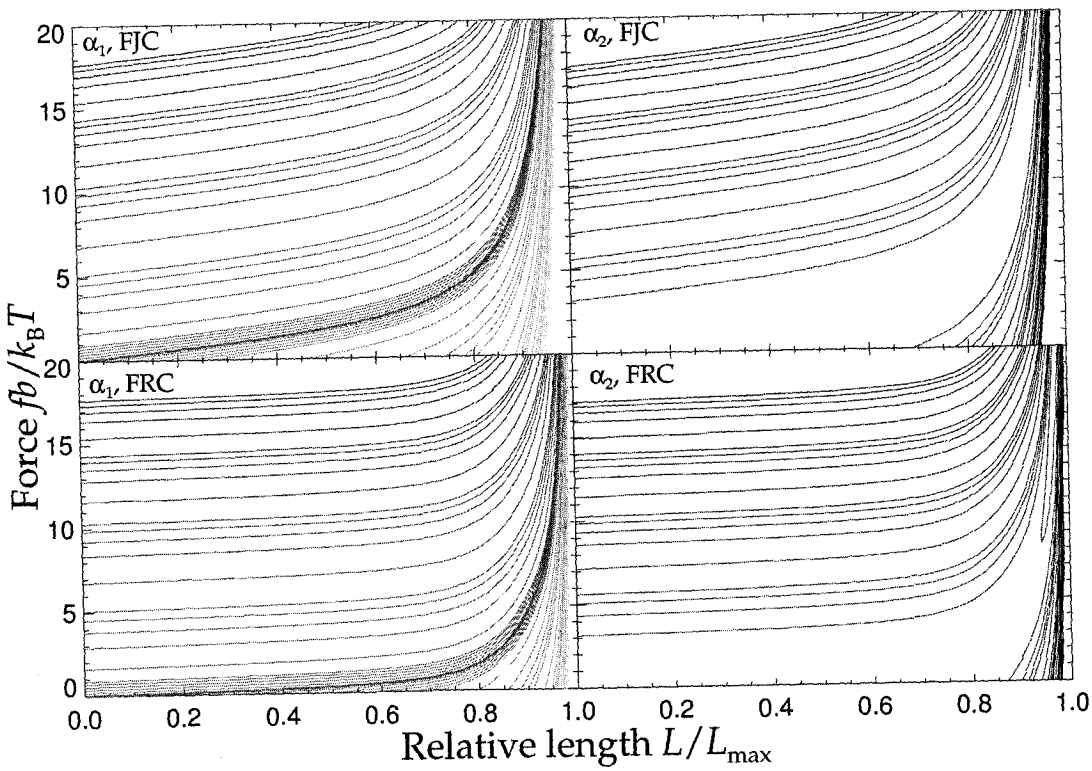

Figure 3.11: Contour plots for the first two moments of the transition probabilities α_1 and α_2 in the Gibbs regime. The contours are plotted using the same scheme as in Fig. 3.10.

required force profile. This velocity v_c roughly corresponds to the instantaneous value of α_1, while again the fluctuations and α_2 only play a minor role in this approximation.

One can now solve the approximate equations (3.28) to (3.31) directly. This approach works for small extensions and very close to equilibrium. However, as one moves further away from equilibrium, the higher moments $\alpha_{i>2}$ and $\zeta_{j>2}$ become more important. In this light, it is much simpler to solve the master equation directly, although the results presented in this section provide a good intuitive understanding of the situation.

3.4 Discussion

In this work we have developed a theory of non-equilibrium polymer stretching in the entropic regime. We use a master equation approach with the length as our stochastic variable. We derived the transition probabilities in both the Gibbs and Helmholtz regimes and showed how they can be obtained from relaxation time measurements. We then calculated force extension curves in and out of equilibrium for two model polymers, a FJC molecule with 150 monomers and an FRC molecule with 100 monomers.

Our calculations show that one should expect non-equilibrium effects to appear when pulling at velocities of the order $0.1bw_0$ or greater. Alternatively, force loading rates of about $10^{-3}w_0k_BT/b$ will generate similar effects. For comparison with actual systems, the Kuhn length a effectively replaces the monomer length b. We also need the transition frequency w_0, which can be estimated from equation (3.15), $w_0 \approx c_{||}\exp(-\beta Q)/L_{\max}$. We have shown in section 3.3 that w_0 can vary over several orders of magnitude, from $10^4 s^{-1}$ for λ-DNA to $10^6 s^{-1}$ for PEG.

We find that the entropic dynamics of shorter polymer chains are much too fast for current AFM experiments to register non-equilibrium effects. However, this changes with long proteins that have contour lengths of the order of many microns. In those cases, equilibrium theories can no longer be applied with force loading rates and pulling velocities of about 5pN/s and 30μm/s respectively. The difference in the two cases is already manifest in the empirical dependence of the relaxation time on the monomer number, $\tau \sim N^2$. One should in fact expect that the longer molecule has

much slower dynamics.

A final point has to be made on the fluctuations, particularly in the analysis of the Gibbs regime. Our whole theory is based on the fact that a cantilever can follow the molecular fluctuations on a similar time scale. This should practically cancel the effect of the cantilever itself. As shown by Kreuzer *et al.* [32], one can achieve these conditions much more easily with a very soft cantilever. Still, the question remains whether or not it is possible in practice to follow these fluctuations one by one. Once again, the relevant quantity here is the frequency w_0. One should only be able to follow the fluctuations if the cantilever position can be monitored with a frequency $w_0 \sim 10^4 - 10^5$ s^{-1} for λ-DNA. If this can be achieved, one should be able to do measurements on polymers in the Gibbs regime in order to verify some of the results presented here. Again, it might be easier to do this at low temperature. Notice that the force fluctuations that correspond to the stiff cantilever actually have been observed for some systems, see for example Ref. [126], and have been shown to yield additional interesting information about the elastic properties of polymers [10]. Current work in progress is the microscopic derivation of the transition probabilities including solvent effects. We are also looking at the derivation of the Fokker-Planck equation.

3.5 Appendix: Theory from the Conformers

In this appendix we briefly outline the approach to non-equilibrium phenomena in the stretching of a polymer starting from the level of probability functions for the conformers themselves. Let $P_i(T, \mathbf{L}, \mathbf{f}, t)$ give the probability that under a force $\mathbf{f}$ the i$^{\text{th}}$ conformer (of end-to-end length $\mathbf{L}$) is realized at time t. Conformers are local minima in the electronic energy surface of the polymer molecule in a space spanned by 3^{nN} coordinates of its atoms where N is the number of monomers and n is the number of atoms per monomer. This energy surface can be mapped for short polymers (invoking a number of criteria) using first principles calculations based, for instance, on density functional theory as recently demonstrated for poly(ethylene glycol). The result is a set of energy curves, $E_i(\mathbf{L})$, for the i$^{\text{th}}$ conformer stretched to a length $\mathbf{L}$ around its minimum at $\mathbf{L_i}$ and also all the vibrational and rotational frequencies.

Likewise, transition states can be identified that lead from one conformer to another.

In equilibrium the conformer probability function is given by

$$P_i^{eq}(T, \mathbf{L}, \mathbf{f}) = \frac{\exp[-\beta E_i(\mathbf{L})] \exp[\beta \mathbf{f} \cdot \mathbf{L}]}{\exp[-\beta g(T, \mathbf{f})]} \tag{3.42}$$

To study non-equilibrium effects we again assume that the stretching the molecule can be described by a homogeneous Markov process satisfying a master equation

$$\frac{\mathrm{d}}{\mathrm{d}t} P_i(T, \mathbf{L}, \mathbf{f}; t) = \sum_{j, \mathbf{L}'} \left[W\left(i, \mathbf{L}; j, \mathbf{L}'; \mathbf{f}\right) P_j(T, \mathbf{L}', \mathbf{f}; t) - W\left(j, \mathbf{L}'; i, \mathbf{L}; \mathbf{f}\right) P_i(T, \mathbf{L}, \mathbf{f}; t) \right]. \tag{3.43}$$

One acceptable form of the transition probabilities is given by transition state theory

$$W\left(j, \mathbf{L}'; i, \mathbf{L}; \mathbf{f}\right) = \frac{z_{ji}^{\#}(\mathbf{L}', \mathbf{L})}{z_i(\mathbf{L})} \exp[-\beta(E_{ji}(\mathbf{L}', \mathbf{L}) - E_i(\mathbf{L}) + \frac{1}{2}\beta \mathbf{f} \cdot (\mathbf{L}' - \mathbf{L})], \tag{3.44}$$

where $z_i(\mathbf{L})$ and $z_{ji}^{\#}(\mathbf{L}', \mathbf{L})$ are the partition functions accounting for the internal vibrations and rotations of the polymer around the minimum of the i-th conformer and at the transition state of energy E_{ij} to the j^{th} conformer. Some of these numbers have been calculated for short chains, for instance n-alkanes and oligo-ethylene.

It should be obvious that all this information needed to specify the transition probabilities (3.44) can at best be obtained for short chains [99, 112] as done very successfully in recent years in the study of proteins [117–119].

To make the connection with the approach presented in this paper we must invoke simplifying assumptions. In particular, if the conformational conversion for a given length and conformer is fast on the time scale of stretching we can write

$$P_i(\mathbf{L}, \mathbf{f}; t) = \exp[-\beta E_i(\mathbf{L})] P(\mathbf{L}, \mathbf{f}; t) \tag{3.45}$$

and the master equation simplifies to

$$\frac{\mathrm{d}}{\mathrm{d}t} P(\mathbf{L}, \mathbf{f}; t) = \sum_{\mathbf{L}'} \left[W\left(\mathbf{L}; \mathbf{L}'; \mathbf{f}\right) P(\mathbf{L}', \mathbf{f}; t) - W\left(\mathbf{L}'; \mathbf{L}; \mathbf{f}\right) P(\mathbf{L}, \mathbf{f}; t) \right], \tag{3.46}$$

where

$$W(\mathbf{L}, \mathbf{L}'; \mathbf{f}) = \frac{\sum_{i,j} W\left(i, \mathbf{L}; j, \mathbf{L}', \mathbf{f}\right) \exp[-\beta E_j(\mathbf{L}')]}{\sum_i \exp[-\beta E_i(\mathbf{L})]} \tag{3.47}$$

is the transition probability specified phenomenologically at the beginning of this work.

Chapter 4

Non-equilibrium Dynamics of Single Polymer Molecules: Relaxation Close To and Far From Equilibrium

This chapter has been published in the International Journal of Quantum Chemistry (vol. **116**, 2953-2959, 2006) as an article with the same title. The authors are Felix Hanke and Hans-Jürgen Kreuzer, Felix Hanke's contribution to this work is the idea for the approach, all numerical and analytic calculations and about 85% of the manuscript preparation. Permission to use this work has been granted by the International Journal of Quantum Chemistry, a copy of the permission letter is attached to this thesis.

Abstract

A master equation approach is used to study the relaxation of single polymer molecules. For relaxation close to equilibrium a Fokker-Planck equation is derived via a Kramers-Moyal expansion. Far from equilibrium two scenarios are studied: (1) an initial force that stretched the molecule to a certain length is suddenly released and the time evolution to the final force-free equilibrium is followed. (2) A force of a certain magnitude is suddenly applied to a molecule and the time evolution to the final equilibrium stretching at that force is followed. Initial transients, dominated by many time scales, are followed by a roughly exponential decay. Final approach to equilibrium is again exponential but on a time scale many orders of magnitude slower.

4.1 Introduction

A microscopic understanding of the mechanical properties of individual natural or synthetic polymer strands is required to model and predict their function in biological or technical processes, *e.g.* DNA replication, muscle contraction, or the rheological properties of polymers. Experimentally, single molecule force spectroscopy with the Atomic Force Microscope or with optical tweezers offers a versatile and powerful

experimental tool to measure the extension of a single molecule as a function of applied force in different environments. The method allows to observe the binding forces between different receptor-ligand systems [107,108] and the unfolding of protein domains [19, 23], or to measure the elastic properties of individual macromolecules [20, 42]. Likewise, the scanning force microscope, optical tweezers and near-field magnetic tweezers have been used to measure the elastic response of chromosomes [109], to study formation of DNA loops by an enzyme [110], and to investigate DNA-binding molecular motors (RNA polymerase, DNA polymerase, etc.) [111], to reveal the dynamics of these molecules during translocation, as well as the effect of external force loads on their performance.

The ultimate aim of polymer science must be the explanation of the macroscopic properties of a long repetitive chain molecule in terms of the structural properties of its subunits. To proceed from the microscopic details of the quantum chemistry of these subunits to a comprehensive description of the long chain a series of well-defined approximations must be invoked that at any stage can be subjected to rigorous scrutiny. Such a program of simplifications has been in place in polymer science for many years [4], but only recently has it become practical to implement this procedure from first principles [50, 99, 112].

Macroscopic properties of immediate interest are the force-extension curve and the corresponding fluctuations of force and length of the polymer molecule. To ensure that a measurement of the force-extension relation of a polymer molecule yields the equilibrium equation of state the rate of change of the external force must be slow on the time scale of the internal relaxation of the polymer chain, which is readily checked by a sufficient variation of this rate. If the rate of increase of the external force is such that equilibrium cannot be maintained internally, non-equilibrium effects are accessed which can be used to study the kinetics and, ultimately, the dynamics of the polymer chain. As long as one stays close to equilibrium relaxation effects can be studied. These same dynamics will then also manifest themselves far from equilibrium in the form of hysteresis and nonlinearities.

Going beyond simple approaches to the dynamics of polymer chains such as the Rouse and Zimm models [1, 5], a mesoscopic theory has recently been developed

which treats conformational changes in the polymer as a Markov process. Taking the end-to-end length as the stochastic variable, one sets up a master equation for which a phenomenological form of the transition probabilities is assumed that reproduces experimental equilibrium relaxation times. Because the transition rates in the master equation must satisfy detailed balance they will contain information about the equilibrium properties of the chain. For the calculation of the latter we will use the Rotationally Isomeric State (RIS) model; in the previous paper two simple models, namely the Freely Jointed Chain (FJC) and the Freely Rotating Chain (FRC) models, were used and the generalisation to more detailed polymer models is straightforward, albeit numerically more involved. The RIS model allows for the chain segments to assume only a discrete set of torsional angles (three in most cases for the trans, gauche(+) and gauche(-) conformers), while bond lengths and angles are fixed. In addition one introduces nearest neighbour interactions of which we only keep the pentane interaction for a gauche defect.

We use a Green function method [6, 7, 11] to obtain the equilibrium properties of these models in the Gibbs ensemble. This method is based on the Chapman-Kolmogoroff equation for a monomer's Green function $\mathcal{G}(i, \Gamma)$

$$\mathcal{G}(i+1;\Gamma) = \int d\Gamma' \; \mathcal{T}(\Gamma, \Gamma')\mathcal{G}(i, \Gamma') \tag{4.1}$$

which relates monomer $i+1$ to monomer i via a transfer operator $\mathcal{T}$ in configuration space $\{\Gamma\}$. The integration of the final Green function over all states gives the partition function $Z(L, T, N)$. In Figure 4.1 we show, for future reference, the partition function for an alkane chain with 300 monomers.

The paper is organised as follows: in the next section we summarise the pertinent features of the master equation approach specifying the specific form of the transition rates in the master equation and derive the macroscopic equations of motion that couple the time dependence of the average length of the polymer to the non-equilibrium evolution of the fluctuations. We then describe how to calculate the relaxation times close to equilibrium and give a derivation of the Fokker-Planck equation starting from the Kramers-Moyal expansion. Section 4 presents results for relaxation far from equilibrium treating the cases of sudden release of a stretched molecule and of sudden stretching from the force-free situation. We conclude with an outlook to future work.

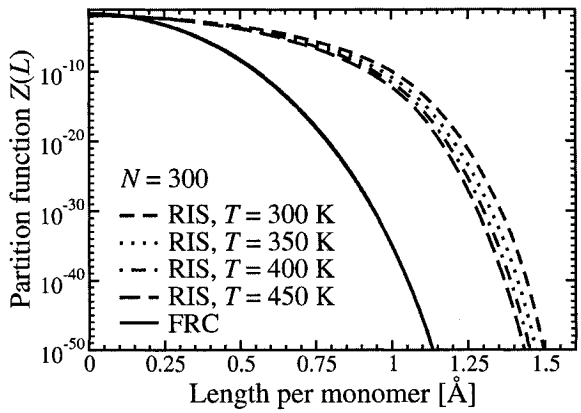

Figure 4.1: The partition functions for RIS chains with 300 monomers and different temperatures as a function of length as calculated from the Transfer Matrix method.

4.2 Master Equation

To set the stage for the study of fast relaxation phenomena in single polymer molecules we summarise the pertinent features of the mesoscopic approach of our previous paper. In a coarse-grained approach one takes the end-to-end length of the polymer as the stochastic variable and treats the stretching behaviour of single polymer molecules as a Markov process that is represented with a master equation. One introduces a function $P(\mathbf{L}, \mathbf{f}, t)$ that gives the probability that at time t the end-to-end length $\mathbf{L}$ is realised under a force $\mathbf{f}$. Its value in equilibrium is given by

$$P_{\text{eq}}(\mathbf{L}, \mathbf{f}) = \frac{Z(N, \mathbf{L}, T) \exp(\beta \mathbf{f} \cdot \mathbf{L})}{\exp[-\beta g(T, \mathbf{f})]}. \tag{4.2}$$

$g(T, \mathbf{f})$ is the free energy in the Gibbs ensemble. Away from equilibrium we postulate a master equation

$$\frac{\mathrm{d}}{\mathrm{d}t} P(\mathbf{L}, \mathbf{f}, t) = \frac{1}{b^3} \int \mathrm{d}^3 L' \left[W(\mathbf{L}, \mathbf{L}'; \mathbf{f}) P(\mathbf{L}', \mathbf{f}, t) - W(\mathbf{L}', \mathbf{L}; \mathbf{f}) P(\mathbf{L}, \mathbf{f}, t) \right]. \tag{4.3}$$

The transition element $W(\mathbf{L}', \mathbf{L}; \mathbf{f})$ gives the probability per unit time that the length of the polymer changes from $\mathbf{L}$ to $\mathbf{L}'$ under a force $\mathbf{f}$. The length of a single monomer is b. These transition rates can in principle be calculated from the microscopic dynamics of the coupled polymer-solute system. However, in the recent paper a phenomenological approach was pursued in which their form is postulated based on

simple ideas, to be

$$W(\mathbf{L}',\mathbf{L};\mathbf{f}) = w_0 \exp\left[\frac{\beta}{2}\mathbf{f}\cdot(\mathbf{L}'-\mathbf{L}) - \frac{\beta\Delta}{b^2}(\mathbf{L}'-\mathbf{L})^2\right]\sqrt{\frac{Z(L',N,T)}{Z(L,N,T)}}. \tag{4.4}$$

This can also be written as

$$W(\mathbf{L}',\mathbf{L};\mathbf{f}) = w_0 \exp\left[\frac{\beta}{2}\mathbf{f}\cdot(\mathbf{L}'-\mathbf{L}) - \frac{\beta\Delta}{b^2}(\mathbf{L}'-\mathbf{L})^2 + \frac{\beta}{2}\int_L^{L'}\mathbf{f}(\mathbf{L}'')\cdot\mathrm{d}\mathbf{L}''\right]. \tag{4.5}$$

The main requirement for the transition probabilities is that they satisfy detailed balance. The parameter Δ controls the width of effective transitions. The dynamical trigger of the length changes, contained in w_0, are transverse and longitudinal sound waves that travel along the backbone of the polymer chain; one finds that

$$w_0 = \gamma(\mathbf{c}\cdot\hat{\mathbf{f}})\exp[-\beta Q]/L_{\max} \tag{4.6}$$

where $\mathbf{c} = (c_{\shortparallel}, c_\perp, c_\perp)$ contains longitudinal and transverse sound velocities and $\hat{\mathbf{f}}$ is a unit vector in the direction of the force, and γ is an accommodation coefficient to account for the probability that not all attempts lead to a length change and also incorporates hydrodynamic effects. The energetic barrier between two different conformers is denoted by Q. The Gaussian dependence of the transition probability on $|\mathbf{L}'-\mathbf{L}|$ makes sure that the end of the molecule cannot jump over long distances.

The non-equilibrium force-extension relation is given by

$$\overline{\mathbf{L}}(\mathbf{f},t) = \frac{1}{b^3}\int \mathrm{d}^3L\ \mathbf{L}P(\mathbf{L},\mathbf{f},t) \tag{4.7}$$

and its equation of motion is obtained from (4.3)

$$\frac{\mathrm{d}\overline{\mathbf{L}}}{\mathrm{d}t} = \langle\alpha_1(\mathbf{L})\rangle. \tag{4.8}$$

We define the mean-square fluctuations of the molecular end-to-end distance as a second rank tensor

$$\left\langle\overleftrightarrow{\sigma^2}\right\rangle = \langle\mathbf{L}\mathbf{L}\rangle - \langle\mathbf{L}\rangle\langle\mathbf{L}\rangle. \tag{4.9}$$

In a coordinate system where the force points along the z-axis, this tensor is diagonal. In this case, the equation of motion for an element is

$$\frac{\mathrm{d}\langle\sigma_{ii}^2\rangle}{\mathrm{d}t} = \langle\alpha_{2ii}\rangle + 2\langle L_i\alpha_{1i}\rangle - 2\langle L_i\rangle\langle\alpha_{1i}\rangle. \tag{4.10}$$

For equations (4.8) and (4.10) we have defined the n^{th} moment of the transition probabilities,

$$\overleftrightarrow{\alpha}_n(\mathbf{L},\mathbf{f}) = \frac{1}{b^3}\int \mathrm{d}^3L'\ (\mathbf{L}'-\mathbf{L})^n W(\mathbf{L}',\mathbf{L};\mathbf{f}) \tag{4.11}$$

as a tensor of rank n.

If one only considers the polymer distribution along the force axis, the problem reduces to one dimension and the transition probabilities have the form

$$W(L',L;f) = w_0 \exp\left[\beta\frac{f}{2}(L'-L) - \frac{\beta\Delta}{b^2}(L'-L)^2\right]\sqrt{\frac{Z(N,L',T)}{Z(N,L,T)}} \tag{4.12}$$

This corresponds to the approximation that the additional two integrations in equation (4.3) have roughly the same effect for all times. We have shown that this approximation corresponds to the limit of small length fluctuations $\sigma_{zz}^2 \ll L_{\max}^2$.

4.3 Relaxation Close to Equilibrium

We first use the master equation approach to study relaxation close to equilibrium. In our previous paper we extracted longitudinal and transverse relaxation times from the equation of motion (4.8) by setting $\overline{\mathbf{L}} = \mathbf{L}_{\text{eq}} + \overline{\delta\mathbf{L}}$ and expanding around $\mathbf{L}_{\text{eq}}$ with $\overrightarrow{\alpha_1}(\mathbf{L}_{\text{eq}},\mathbf{f}) = \mathbf{0}$ so that

$$\frac{\mathrm{d}\overline{\delta L_i}}{\mathrm{d}t} = \left.\frac{\partial\alpha_{1i}(\mathbf{L}_{\text{eq}},\mathbf{f})}{\partial\overline{L_i}}\right|_{\mathbf{f}} \overline{\delta L_i} \tag{4.13}$$

$$= -\frac{1}{\tau_i}\overline{\delta L_i}. \tag{4.14}$$

This defines two relaxation times $\tau_{\|}$ and $\tau_{\perp}$ in the directions parallel and perpendicular to the applied force. To evaluate the moments of the transition rates analytically we introduce $r = L' - L$ and rewrite expression (4.12) as

$$W(r,L;f) = w_0 \exp\left[-\frac{\beta\Delta}{b^2}r^2 + \frac{\beta}{2}\left(fr - \int_0^r f_{eq}(r'+L)\mathrm{d}r'\right)\right]. \tag{4.15}$$

It is now fairly straight forward to approximate $\alpha_1(L;f)$ via the method of steepest descent. Inserted into equation (4.14), this yields the inverse transverse and longitudinal relaxation times as

$$\frac{1}{\tau_{\|}} = \xi_{\|}\frac{\partial f}{\partial\ell} \tag{4.16}$$

$$\frac{1}{\tau_{\perp}} = \xi_{\perp}\sqrt{\frac{f}{\ell}\frac{\partial f}{\partial\ell}}. \tag{4.17}$$

In our theory, the longitudinal and transverse friction parameters have the explicit form

$$\xi_{\parallel/\perp} = \frac{\pi^{\frac{3}{2}}}{4} \frac{c_{s\parallel/\perp}}{L_{\max}^2} e^{-\beta Q} \frac{b}{(\beta\Delta)^{\frac{5}{2}}}. \tag{4.18}$$

Notice that we need to differentiate between longitudinal and transverse pulse velocities due to the different nature of the two relaxation modes.

Next we consider the derivation of the Fokker-Planck equation. To this end we employ the Kramer's Moyal expansion, truncated to second order,

$$\dot{P}(L,t) = \sum_{n=1}^{\infty} \frac{(-1)^n}{n!} \frac{\mathrm{d}^n}{\mathrm{d}L^n} [P(L)\alpha_n(L,f)] \approx -\frac{\mathrm{d}}{\mathrm{d}L}[P(L)\alpha_1(L,f)] + \frac{1}{2}\frac{\mathrm{d}^2}{\mathrm{d}L^2}[P(L)\alpha_2(L,f)] \tag{4.19}$$

Using the expansion (4.19) one finds straightforwardly

$$\frac{\partial P}{\partial t} = \frac{\sqrt{\pi}}{4} \frac{w_0 b^2}{(\beta\Delta)^{3/2}} \frac{\partial^2 P}{\partial L^2} + \frac{\sqrt{\pi}}{4} \frac{w_0 b}{(\beta\Delta)^{3/2}} (f - f_{\mathrm{eq}}) \frac{\partial P}{\partial L} \tag{4.20}$$

Note that this Fokker-Planck equation describes correctly the relaxation close to equilibrium and also gives the correct equilibrium distribution.

4.4 Relaxation far from Equilibrium

In this section we look at two situations, one in which the external force that has stretched the polymer to a given length is suddenly released and the other situation where the force is suddenly applied to a polymer; sudden means fast on the timescale of the internal relaxation of the molecule. For both situations we solve the master equation starting from initial conditions of equilibrium in which the molecule is stretched under a given force (which may be zero) with the transition probabilities calculated at a different, final force to which the molecule is relaxing. If initial and final forces are substantially different then all eigenvalues, or time scales, of the transition matrix will contribute in the time evolution. The aim of this study is to identify initial transients, possible regimes dominated by a single time scale leading to intermittent exponential behaviour, and approach to the final equilibrium. All the calculations have been done using the RIS model with 300 monomers. In order to estimate the attempt frequency, we used a transition barrier of 0.1 eV and a velocity

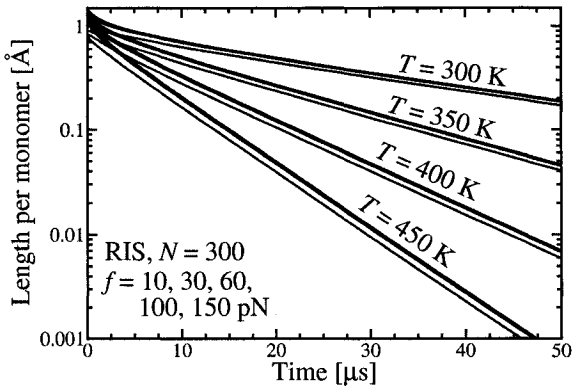

Figure 4.2: The RIS relaxation data ($N = 300$) for several different temperatures is shown on a logarithmic scale. Each set of curves contains curves for the forces $f = 10, 30, 60, 100$,and 150 pN (bottom to top within each set for a given temperature).

of sound of about 4500 m/s. The bond length $b = 1.54$Å was chosen appropriately for alkanes as were bond angles and conformer energies. See reference [9] for details.

As a first case we looked at the situation where initial and final forces were close so that relaxation is near equilibrium. What we find, not surprisingly, is that the numerical solution of the master equation is dominated by a single time scale, i.e. an exponential approach to the final equilibrium, with a relaxation time that agrees numerically with our simple analytical results (4.16) obtained by an expansion of the transition probabilities.

4.4.1 Sudden Release

We first discuss the situation of a sudden release of the molecule from a given force f, see in figure 4.2. The initial time evolution shows over exponential transients where many relaxation modes contribute. This is followed by a long, almost pure exponential decay. A fit to this regime yields the non-equilibrium relaxation time for the molecule. Note however, that this does not correspond to the equilibrium relaxation mode. This is most obviously demonstrated when we look at the length fluctuations. As indicated in previous work [32, 33, 106], the fluctuations are extremely important when one wants to understand stretching processes completely. In the situation of sudden release, the molecule retains its narrower length distribution throughout the release process, which means that the fluctuations are controlled by the previous

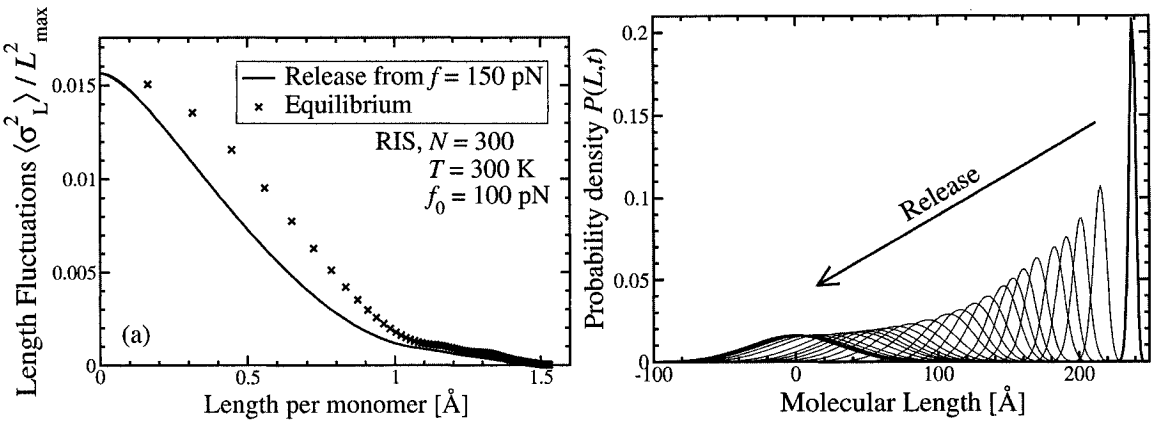

Figure 4.3: (a) The fluctuations of a sudden release of the $N = 300$ RIS model from 100 pN at 300 K compared to the corresponding equilibrium fluctuations. (b) Selected snapshots of the time-dependent probability density function $P(L,t)$ during the release shown in panel (a).

history of the release process. This is demonstrated in figure 4.3 (a), which shows that the non-equilibrium fluctuations are always less than those in equilibrium. We also show some intermediate probability distributions in figure 4.3(b) from which one can see that the probability distribution of the molecule retains a roughly Gaussian shape. Deviations from this form are important but only start to occur in the wings of the distribution several orders of magnitude below its maximum. To understand this remarkable feature a calculation of the eigenvalue spectrum of the transition matrix is needed from which the density of states can be extracted and also the distribution of weights of the individual exponential terms.

This can be done quite easily by rewriting equation (4.3) as

$$\dot{\mathbf{P}}(t) = \overleftrightarrow{W} \cdot \mathbf{P}(t). \tag{4.21}$$

Here $\mathbf{P}$ contains the probability density function for the whole molecule, while the operator $\overleftrightarrow{W}$ is obtained from the original transition probabilities as

$$\overleftrightarrow{W}(L', L) = W(L', L) - \delta(L' - L)\frac{1}{b}\int \mathrm{d}L'' W(L'', L) \tag{4.22}$$

We now have the Master Equation as a simple first-order differential equation, which is solved by diagonalisation for a given value of a force. The relaxation time for a given eigenmode corresponds to the inverse eigenvalue of the operator (4.22). From

the left and right eigenvectors of $\overleftrightarrow{W}$ one can subsequently obtain the weights of the individual exponential terms in the time evolution.

Final approach to equilibrium is again exponential but on a time scale that is many orders of magnitude slower in agreement with relaxation close to equilibrium. Note that the initial force has virtually no influence on the relaxation behaviour.

4.4.2 Sudden Stretching

Next is the situation where the molecule is initial unstretched, *i.e.* where no force is present, and the force is suddenly raised to values from 10 to 150 pN. Figure 4.4(a) shows the result for three different forces, each at four different temperatures. In each case, the molecule relaxes to some equilibrium length L_{eq}, starting from zero extension. Not quite unexpectedly, the higher forces reach their equilibrium much faster. The same goes for higher temperatures. In order to gain some insight into the non-equilibrium relaxation times involved in this process, we replot the data in the form

$$t = \tau \ln\left(1 - \frac{L(t)}{L_{\mathrm{eq}}}\right). \tag{4.23}$$

The slope of such a plot corresponds to the relaxation time τ at a given extension $L(t)$. Some of these results are shown in figure 4.4(b) for a force $f = 10$ pN. One can clearly see when the molecule approaches equilibrium (corresponding to $\tau = 0$), at times longer than 35 μs depending on the temperature.

Once again we see that there is no single relaxation time, but a superposition of quite a number of relaxation modes. The striking feature of all the data is however, that there is one dominant relaxation mode that does *not* correspond to the equilibrium relaxation time τ_{eq}. We hope to gain more insight into this feature by calculating the relaxation modes directly from our Master Equation.

4.5 Outlook

In this paper we have used a master equation approach to study the relaxation of a polymer molecule far from equilibrium for two situations, namely when a force is suddenly reduced to zero or increased from zero. Not surprisingly, the complete

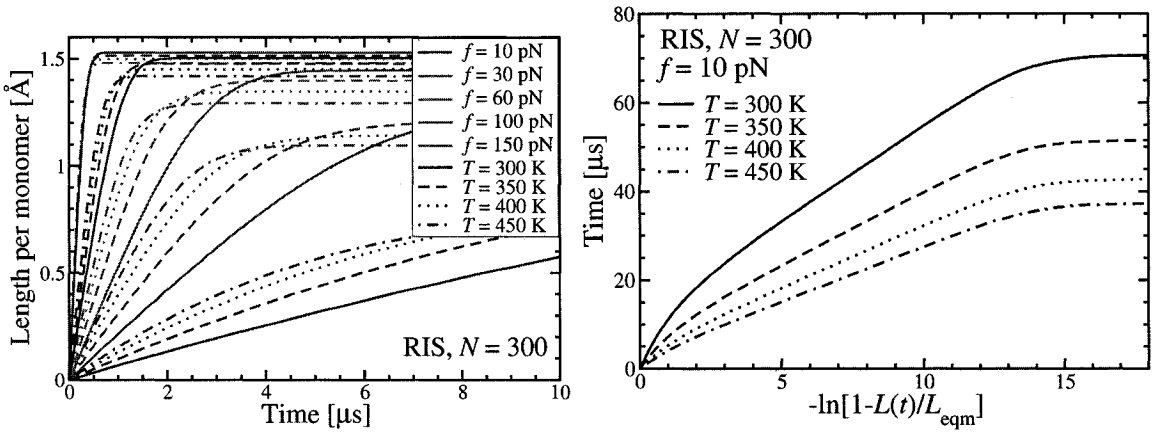

Figure 4.4: (a) The relaxation data for a RIS model with an instantly applied force f. There are three sets of data for $f = \{10\text{pN}, 60\text{pN}, 150\text{pN}\}$, each for the temperatures indicated in the legend. (b) The data for $f = 10\text{pN}$ has been replotted to facilitate the extraction of the relaxation times.

eigenvalue spectrum of the matrix of transition probabilities contributes, in particular in the initial regime of transients but there is also a long intermediate regime dominated by a single time scale. To go further we intend to calculate the eigenvalue spectrum of the transition matrix and extract the density of states. Together with the distribution of weights of the individual exponential terms this will hopefully lead the way to find simple approximation schemes.

Chapter 5

Breaking Bonds in the Atomic Force Microscope: Extracting Information

This chapter has been published in Biointerphases (vol. **1**, pages 11-17 , 2006) as an article with the same title. The authors are Felix Hanke and Hans-Jürgen Kreuzer. Felix Hanke's contribution to this work consists of all calculations, the details of the Gibbs and Helmholtz approaches as well as 75% of the manuscript preparation. Permission to use this work has been granted by the editor of Biointerphases, a copy of the permission letter is attached to this thesis.

Abstract

A theoretical framework is developed to analyze molecular bond breaking in dynamic force spectroscopy using Atomic Force Microscopy (AFM). An analytic expression of the observed bond breaking probability as a function of force is obtained in terms of the relevant physical parameters. Three different experimental realizations are discussed, in which (*i*) the force is increased linearly in time, and (*ii*) the AFM cantilever is moved at constant speed, and (*iii*) the force is held constant. We find that unique fitting of the bond parameters such as the potential depth and its width is possible only when data from rather different force-loading rates is used. The complications in the analysis of using the constant velocity mode arising from the intermediate polymer spacer are discussed at length.

5.1 Introduction

The molecular interactions between small molecular aggregates can be manipulated in nanoarchitectures to construct a molecular switch with bond forming and bond breaking providing the on/off states of a switch, respectively. For a molecular bond with a binding energy E extending over a distance d the force needed is of the order of E/d. Thus controlled bond breaking can be achieved at temperatures $T \ll E/k_B$

provided the applied force is controlled to better than k_BT/d. For a covalent bond we have $E \sim$ eV and $d \sim$ Å so that the force is of the order of nN and must be controlled at the level of pN.

Bond breaking implies the separation of the two molecular fragments along their reaction coordinate. For a diatomic molecule AB the reaction coordinate is the $A - B$ distance and the energy surface is the intra molecular potential as a function of that distance. For a molecular switch such as the bis-terpyridine moiety TP-Ru-TP separating into TP-Ru and TP fragments [72] their separation involves rotations relative to each other and changes in their internal structures so that the reaction coordinate is to be understood as the minimum energy pathway in a multidimensional coordinate space in which the center of mass separation with local adjustments in relative orientation is the dominant one. Excitations in the rotational and internal vibrational degrees of freedom extend the reaction coordinate into a multidimensional valley in the free energy surface. The latter can and has been calculated for many systems by first principles methods of quantum mechanics. For a simple molecular bond the free energy curve along the reaction coordinate has just one minimum of depth E and width d [81]. For more complex bonds that may entail several unfolding steps before breakage further minima at larger separations appear [23].

Experimentally controlled bond breakage has been achieved with laser tweezers and with the atomic force microscope (AFM). A typical experiment using single-molecule force microscopy is the recent study of the TP-Ru-TP system [72] in which the TP moieties were first linked to a poly(ethylene glycol) spacer which in turn was attached to the AFM cantilever. Similarly the spacer of a mono-complexed TP-Ru^{3+} was attached to a suitably prepared surface. In the course of the AFM experiment, the non-complexed moieties on the tip were brought in contact with the mono-complexed units on the surface resulting in the formation of a bonded bis-terpyridine moiety, TP-Ru^{2+}-TP, in which the Ru atom is reduced. Withdrawing the tip first stretched the spacers and eventually lead to the breaking of one of the Ru-TP bonds. In a typical experiment the cantilever speed was around 120 nm/s which lead to average bond breaking forces of the order of 100pN and a statistical width of the force distribution of the order of 50 pN. At this pulling speed, the cantilever forces the system away

from equilibrium so that the distribution of bond-breaking forces depends strongly on the velocity used.

Several studies have been published that model dynamic force spectroscopy as described in the last paragraph. An initial molecular dynamics study of bond breaking in proteins [90] suggested that it might be possible to model the reaction paths exactly for extremely fast loading rates or pulling speeds. The most widely cited approach to model this type of experiment was put forward by Evans and Ritchie [86], who used a simplified form of the bond potential in order to calculate the loading-rate dependent breaking probability. Various authors have since extended this model taking into account rebinding [82], multiple strands [96], specific force profiles [91], and to describe experiments with a constant force loading rate [88,127]. A lot of data has been analyzed recently with the help of Monte Carlo simulations [89].

A problem that has not received enough attention concerns the uniqueness of modeling any data for the purpose of extracting underlying microscopic parameters. This will be done in this paper by setting up an analytic theory, based on previous work [127], that can explain breaking force distributions and can be used to extract the relevant physical parameters, such as activation energies, attempt frequencies and bond lengths, from experimental data. We will delineate a set of criteria to ensure uniqueness of such a procedure. Concentrating on bond breaking with the AFM we examine the different experimental modes including the constant velocity [72], the constant force-loading rate, or force ramp [46], set ups, and the force-clamp mode [23].

5.2 Theory

We treat bond breaking by an external force as a thermally activated process for which we write down an Arrhenius rate equation for the probability, $P(t)$, that the molecule is still intact at time t [127]

$$\frac{\mathrm{d}P}{\mathrm{d}t} = -A \exp[-\beta \Delta V(f)] P. \tag{5.1}$$

Here $\Delta V(f)$ is the activation energy or energy difference between the free energy minimum of the bond and the barrier to be overcome in bond breaking under the influence of an applied force, see Fig. 5.1. The prefactor A contains information

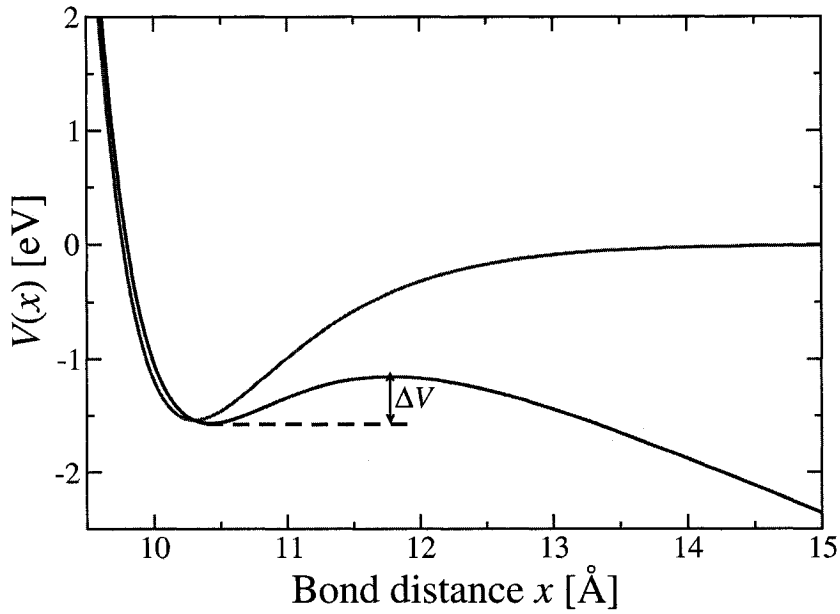

Figure 5.1: The bond potential under an external force (solid line) is the linear combination of the unperturbed Morse potential (curved dashed line) and an external force $V_{\text{force}} = -f(x - x_0)$ (straight dashed line). The resulting force-dependent barrier is shown as ΔV.

about the changes in entropy due to the breakup of the molecule and also about the internal energy re-distribution into the bond that eventually breaks. According to transition state theory it is given by $A = \kappa\nu q^*/q$ where ν is the attempt frequency, κ the accommodation coefficient and q^*/q the ratio of the internal partition functions of the activation complex to that of the molecule in the initial state. In the simplest scenario ν can be interpreted as the attempt frequency to break the bond *i.e.* roughly that of the oscillations around the minimum of the bond potential, which in vacuo is given by

$$\nu = \frac{1}{2\pi}\sqrt{\frac{2V_0\gamma^2}{\mu}}, \tag{5.2}$$

where μ is the reduced mass of the two fragments and V_0 the maximum depth of the potential. The frequency ν is typically around 10^{12}s^{-1} but it is drastically reduced in a liquid mostly due to solvation effects. In addition, the accommodation coefficient is typically much smaller than unity for a reaction in a liquid and the ratio of the partition functions is significantly smaller than unity so that one expects $A \ll \nu$.

What is usually measured in an experiment is not the probability of the bond still being intact at time t but the probability that the bond is broken at time t, $P_b(t) = 1 - P(t)$.

In the force ramp mode, the force f is increased linearly in time with a force loading rate α

$$f = f_0 + \alpha t. \tag{5.3}$$

Eliminating t in favor of f we rewrite the Arrhenius rate equation (5.1) as

$$\frac{\mathrm{d}P}{\mathrm{d}f} = -\frac{A}{\alpha}\exp[-\beta\Delta V(f)]P, \tag{5.4}$$

which can be solved analytically to give

$$P(f) = \exp\left[-\frac{A}{\alpha}\int_{f_0}^{f}\exp[-\beta\Delta V(f')]\mathrm{d}f'\right] \tag{5.5}$$

or

$$P(t) = \exp\left[-A\int_{0}^{t}\exp[-\beta\Delta V(f_0+\alpha t')]\mathrm{d}t'\right]. \tag{5.6}$$

We obtain the distribution of bond breaking forces by taking the derivative of $P_b(f) = 1 - P(f)$. Its maximum gives the most probable bond breaking force, and is obtained by equating the second derivative of (5.5) to zero, which yields

$$\left.\frac{\mathrm{d}\beta\Delta V}{\mathrm{d}f}\right|_{f_b} = -\frac{A}{\alpha}\exp[-\beta\Delta V(f_b)] \tag{5.7}$$

Likewise, we calculate the width of the breaking force distribution by setting the third derivative equal to zero.

To go further analytically we need to specify the bond potential $V(x)$ to obtain $\Delta V(f)$. For a simple bond the Morse potential is known to capture its essential features including the all important dissociative state at large separation (which a harmonic potential obviously does not). In the presence of an external potential it reads

$$V(x) = V_0\{\exp[-2\gamma(x-x_0)] - 2\exp[-\gamma(x-x_0)]\} - f(x-x_0) \tag{5.8}$$

Here γ^{-1} is the range of the potential, $-V_0$ its depth and x_0 the position of its minimum. From the force-dependent local minimum and maximum of the potential

(5.8) we can calculate the dissociation barrier

$$\begin{aligned}\Delta V(f) &= V_{\max} - V_{\min} \\ &= -f(x_+ - x_-) + V_0 \{\exp[-2\gamma(x_+ - x_0)] - \exp[-2\gamma(x_- - x_0)] \\ &\quad -2\exp[-\gamma(x_+ - x_0)] + 2\exp[-\gamma(x_- - x_0)]\} \end{aligned} \tag{5.9}$$

The exponential argument is given by

$$\gamma(x_\pm - x_0) = \ln 2 - \ln\left[1 \mp \sqrt{1 - \frac{2f}{\gamma V_0}}\right] \tag{5.10}$$

Note that the barrier is not dependent on x_0. $f_{\max} = \gamma V_0/2$ is the maximum force at which the barrier goes to zero, which however can only be reached by applying the force adiabatically at zero temperature. Explicitly we get for the barrier

$$\Delta V/V_0 = \sqrt{1-\widetilde{f}} - \widetilde{f}\tanh^{-1}\sqrt{1-\widetilde{f}}, \tag{5.11}$$

where $\widetilde{f} = f/f_{\max}$. One can show that this function can be approximated to within a few percent over its complete range $0 < \widetilde{f} < 1$ by

$$\Delta V \simeq V_0(1-\widetilde{f})^2. \tag{5.12}$$

It turns out that the approximation (5.12) is remarkably good for a variety of possible bond potentials, as long as one chooses V_0 to be the depth of the unperturbed potential and defines the dimensionless force in terms of the maximally possible force for a given potential. For example in the case of a Lennard-Jones potential

$$V(x) = 4\varepsilon\left[\left(\frac{\sigma}{x-x_0}\right)^{12} - \left(\frac{\sigma}{x-x_0}\right)^{6}\right] \tag{5.13}$$

we would have $V_0 = \varepsilon$ and $f_{\max} = (7/26)^{7/6}(144\varepsilon/13\sigma)$. A cut-off harmonic potential as it is used in the Ritchie-Evans model satisfies equation (5.12) exactly, as we show in Appendix 5.8.

The form (5.12) allows us to do the integral in our force distribution (5.5) explicitly to find

$$P(\widetilde{f}) \simeq \exp\left[-\frac{A}{2\alpha}\sqrt{\frac{\pi}{\beta V_0}} f_{\max}\left\{\operatorname{erf}(\sqrt{\beta V_0}) - \operatorname{erf}[\sqrt{\beta V_0}(1-\widetilde{f})]\right\}\right]. \tag{5.14}$$

The most probable breaking force f_b is calculated from from the equation

$$1 - 2\frac{f_b}{\gamma V_0} = \frac{\gamma A}{4\beta\alpha}\exp[-\beta V_0(1-2\frac{f_b}{\gamma V_0})^2]. \tag{5.15}$$

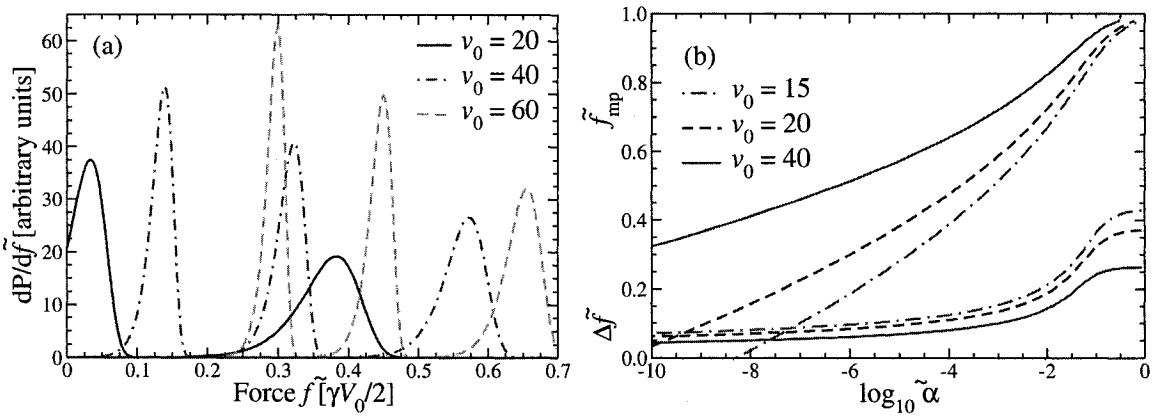

Figure 5.2: (a) Breaking force distribution $\mathrm{d}P(\tilde{f})/\mathrm{d}\tilde{f}$ for three potential depths (as shown by the colours) and for three force loading rates $\tilde{\alpha} = \alpha/(\gamma A V_0) = 10^{-10}, 10^{-5}, 10^{-1}$ (left to right within each group). Notice that the peak for $\tilde{\alpha} = 10^{-10}$ would be so low that all systems essentially dissociate at zero force, see plot (b). (b) Most probable breaking force and width of the force distribution as a function of force load rate for three potential depths (all in dimensionless form).

5.3 Results: Force Ramp

The rates $\mathrm{d}P_b(f)/\mathrm{d}f = -\mathrm{d}P(f)/\mathrm{d}f$, or the breaking force distributions, are shown in Fig. 5.2(a) for three potentials and three values of $\tilde{\alpha} = \alpha/(\gamma A V_0) = 1$, 10^{-5}, 10^{-10} and $v_0 = V_0/k_B T = 20$, 40, 60. The shapes of these curves are certainly in qualitative agreement with the experimental results, including their slight asymmetry.

To get a quantitative understanding we plot in Fig. 5.2(b) the most probable breaking force and the width of the force distribution as a function of $\tilde{\alpha}$. From (5.15) we see that as $\tilde{\alpha} \to \infty$ the most probable breaking force $\tilde{f}_b$ goes to 1. This occurs either if the loading rate α is very large or if the attempt frequency A is very low. But note that in this case one does not obtain the experimentally observed breaking force distributions.

A fit of our theory to the experimental results of the TP-Ru-TP complex [72] is shown in Fig. 5.3 with best parameters $\tilde{\alpha} = 2 \times 10^{-5}$ and $v_0 = 14$. This implies that $V_0 = 0.35\mathrm{eV}$ and $\gamma V_0 \simeq 0.5\mathrm{eV/\AA} = 0.7\mathrm{nN}$. From $\tilde{\alpha}$ we obtain $A = 6 \times 10^5 \mathrm{s}^{-1}$. Also shown in Fig. 5.3 are our predictions of multiple bond breaking for the situations

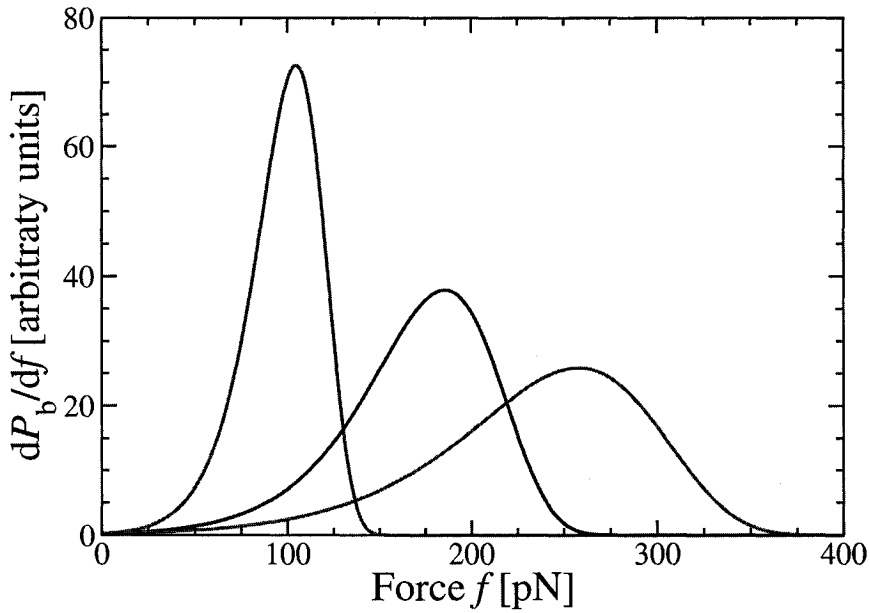

Figure 5.3: Theoretical predictions of the breaking force distribution for single, double and triple strands (left to right) for TP-Ru-TP. Same parameters for all curves, see text.

where the AFM tip has picked up two and three complexes. Following the experimental paper [72] we assume that by the time the first bond breaks the force is so high that the other bonds break instantaneously. This implies that in (5.14) we need to replace f by $f/2$ and $f/3$, respectively, shifting the original peak from 103pN to 185pN and 255pN, This procedure also widens the peaks asymmetrically, in excellent agreement with experiment.

Next, we would like to make the connection with the Ritchie-Evans version of Bell's model [80,86] employed in numerous experimental papers for the data analysis, for which the rate equation (5.1) reads

$$\frac{\mathrm{d}P}{\mathrm{d}t} = -k^*_{\mathrm{off}} \exp[\beta f \Delta x_e] P, \tag{5.16}$$

where Δx_e is interpreted as the maximum elongation of the molecule in quasi-equilibrium before breaking. Note that Δx_e is not a constant (as frequently assumed) but a function of f (as it is in our theory). We obtain this simplified model from the present theory if we assume that the breaking force is much smaller that the maximum, i.e. $f \ll \gamma V_0/2$, which is generally applicable for small loading rates. In this case we can

expand the Arrhenius rate equation (5.4) using our harmonic approximation (5.12) and obtain the rate expression (5.16) with $\Delta x_e = 4/\gamma$ and

$$k^*_{\text{off}} = A \exp[-\beta V_0]. \tag{5.17}$$

Recall that the prefactor in equation (5.1) has a simple physical meaning: it is an attempt frequency weighted by entropic factors as discusses in section 5.1. On the other hand, k^*_{off} includes a Boltzmann weight involving the potential depth V_0. Thus it is a hybrid that appears to defy physical interpretation if V_0 is not explicitly known.

The expressions for Δx_e and k^*_{off} above enable direct comparison with the TP-Ru-TP data by Kudera *et al.* [72], where we can use our values for A, V_0 and γ to get $\Delta x_e = 2\text{Å}$, and $k^*_{\text{off}} = 0.5\text{s}^{-1}$, agreeing with their values of 3.3Å and 0.05s^{-1} to within an order of magnitude. The reason for these discrepancies in the two parameters k^*_{off} and Δx_e is the approximate nature of the Ritchie-Evans model: the data extend over an interval $f_b \pm \Delta f/2$, and do not satisfy the condition $f \ll \gamma V_0/2$ for the top 20% of this range.

In concluding this discussion we note that the Ritchie-Evans model lacks an important physical parameter, namely the strength of the bond. It thus appears to be limited to forces with $f \ll \gamma V_0/2$, a restriction not imposed in our general model. We will show in sections 5.4 below, that it is advisable to use force loading rates as large as technically possible. This would hopefully enable observations close to the maximally possible force f_{max} and should facilitate the extraction of microscopic parameters.

5.4 Data Analysis: Force Ramp

Our theory of bond breaking has three independent parameters A, V_0 and γ in terms of which the probability of finding and intact bond (5.14) reads

$$P(f) \simeq \exp\left[-\frac{A}{4\alpha}\gamma V_0 \sqrt{\frac{\pi k_B T}{V_0}} \left\{ \text{erf}\left(\sqrt{V_0/k_B T}\right) - \text{erf}\left(\sqrt{V_0/k_B T}(1 - 2\frac{f_b}{\gamma V_0})\right)\right\}\right] \tag{5.18}$$

To extract these parameters from experimental data one has several options: (i) measure the force distribution for several force loading rates α and fit them with the

theoretical curve; and (*ii*) to measure the breaking force distributions when several strands are attached. A third option, namely to determine the maximum and width of the breaking force distribution for several force loading rates α is also possible provided data with good statistics are available.

We have first checked option (*i*) and found that a unique fit is obtained if we take three α that span two orders of magnitude. Our experimental *data* were force distributions calculated from (5.14). The extracted fit parameters agree with the original input data to arbitrary precision. The uniqueness of the extracted parameters is quickly lost if the force loading rates differ by less than two orders of magnitude. Similarly, option (*ii*), *i.e.* measuring the force distributions for several attached strands (for 1, 2 and 3 attached strands) also leads to a unique and perfect fit if two force loading rates are used that differ by one order of magnitude. Notice that we have used input data which was directly derived from equation (5.5), without considering any noise - this is to highlight the difficulty in extracting physically meaningful parameters.

To demonstrate the pitfalls of insufficient data, we have analyzed the force distributions for one, two, and three strands for a single force loading rate α. As Fig. 5.4(a) shows we can easily produce a *good* fit; however, the parameters extracted via least-square fitting can be different from the input and strongly depend on the initial guesses in the fitting procedure, *i.e.* the fit is *not* unique. This is shown in Fig. 5.4(a) where the input data (triangles) were calculated for $V_0/k_B = 4200K$, $A = 10^6 s^{-1}$, and $\gamma = 1.4\text{Å}^{-1}$. The fit shown yielded, instead, $V_0/k_B = 6200\text{K}$, $A = 10^9\text{s}^{-1}$, and $\gamma = 1.5\text{Å}^{-1}$. However, it is easy to demonstrate that this is wrong by using the same fit parameters for the three curves at a higher α. Fig. 5.4(b) shows that the latter fit is unacceptable.

What we have concluded so far about the analysis of data to extract the underlying physical parameters controlling bond breakage was based on perfect theoretical breaking force distributions. Noise in experimental data and limited statistics complicate the fitting procedure significantly. thus one can only expect that the data analysis yields a unique set of parameters if lots of data with good statistics are available, in particular spanning a wide range of force loading rates.

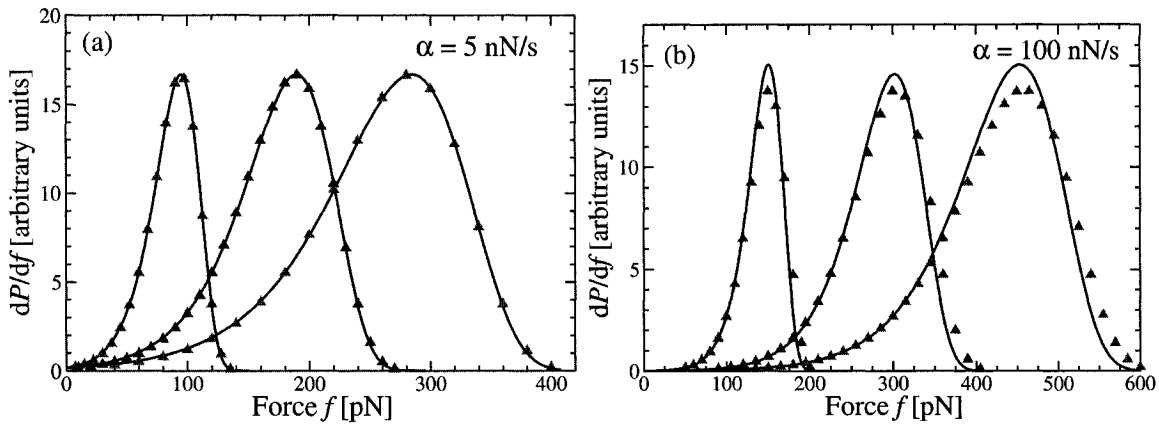

Figure 5.4: A numerical fit to generated data ($V_0/k_B = 4200K$; $A = 10^6 s^{-1}$; $\gamma = 1.4\text{Å}^{-1}$; see text) that utilized only the input data shown in (a). The same fit can be corrected only by taking into account data for a higher force loading rate, as done in panel (b).

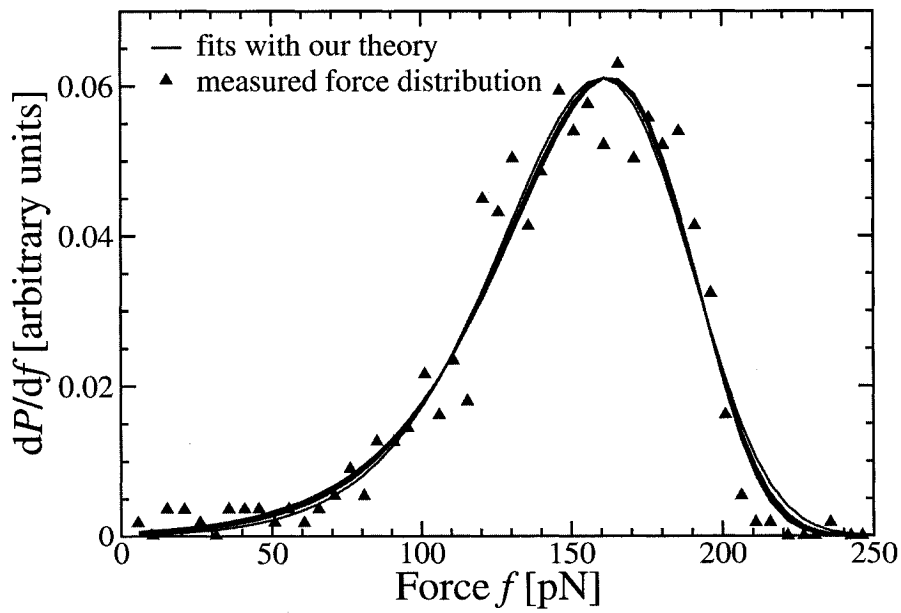

Figure 5.5: The unfolding forces for ubiquitin, as measured by Schlierf *et al.* [78] and fitted with our theory. All parameters are given in Table 5.1

Table 5.1: The parameters V_0, γ, and A for the ubiquitin experiment, the corresponding k^*_{off} from the Ritchie-Evans model, and the maximum force $f_{\max} = \gamma V_0/2$ for each Morse potential.

V_0 [eV]	γ [Å^{-1}]	A [s^{-1}]	k^*_{off} [s^{-1}]	Δx_e [Å]	$f_{\max}$ [pN]
0.236	1.76	1.06×10^2	9.78×10^{-3}	2.27	334
0.273	2.09	8.02×10^2	1.75×10^{-2}	1.91	457
0.319	2.29	6.58×10^3	2.28×10^{-2}	1.75	585
0.371	2.41	5.78×10^4	2.65×10^{-2}	1.66	717
0.403	2.47	2.21×10^5	2.82×10^{-2}	1.62	799
0.427	2.51	5.81×10^5	2.93×10^{-2}	1.60	857

A second, even more striking example is the analysis of unfolding of ubiquitin data, which was recently measured by Schlierf, Li, and Fernandez [78]. The Ritchie-Evans model gives a perfect fit to their data, if the (physically questionable) quantity Δx_e is used as a fitting parameter. We have done the analysis for their data using the model outlined in the previous section. As indicated above the resulting fit is not unique. In fact, Fig. 5.5 shows six different numerically equivalent fits. We compare the obtained fit parameters in Table 5.1 and calculate the corresponding values of k^*_{off} -and Δx_e in the Ritchie-Evans model as outlined above. The latter are remarkably constant and match those obtained by Schlierf *et al.* in the original reference [78]. The last column in our table shows why the Ritchie-Evans model is such a good approximation for this experiment - all data remains in the limit $f \ll f_{\max}$. Apparently, the information provided by using a single force loading rate is insufficient to determine the actual physical parameters of the system. We point out that a simultaneous analysis including the same information for a different force-loading rate should result in unique values of the bond parameters.

The main numerical difficulties with fitting experimental data with the theoretical breaking force distribution arise from the fact that three parameters must be fitted simultaneously. This can be circumvented with an alternative fitting procedure: (a) integrate the experimental breaking force distribution $\mathrm{d}P_b(f)/\mathrm{d}f$ to obtain $P_b(f)$. (b) Plot

$$\ln\left[\frac{1}{1-P_b(f)}\frac{\mathrm{d}P_b(f)}{\mathrm{d}f}\right] = \ln A - \beta\Delta V(f) \tag{5.19}$$

as a function of f. At the lowest possible force this function approaches $[\ln A - \beta V_0]$ and as the force approaches its maximum it yields $\ln A$. Next fit $[\ln A - \beta V_0(1 - f/f_{\max})^2]$ (which should be possible numerically in the small force regime) and get $f_{\max} = \gamma V_0/2$ and thus γ. This way one obtains first estimates for the three parameters which can then be used for the curve fitting described above.

5.5 Data Analysis: Pulling at Constant Cantilever Speed

Pulling at constant cantilever speed is the (experimentally) simpler mode of breaking a molecular bond in that a feedback loop to control the force loading rate is not required. However, it adds considerable difficulties in the interpretation of the data. A detailed knowledge of the elastic response of the polymer spacer itself is required. The rate equation (5.1) now contains an additional integration over all accessible forces

$$\frac{\mathrm{d}P_{\mathrm{intact}}(t)}{\mathrm{d}t} = P_{\mathrm{intact}}(t) \times \int \mathrm{d}f' \; P_f(f',t) A \exp(-\beta\Delta(f')). \tag{5.20}$$

Here, P_f is the probability of having a force f at time t. As before, the formal solution to this simple differential equation is given by

$$P_{\mathrm{intact}}(t) = \exp\left[\int_0^t \mathrm{d}t' \int \mathrm{d}f' \; P_f(f',t') A \exp[-\beta\Delta(f')]\right] \tag{5.21}$$

For the force ramp mode we simply have $P_f(f,t) = \delta(f - \alpha t)$. In general, the controlled position scenario has finite force fluctuations [32,33]. These become particularly important when the polymer spacer is pulled very fast and equilibrium theories become inapplicable. In such a scenario, one might consider an approach as outlined elsewhere [106]. Restricting ourselves to slow pulling such that the spacer molecule is always in equilibrium, we find [33]

$$P_f(f,t) = \frac{Z(vt - f/k_c, N, T)\exp(-\beta f^2/(2k_c))}{\int \mathrm{d}\bar{f}\; Z(vt - \bar{f}/k_c, N, T)\exp(-\beta \bar{f}^2/(2k_c))}. \tag{5.22}$$

Equation (5.22) requires the canonical partition function of the polymer spacer Z, the pulling velocity v and the cantilever spring constant k_c. Using stiff cantilevers in this case has the advantage that one does not need to care about the fluctuations in the polymer-spacer systems and one can approximate $P_f(f,t) \approx \delta(f - f_{\mathrm{eqm}}(vt))$,

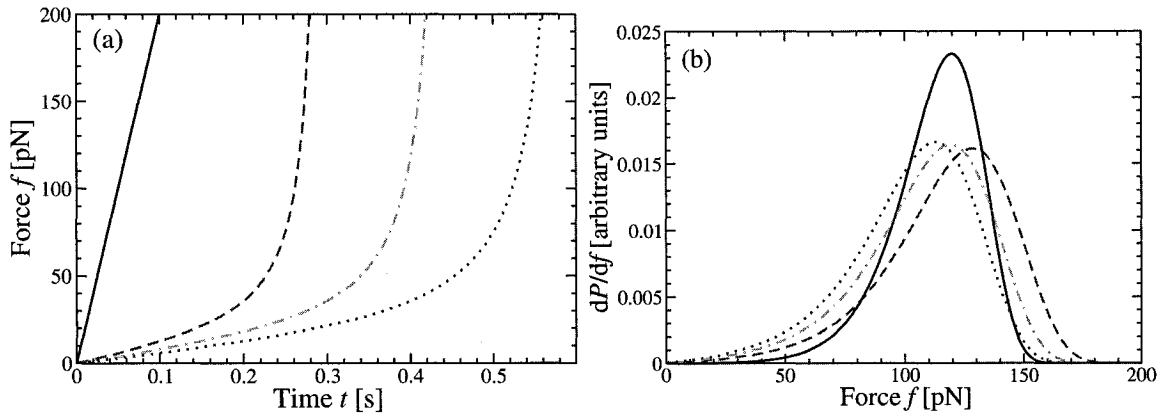

Figure 5.6: (a) the $f(t)$ traces for a constant force loading rate $\alpha = 2$nN/s (solid line) compared with constant velocity traces for $v = 118$ nm/s with polymer spacers of length $N = 100$ (dashed), 150 (dot-dashed), and 200 (dotted) monomers. These correspond roughly to the spacers used in reference [72] (b) the calculated breaking spectra for the same traces as in (a) are done for the parameters $A = 4 \times 10^6 \text{s}^{-1}$, $\gamma = 1$ Å^{-1}, and $V_0 = 0.52$ eV.

which we will use in the following analysis. One then needs the force-extension relation, $f_{\text{eqm}}(L_p)$, where $L_p = vt$ is the time-dependent length of the polymer spacer. This information is available from experimental data or detailed theories of polymer stretching [9, 42, 99] For a proof of principle, we use the simple freely joined chain (FJC) model with N monomers of length b whose length L is given in terms of the force f by the Langevin function

$$L(f) = Nb[\coth(\beta f b) - 1/(\beta f b)]. \tag{5.23}$$

Fig. 5.6(a) shows the time dependence of the applied force when the cantilever position is changed at constant force-loading rate and contrasts it with that of a constant velocity experiment. The nonlinearity will effect the breaking force distributions considerably as shown in Fig. 5.6(b). An additional difficulty arises from the fact that the exact monomer length of the spacer is hard to control and in any given experiment will have some distribution over which (5.22) must be averaged. We show traces for $N = \{100, 150, 200\}$ monomers to demonstrate the effect of a finite distribution monomer numbers.

There are claims that a Gaussian length distribution leads to no noticeable change

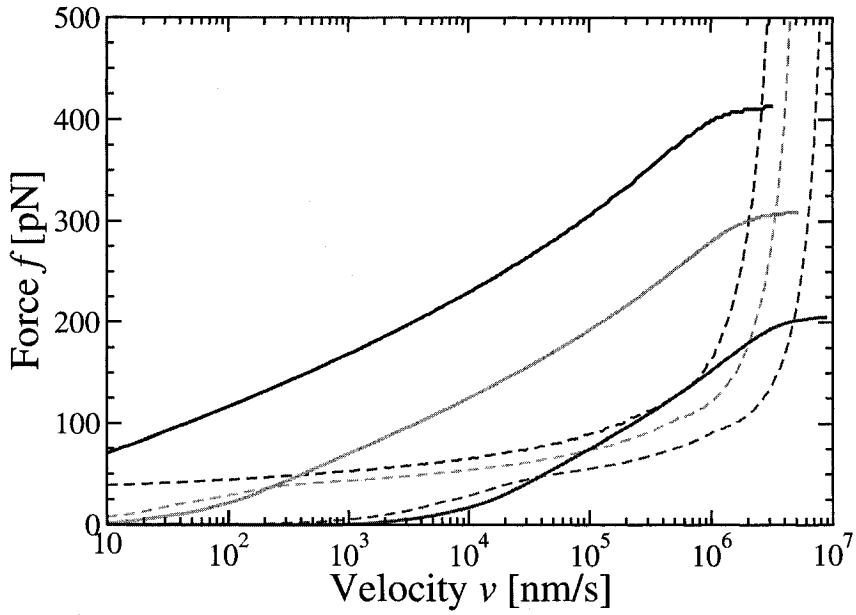

Figure 5.7: Most probable breaking force (solid lines) and the width of the $\mathrm{d}P/\mathrm{d}f$ distribution (dashed lines) is shown for the case of constant velocities with $A = 4 \times 10^6 \mathrm{s}^{-1}$ and $\gamma = 1\text{Å}^{-1}$. The potential depths are (from top to bottom, in units of $k_\mathrm{B}T$) 10, 15, 20.

in the overall breaking spectra [89]. However, we would like to point out that even a well characterized and narrow length distribution will introduce additional uncertainties in the fitting procedure since it adds two additional parameters, namely the average number of monomers and the distribution width. As pointed out in the last section, one needs very good data for a meaningful interpretation of dynamic force spectroscopy. The finite distribution width of different polymer spacers leads to a slight smearing of the observed distributions, which results in extreme difficulty in the fitting of data. This and other complications related to the use of constant velocity experiments would be completely circumvented by using the force-clamp technique.

5.6 Force-Clamp Mode

The force-clamp mode [23] is similar to that with the constant force-loading rate, but here the force is raised rapidly to some value f and held constant. The Arrhenius rate equation (5.1) then has a very simple solution that shows an exponential decay

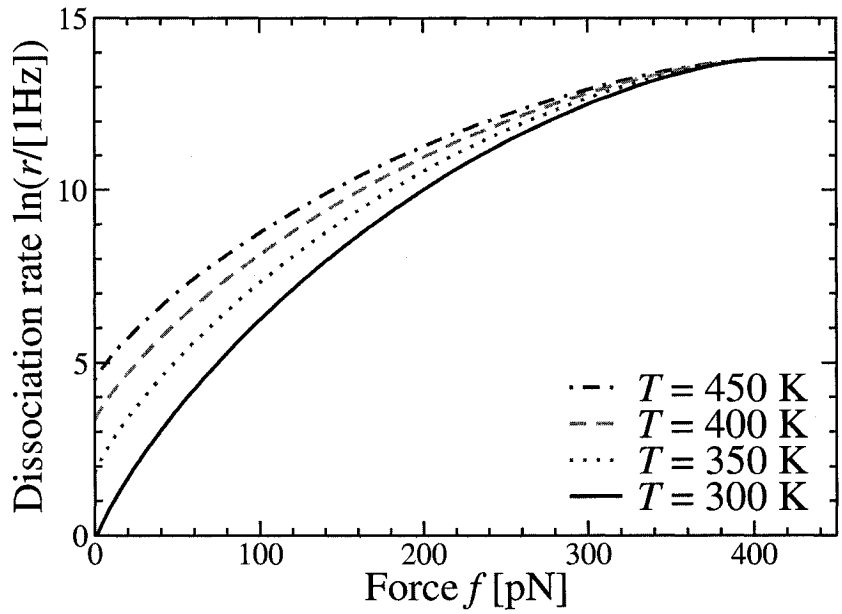

Figure 5.8: Force clamp spectra for different temperatures, the parameters are $A = 10^6 s^{-1}$, $V_0 = 0.35eV$, and $\gamma = 1.4Å^{-1}$. These plots were generated using the barrier $\Delta V(f)$ for a Morse potential as given in equation (5.11).

with a constant decay rate

$$\begin{aligned} P(t) &= \exp(-rt) \\ r &= A\exp[-\beta\Delta V(f)] \end{aligned} \tag{5.24}$$

In this setup one would have to measure the bond decay time (over several orders of magnitude) many times for each force, which can be used to extract the decay rate r. If we now plot the logarithm of the rate r vs. the force f, we find a spectrum such as given in figure 5.8 for four different temperatures. The further analysis then proceeds as discussed around equation (5.19).

5.7 Summary

We have shown in this paper that a simple analytical theory can be adapted for an analysis of bond breaking in the atomic force microscope. Since the probabilities distribution of bond breaking forces have rather simple shapes and not much structure apart from some asymmetry a large set of data must be available to obtain the

underlying physical parameters such as bond strength, bond width and Arrhenius prefactor uniquely. Extracting the actual shape of the energy surface requires much additional work. A large set of data means data obtained under different experimental conditions such as vastly different force loading rates. Fig. 5.2 shows that increasing the pulling rate will eventually lead to the direct measurement of the maximum bond breaking force. We emphasize that three independent parameters are necessary for a complete microscopic explanation of this situation, compared to two in models derived from Ritchie and Evans' work.

5.8 Appendix: Cut-Off Harmonic Bond Potential

In this appendix we show that the simplest of bond potentials namely a cut-off harmonic oscillator, confirms our conclusion that the Evans-Ritchie model is only valid for forces small compared to the maximum forces allowed for a given bond potential.

We assume that the unperturbed bond potential is given by a harmonic potential as $V(x) = -V_0 + k(x - x_{\min})^2/2$ so that in the presence of an external force we have

$$V(x) = -V_0 + \frac{1}{2}k(x - x_{\min})^2\theta(\sqrt{2V_0/k} - x) - fx \tag{5.25}$$

For purposes of comparison, we choose the force constant to be the same as that for small oscillations in a Morse potential *i.e.* $k = 2V_0\gamma^2$. Following the procedure outlined in section 5.2 we calculate the force-dependent activation energy as

$$\begin{aligned} \Delta V &= V_{\max} - V_{\min} \\ &= V_0 - \frac{\sqrt{2V_0}}{k} + \frac{1}{2k}f^2 \\ &= V_0 - \frac{f}{\gamma}(1 - \frac{f}{2f_{\max}}), \end{aligned} \tag{5.26}$$

where the maximum sustainable force (for which $\Delta V = 0$) is $f_{\max} = 2V_0\gamma$. Again we find that $k^*_{\text{off}} = A\exp[-\beta V_0]$. Dropping the quadratic term for forces $f \ll f_{\max}$ we again obtain the Evans-Ritchie model with an activation energy linear in the force and, not surprisingly, no dependence on the depth of the potential. We finally observe that the barrier (5.26) in this calculation has the form $\Delta V/V_0 = (1 - f/f_{\max})^2$, which is exactly the approximation made in equation (5.12).

Chapter 6

Discussion and Summary

The questions considered in this thesis revolve around conformational statistics and dynamics of single polymer molecules. Many analytical methods are used in conjunction with extensive numerical calculations to explain a variety of phenomena. However, the fundamental approach to the different problems is the same in all cases. The starting point is a reasonable assumption about the underlying energy landscape in a given system, which is followed by an exact statistical mechanical analysis that directly leads to experimentally observable results. The Transfer Matrix (TM) method provides a very useful vehicle for the equilibrium partition and Green functions from which many of the remaining results are derived. To summarize this thesis, the energy functions and surfaces used in all projects will be reviewed together with the primary results.

The theory of conformational transitions in polymer stretching starts with an arbitrary potential of the conformer length $V(b)$, which can be integrated analytically using a parabolic expansion about the conformer's potential minimum at length b_0. The resulting partition function $\Gamma(f)$, Eqn. (2.8), contains the full description of a single conformer in a parabolic potential under the application of an external force. An attempt to calculate further closed-form results is futile, but the analytically available partition function can easily be processed by numerical differentiation to obtain physically observable quantities in the Gibbs ensemble. These results are shown in Fig. 2.3. In fact, all of the calculations and data fitting procedures in the Gibbs ensemble can be done with a spreadsheet. Unfortunately the pure Gibbs ensemble is insufficient to model all of the available data, which is where TM calculations become extremely useful. The work presented goes well beyond previous theories that use non rigorous variations on the Langevin formula to model the force response during conformational transitions. Combining the use of analytical fitting procedures with sophisticated numerical methods to obtain further information is shown to be an

excellent way to approach single polymer stretching experiments.

Chapters 3 and 4 make use of the simplest of all energy surfaces, a constant. The description of polymer stretching in terms of a Markov process is a definition that brings an approximation of the transition rates $W(L, L')$, equations (3.8) or (3.17), along with it. It is important to note, however, that these rates were picked as the simplest, obvious choice that satisfies detailed balance. The numerical integration of the Master equation (3.3) in the two regimes yields the force-extension curves that one would expect for molecules that are stretched very quickly. The results are presented in Figs. 3.5 and 3.7.

Interestingly enough, the length fluctuations in the controlled force regime change significantly when a molecule is stretched out of equilibrium, whereas there is little to no change in the controlled position regime, see Figs. 3.6 and 3.8. It remains to be noted that there is a graphical interpretation for the theory when it is applied to experiments barely out of thermodynamic equilibrium. A truncation of the Kramer's-Moyal expansion of the Master Equation [67,68,128], yields approximate equations of motion, Eqns. (3.28) and (3.29), that can be represented graphically via contour plots (Figs. 3.10 and 3.11). For given pulling speed or loading rate, the force-extension curve is almost exactly given by the contour lines of the first moment of the transition rates.

Incidentally, the same expansion also leads to the Fokker-Planck equation (4.20) of the fast stretching problem, which is one of the important results in chapter 4. The same chapter also presents a theory of the relaxation behaviour of single molecules far from equilibrium, which is governed by a continuous spectrum of relaxation times, as shown in Figs. 4.2, 4.3, and 4.4. These calculations form the first comprehensive analytical theory of polymer stretching out of equilibrium, which is again based on the availability of an exact partition function via the Transfer Matrix method. Previous models were only possible with Monte Carlo studies [60,61] or for semiflexible molecules [64,66].

Another energy surface, used to model the breaking of molecular bonds in chapter 5, is based on the Morse potential (see Fig. 5.1). It is easy to show numerically that most reasonable potentials for this problem lead to similar results for the barrier

height as a function of force, if they are appropriately scaled. Again, this theory is purely analytic when it is evaluated for an experiment that includes a controlled force. The probability of finding a single molecular bond intact is given by Eqn. 5.5 for the case of a force-ramp experiment and by Eqn. 5.24 for the force-clamp calculation. The primary results of the theory are fits for three important parameters that can be used to uniquely specify the process; these are the depth of the potential well V_0, the attempt frequency of escaping the well A, and the potential width γ.

As indicated in Chapter 5, experiments generally use a long polymer spacer that is very important for two reasons. First, it serves to physically separate the molecule to be broken and the substrate. Second, it provides an easily recognizable signature of the breaking event that allows one to extract the exact conditions under which the molecule breaks. The work presented here gives a way to interpret and fit the observed spectra, given that they are measured with a constant force-loading rate. In this context, one has to be very careful with making the distinction between constant speed and constant force-loading rate experiments. As current theories are primarily concerned with the physics of the breaking bond itself, the importance of properly accounting for the effect of a polymer spacer is largely overlooked. A look at any spacer force-extension curve should convince one that the approximation $f \approx kvt$ (where k is an effective spring constant, and v is the pulling velocity) commonly used to model the force in a constant-speed experiment (see for example Dudko *et al.* [85] or Hummer and Szabo [92]) is insufficient.

Monte Carlo methods were used by Friedsam *et al.* to partially solve the spacer problem [89]. It was found that there are almost no measurable effects of polydispersity and the non-constancy of the force-loading rate. Unfortunately, their model is based only on the Ritchie-Evans framework, which does not lead to unique results in the first place, see Fig. 5.5. Moreover, the results presented in Fig. 5.6 show that the variable spacer length leads to vastly different breaking spectra. These effects should be investigated in much more detail before attempting to model constant-speed experiments rigorously.

The primary reason for the easy analytic evaluation of the force-ramp model in Chapter 5 is that the applied force is the fundamental variable of the bond breaking

physics. If one starts to do the calculation for fixed-velocity regimes where the length is controlled, the theory instantly becomes more complicated as the force is now a fluctuating quantity that is only described by a probability density function $P(f,t)$, given by Eqn. (5.22). It is still possible to integrate the differential equation of the problem numerically, but there are many more factors that have to be considered and, to the author's knowledge, a complete solution at constant velocity is not yet available.

A procedure to successfully model breaking experiments that include a polymer spacer and are done at constant speed would be as follows. For each single AFM trial it will be necessary to obtain a reasonable fit to the spacer's force-extension response. This can be done for example via the theory and fitting procedure presented in chapter 2, by using a Worm-like Chain model or by any other method of choice. It is important to know how the extension trace would have continued if the spacer would not have been disconnected. For *each* of these trials, the differential equation describing the molecular breaking probability (*i.e.* Eqn. (5.1)) should be integrated as a function of some model parameters. One can then obtain a statistical measure, based on Student's t-test, that gives a probability $P_{A,V_0,\gamma}$ that all of the different trials come from the same input quantities A, V_0, and γ. To calculate a fitting result, this probability has to be maximised with respect to the input parameters. While this proposed procedure is numerically rather involved, it is the only possible choice that retains experimental realism as well as statistical rigour. Moreover, it would make use of all the available data, *i.e.* the force-extension traces and the observed breaking forces; this is theoretically satisfying as well.

In principle, the theories presented in chapters 2 and 5 could be used without regard to fitting, by way of obtaining the energy landscape directly from *ab initio* calculations. As a first attempt at such a theory, preliminary Density Functional theory (DFT) calculations were done using Gaussian 03 [129] to determine the properties of α-*D*-glucopyranose, which is the monomer of Dextran. The energy landscape obtained by these calculations, shown in figure 6.1, is very similar to that available in the literature [102]. The bond breaking theory in chapter 2 is easily adopted for a numerically specified bond potential. Based on the numerical evaluation of the

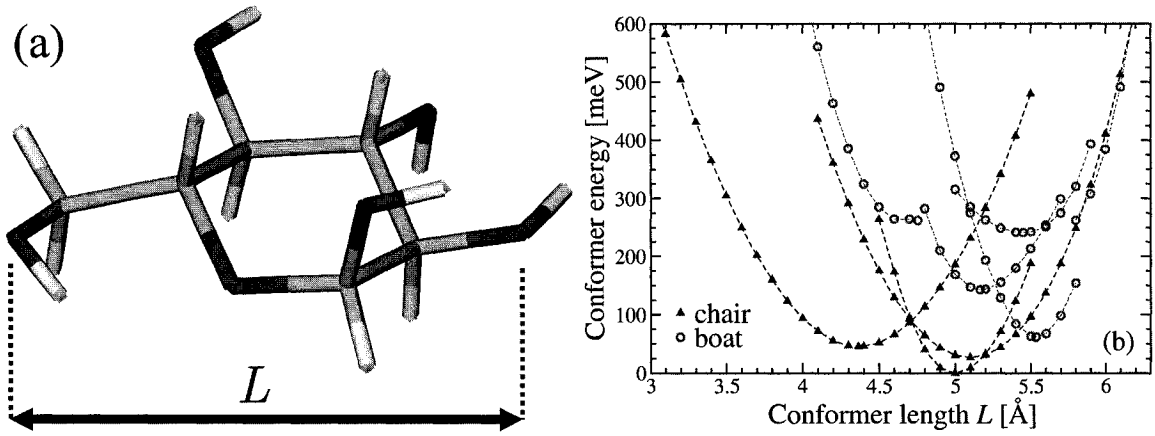

Figure 6.1: (a) schematic drawing of a chair configuration in a *D*-glucopyranose molecule used as starting point for DFT calculations. This is the fundamental building block of Dextran. DFT calculations were done at the B3LYP/6-31g level using Gaussian 03 [129]. (b) DFT stretching results for a variety of chair and boat conformers. The conformer length L is defined in panel (a). The lowest conformer energy is used as reference.

integral in the partition function (2.4) it is possible to obtain all the statistical results presented in that chapter.

Unfortunately, it is already obvious from figure 6.1(b) that the prediction for the force extension curve in this model can not show a conformational transition as observed in the experimental results. As discussed in Chapter 2, one requirement for the observation of an obvious conformational transition is an energetic step with energy differences much larger than the thermal energy $k_{\mathrm{B}}T$, as shown in Fig. 2.3 for the fits of experimental data to the Dextran response. An important question to be answered is why these DFT calculations fail to produce a monomer energy landscape that correctly predicts the observed force-extension curve.

There are two possible explanations, which may form the basis of future work on this topic. First, the present analysis is done in vacuum, without taking into account the solvent. Extensive DFT calculations by Momany *et al.* [130] show that there are several hydration shells around a single glucopyranose molecule, let alone around an n-mer. These shells have thus far only been calculated for unperturbed molecules and it remains to be seen whether it would be possible to use *ab initio* simulations for the analysis of molecular stretching. It is to be expected that there are large

energetic effects due to solvents that have not been captured in the preliminary DFT calculations. The second possibility for the failure of current calculations is that the DFT calculations need to be done for more than one monomer. Steric interactions between neighbouring monomers could prevent certain configurations included in Fig. 6.1 to be possible in long molecules. A single monomer calculation will not be able to take these effects into account.

The latter procedure is a daunting task that has not yet been attempted for any polysaccharide, but it has worked previously on poly(ethylene-glycol) using extensive three-monomer calculations [99,104]. For the proper modeling of such a system, it is suggested to do *ab initio* calculations for polysaccharides (such as Dextran) containing several monomers as well some of the solvent molecules. To give decent results, it would be necessary to go well beyond the static calculations such as the one presented in Fig. 6.1, due to the thermal effects of the solvent.

The final comment of this work regards the modeling of polymer fluctuations in a non-equilibrium experimental environment. Due to the availability of exact equilibrium statistics, the Master equation approach in conjunction with the use of the TM method forms a valuable tool for the analysis of fast stretching experiments. It can also be used to model experiments that are reversible but where conventional equilibrium theories fail such as the recent measurement of length and force fluctuations in force-ramp AFM spectroscopy [22]. The experiment uses a feedback that regularly update of the cantilever position to keep the average force-loading rate $\langle \alpha \rangle = \mathrm{d} \langle f \rangle / \mathrm{d}t$ constant. The Master equation formulation in the Helmholtz regime, Eqn. (3.17), can be modified in such a way that this update process is mimicked numerically. This calculation should yield an exact numerical replication of the experimental conditions, which would provide an explanation for the unusual fluctuations.

In conclusion, this thesis develops several applications to explain a wide variety of phenomena in the field of polymer stretching. Analytic approaches are used wherever possible, and are supplemented with appropriate numerical techniques when necessary. The Transfer Matrix technique was further developed into a versatile tool that, due to its many advantages, stands equal among a host of other theoretical methods. The systems modeled in this work correspond to well-defined experiments using the

Atomic Force microscope. The exact experimental conditions and the mode of operation of the AFM are important factors in the proper interpretation of experiments. This thesis shows how to account for these conditions properly.

Bibliography

[1] de Gennes, P.-G. *Scaling Concepts in Polymer Physics.* Cornell University Press (1979)

[2] Doi, M. and Edwards, S. F. *The Theory of Polymer Dynamics.* Oxford University Press (1986)

[3] Hanke, F. *Applications of the Transfer Matrix Method to Single Polymer Molecules.* Master's thesis, Dalhousie University, Halifax (2004)

[4] Flory, P. J. *Statistical Mechanics of Chain Molecules.* Hanser/Gardner Publications, Inc., Cincinnati (1988)

[5] Grosberg, A. Y. and Khokhlov, A. R. *Statistical Physics of Macromolecules.* AIP Press (1994)

[6] Livadaru, L. *Transfer Matrix Approach to the Statistical Mechanics of Single Polymer Molecules.* Ph.D. thesis, Dalhousie University, Halifax (2002)

[7] Livadaru, L., Netz, R. R., and Kreuzer, H. J. *Stretching Response of Discrete Semiflexible Polymers.* Macromolecules, **36**, (2003), 3732–3744

[8] Livadaru, L., Netz, R. R., and Kreuzer, H. J. *Interacting chain model for poly(ethylene glycol) from first principles - stretching of a single molecule using the transfer matrix approach.* J. Chem. Phys., **118**, (2003), 1404–1416

[9] Livadaru, L. and Kreuzer, H. J. *Statistical Mechanics of an $n-$alkane chain in $\theta-$condition: Going beyond the RIS model.* Phys. Chem. Chem. Phys., **6**, (2004), 3872–3878

[10] Hanke, F., Livadaru, L., and Kreuzer, H. J. *Adsorption forces on a single polymer molecule in contact with a solid surface.* Europhys. Lett., **69**, (2005), 242–248

[11] Livadaru, L. and Kreuzer, H. J. *Confinement of a Polymer Chain in a tube.* New J. Phys., **5**, (2003), 95

[12] Livadaru, L. and Kreuzer, H. J. *A Statistical Mechanical Model of Polymer Brushes: Equilibrium and Growth.* Z. Phys. Chem., **218**, (2004), 929–956

[13] Mogilner, A. and Oster, G. *Cell Motility Driven by Actin Polymerization.* Biophys. J., **71**, (1996), 3030–3045

[14] Dickinson, R. B. and Purich, D. L. *Clamped-Filament Elongation Model for Actin-Based Motors.* Biophys. J., **82**, (2002), 605–617

[15] Mogilner, A. and Oster, G. *Force Generation by Actin Polymerization II: The Elastic Ratchet and Tethered Films.* Biophys. J., **84**, (2004), 1591–1605

[16] Binnig, G., Quate, C. F., and Gerber, C. *Atomic Force Microscope.* Phys. Rev. Lett., **56**, (1986), 930–933

[17] Zhang, W. and X, Z. *Single molecule mechanochemistry of macromolecules.* Prog. Polym. Sci., **28**, (2003), 1271–1295

[18] Florin, E., Rief, M., Lehmann, H., Ludwig, M., Dornmair, C., Moy, V., and Gaub, H. *Sensing specific molecular interactions with the atomic force microscope.* Biosensors and Bioelectronics, **10**, 9, (1995), 895–901

[19] Rief, M., Oesterhelt, F., Heymann, B., and Gaub, H. E. *Single Molecule Force Spectroscopy on Polysaccharides by Atomic Force Microscopy.* Science, **275**, (1997), 1295–1297

[20] Rief, M., Gautel, M., Oesterhelt, F., Fernandez, J. M., and Gaub, H. E. *Reversible Unfolding of Individual Titin Immunoglobin Domains by AFM.* Science, **276**, (1997), 1109–1112

[21] Zhang, Q. and Marszalek, P. E. *Solvent effects on the elasticity of polysaccharide molecules in disordered and ordered states by single-molecule force spectroscopy.* Polymer, **47**, (2006), 2526–2532

[22] Walther, K. A., Brujic, J., Li, H., and Fernandez, J. M. *Sub-Angstrom Conformational Changes of a Single Molecule Captured by AFM Variance Analysis.* Biophys. J., **90**, (2006), 3806–3812

[23] Oberhauser, A. F., Hansma, P. K., Carrion-Vasquez, M., and Fernandez, J. M. *Stepwise unfolding of titin under force-clamp atomic force microscopy.* Proc. Natl. Acad. Sci. USA, **98**, (2001), 468–472

[24] Wang, M. D., Yin, H., Landick, R., Gelles, J., and Block, S. M. *Stretching DNA with optical tweezers.* Biophys. J., **72**, (1997), 1335–1346

[25] Perkins, T. T., Quake, S. R., Smith, D. E., and Chu, S. *Relaxation of a Single DNA Molecule Observed by Optical Microscopy.* Science, **264**, (1994), 822–826

[26] Quake, S. R., Babcock, H., and Chu, S. *The dynamics of partially extended single molecules of DNA.* Nature (London), **388**, (1997), 151–154

[27] Meiners, J.-C. and Quake, S. R. *Femtonewton Force Spectroscopy of Single Extended DNA Molecules.* Phys. Rev. Lett., **84**, (2000), 5014–5017

[28] Callen, H. B. *Thermodynamics and an introduction to thermostatistics.* John Wiley & Sons, 2 ed. (1985)

[29] Hill, T. L. *An introduction to Statistical Mechanics.* Dover, New York (1986)

[30] Hill, T. L. *Statistical Mechanics - Principles and Selected Applications.* Dover, New York (1987)

[31] Landau, L. D. and Lifshitz, E. M. *Statistical Physics, Part 1.* Butterworth-Heineman, 3 ed. (1980)

[32] Kreuzer, H. J., Payne, S. H., and Livadaru, L. *Stretching a macromolecule in an atomic force microscope: statistical mechanics analysis.* Biophys. J., **80**, (2001), 2505–2514

[33] Kreuzer, H. J. and Payne, S. H. *Stretching a macromolecule in an atomic force microscope: statistical mechanics analysis.* Phys. Rev. E, **63**, (2001), 021906

[34] Keller, D., Swigon, D., and Bustamante, C. *Relating Single-Molecule Measurements to Thermodynamics.* Biophys. J., **84**, (2003), 733–738

[35] Volkenstein, M. V. *Configurational statistics of polymeric chains.* John Wiley & Sons (1963)

[36] Abu-Lail, N. and Carmesano, T. A. *Polysaccharide properties probed with atomic force microscopy.* J. Microscopy, **212**, (2003), 217–238

[37] Kratky, O. and Porod, G. *Röntgenuntersuchung gelöster Fadenmoleküle.* Rec. Trav. Chim. Pays-Bas, **68**, (1949), 1106–1123

[38] Bustamante, C., Marko, J. F., Siggia, E. D., and Smith, S. *Entropic Elasticity of λ-phage DNA.* Science, **265**, (1994), 1599–1600

[39] Marko, J. F. and Siggia, E. D. *Stretching DNA.* Macromolecules, **28**, (1995), 8759–8770

[40] Underhill, P. T. and Doyle, P. S. *Alternative spring force law for bead-spring chain models of the worm-like chain.* J. Rheol., **50**, (2006), 513–529

[41] Bustamante, C., Bryant, C., and Smith, S. B. *Ten Years of Tension: Single Molecule DNA mechanics.* Nature, **421**, (2003), 423–427

[42] Oesterhelt, F., Rief, M., and Gaub, H. E. *Single molecule force spectroscopy by AFM indicates helical structure of poly(ethylene-glycol) in water.* New J. Phys., **1**, (1999), 6.1–6.11

[43] Li, H., Rief, M., Oesterhelt, F., and Gaub, H. E. *Single-molecule force spectroscopy on Xanthan by AFM.* Adv. Mat., **3**, (1998), 316–319

[44] Marszalek, P. E., Oberhauser, A. F., Pang, Y.-P., and Fernandez, J. M. *Polysaccharide elasticity governed by chair-boat transitions of the glucopyranose ring.* Nature, **396**, (1998), 661–664

[45] Marszalek, P. E., Pang, Y.-P., Li, H., Yazal, J. E., Oberhauser, A. F., and Fernandez, J. M. *Atomic levers control pyranose ring conformations.* Proc. Natl. Soc., **96**, (1999), 7894–7898

[46] Marszalek, P. E., Li, H., Oberhauser, A. F., and Fernandez, J. M. *Chair-boat transitions in single polysaccharide molecules observed with force-ramp AFM.* Proc. Natl. Acad. Sci., **99**, (2002), 4278–4283

[47] Li, H., Rief, M., Oesterhelt, F., Gaub, H. E., Zhang, X., and Shen, J. *Single-molecule force spectroscopy on polysaccharides by AFM nanomechanical fingerprint of* $\alpha - 1,4-$*linked polysaccharides.* Chem. Phys. Lett., **305**, (1999), 197–201

[48] Marszalek, P. E., Li, H., and Fernandez, J. M. *Fingerprinting polysaccharides with singlemolecule atomic force microscopy.* Nature Biotech., **19**, (2001), 258–262

[49] Yoshiba, K., Hama, R., Teramoto, A., Nakamura, N., Maeda, K., Okamoto, Y., and Sato, T. *Stiffness and Conformational Transition of Poly3-[(S)-2-methylbutoxy]phenyl isocyanate in Dilute Solution.* Macromolecules, **2**, (2006), 3435–3440

[50] Hugel, T., Rief, M., Seitz, M., Gaub, H. E., and Netz, R. R. *Highly Stretched Single Polymers: Atomic-Force-Microscope Experiments Versus Ab-Initio Theory.* Phys. Rev. Lett., **94**, (2005), 048301

[51] Neuertm, G., Hugel, T., Netz, R. R., and Gaub, H. E. *Elasticity of Poly(azobenzene-peptides).* Macromolecules, **39**, (2006), 789–797

[52] Rouse, P. E. *A Theory of the Linear Viscoelastic Properties of Dilute Solutions of Coiling Polymers.* J. Chem. Phys., **33**, (1953), 1272–1280

[53] Speck, T. and Seifert, U. *Dissipated wirk in driven harmonic diffusive systems: General solution and application to stretching Rouse polymers.* Eur. Phys. J. B, **43**, (2005), 521

[54] Rzehak, R., Kromen, W., Kawakatsu, T., and Zimmermann, W. *Deformation of a tethered polymer in flow.* Eur. Phys. J. E, **2**, (2000), 3–30

[55] Rzehak, R. and Zimmermann, W. *Dynamics of strongly deformed polymers in solution.* Europhys. Lett., **59**, (2002), 779–785

[56] Rzehak, R. and Zimmermann, W. *Static dynamics approach to relaxation modes and times for deformed polymers.* Phys. Rev. E, **68**, (2003), 021804

[57] Heymann, B. and Grubmüller, H. *Elastic properties of poly(ethylene-glycol) studied by molecular dynamics stretching simulations.* Chem. Phys. Lett., **307**, (1999), 425–432

[58] Kreitmeier, S., Wittkop, M., and Göritz, M. *Computer simulations on the cyclic deformation of a single polymer chain above and below the θ temperature.* Phys. Rev. E, **59**, (1999), 1982–1988

[59] Kreitmeier, S. *Equilibrium and nonequilibrium effects of a single polymer chain during cyclic deformation: A Monte Carlo study.* J. Chem. Phys., **112**, (2000), 6925–6932

[60] Sheng, Y.-J., Lai, P.-Y., and Tsao, H.-K. *Nonequilibrium relaxation of a stretched polymer chain.* Phys. Rev. E, **56**, (1997), 1900–1909

[61] Lai, P.-Y., Sheng, Y.-J., and Tsao, H.-K. *Releasing a stretched polymer chain: scaling and Monte Carlo studies.* Physica A, **254**, (1998), 280–291

[62] Seifert, U., Wintz, W., and Nelson, P. *Straightening of Thermal Fluctuations in Semiflexible Polymers by Applied Tension.* Phys. Rev. Lett., **77**, (1996), 5389–5392

[63] Winkler, R. G. *Analytical Calculation of the Relaxation Dynamics of Partially Stretched Flexible Chain Molecules: Necessity of a Wormlike Chain Description.* Phys. Rev. Lett., **82**, (1999), 1843–1846

[64] Hallatschek, O. *Semiflexible polymer dynamics.* Ph.D. thesis, Freie Universität Berlin (2005)

[65] Hallatschek, O., Frey, E., and Kroy, K. *Overdamped stress relaxation in buckled rods.* Phys. Rev. E, **70**, (2004), 031802

[66] Hallatschek, O., Frey, E., and Kroy, K. *Propagation and Relaxation of Tension in Stiff Polymers.* Phys. Rev. Lett., **94**, (2005), 077804

[67] Kreuzer, H. J. and Gortel, Z. W. *Physisorption Kinetics.* No. 1 in Springer Series in Surface Sciences. Springer Verlag, Berlin Heidelberg (1986)

[68] Kreuzer, H. J. *Nonequilibrium thermodynamics and its Statistical Foundations.* Oxford University Press (1981)

[69] Janoviak, H., Struckmeier, J., and Müller, D. J. *Hydrodynamic effects in fast AFM single-molecule force measurements.* Eur. Biophys. J., **34**, (2005), 91–96

[70] Braun, O. and Seifert, U. *Force spectroscopy of single multidomain biopolymers: A master equation approach.* Eur. Phys. J. E, **18**, (2005), 1–13

[71] Grandbois, M., Beyer, M., Rief, M., Clausen-Schaumann, H., and Gaub, H. E. *How Strong Is a Covalent Bond?* Science, **283**, (1999), 1727–1730

[72] Kudera, M., Eschbaumer, C., Gaub, H. E., and Schubert, U. S. *Analysis of Metallo-Supramolecular Systems Using Single-Molecule Force Spectroscopy.* Adv. Funct. Mat., **13**, (2003), 615–620

[73] Brujic, J., Hermans Z., R. I., Walther, K. A., and Fernandez, J. M. *Single-molecule force spectroscopy reveals signatures of glassy dynamics in the energy landscape of ubiquitin.* Nature Physics, **2**, (2006), 282–286

[74] Fernandez, J. M. and Li, H. *Force-Clamp Spectroscopy Monitors the Folding Trajectory of a Single Protein.* Science, **303**, (2004), 1674–1678

[75] Strunz, T., Oroszlan, K., Schäfer, R., and Güntherodt, H. *Dynamic force spectroscopy of single DNA molecules.* Proc. Natl. Acad. Sci., **96**, (1999), 11277–11282

[76] Green, N. H., Williams, P. M., Wahab, O., Davies, M. C., Roberts, C. J., B., T. S. J., and Allen, S. *Single-Molecule Investigations of RNA Dissociation.* Biophys. J., **86**, (2004), 3811–3821

[77] Merkel, R., Nassoy, P., Leung, A., Ritchie, K., and Evans, E. *Energy landscapes of receptor-ligand bonds studied with dynamic force spectroscopy.* Nature, **397**, (1999), 50–53

[78] Schlierf, M., Li, H., and Fernandez, J. M. *The unfolding kinetics of ubiquitin captured with single-molecule force-clamp techniques.* Proc. Natl. Acad. Sci., **101**, (2004), 7299–7304

[79] Bartolo, D., Derenyi, I., and Ajdari, A. *Dynamic response of adhesion complexes: beyond the single path picture.* Phys. Rev. E, **65**, (2002), 051910

[80] Bell, G. I. *Models for the Specific Adhesion of Cells to Cells.* Science, **200**, (1978), 618–627

[81] Beyer, M. K. *The mechanical strength of a covalent bond calculated by density functional theory.* J. Chem. Phys., **112**, (2000), 7307–7312

[82] Chen, H.-Y. and Chu, Y.-P. *Theoretical determination of the strength of soft noncovalent molecular bonds.* Phys. Rev. E, **71**, (2005), 010901

[83] Dudko, O. K., Fillipov, A. E., Klafter, J., and Urbakh, M. *Beyond the conventional description of dynamic froce spectroscopy of adhesion bonds.* PNAS, **100**, (2003), 11378–11381

[84] Dudko, O. K., Fillipov, A. E., Klafter, J., and Urbakh, M. *Following Single Molecules by Force Spectroscopy.* Israel J. Chem., **44**, (2004), 363–372

[85] Dudko, O. K., Hummer, G., and Szabo, A. *Intrinsic Rates and Activation Free Energies from Single-Molecule Pulling Experiment.* Phys. Rev. Lett.

[86] Evans, E. and Ritchie, K. *Dynamic Strength of Molecular Adhesion Bonds.* Biophys. J., **72**, (1997), 1541–1555

[87] Evans, E. and Ritchie, K. *Strength of a Weak Bond Connecting Flexible Polymer Chains.* Biophys. J., **76**, (1999), 2439–2447

[88] Evstigneev, M. and Reimann, P. *Dynamic force spectroscopy: Optimized data analysis.* Phys. Rev. E, **68**, (2003), 045103(R)

[89] Friedsam, C., Wehle, A. K., Kühner, F., and Gaub, H. E. *Dynamic single molecule force spectroscopy: bond rupture analysis with variable spacer length.* J. Phys.: Condens. Matt., **15**, (2003), S1709–S1723

[90] Grubmüller, H., Heymann, B., and Tavan, P. *Ligand Binding: Molecular Mechanics Calculation of the Streptavidin-Biotin Rupture Force.* Science, **271**, (1997), 997–999

[91] Heymann, B. and Grubmüller, H. *Dynamic Force Spectroscopy of Molecular Adhesion Bonds.* Phys. Rev. Lett., **84**, (2000), 6126

[92] Hummer, G. and Szabo, A. *Kinetics from Nonequilibrium Single-Molecule Pulling Experiments.* Biophys. J., **85**, (2003), 5–15

[93] Raible, M., Evstigneev, M., Reimann, P., Bartels, F. W., and Ros, R. *Theoretical analysis of dynamic force spectroscopy experiments on ligand-receptor complexes.* J. Biotech., **112**, (2004), 13–23

[94] Seifert, U. *Dynamic strength of adhesion molecules: Role of rebinding and self-consistent rates.* Europhys. Lett., **58**, (2002), 792–798

[95] Shillcock, J. and Seifert, U. *Escape from a metastable well under a time-ramped force.* Phys. Rev. E, **57**, (1998), 7301–7304

[96] Williams, P. M. *Analytical descriptions of dynamic force spectroscopy: behaviour of multiple connections.* Anal. Chim. Acta, **479**, (2003), 107–115

[97] Hänggi, P., Talkner, P., and Borkovec, M. *Reaction-rate theory: fifty years after Kramers.* Rev. Mod. Phys., **62**, (1990), 251–341

[98] Hanke, F. and Kreuzer, H. J. *Breaking bonds in the atomic force microscope: extracting information.* Biointerphases, **1**, (2006), 11–17

[99] Kreuzer, H. J. and Grunze, M. *Stretching of single polymer strands: A first-principles theory.* Europhys. Lett., **55**, (2001), 640–646

[100] Zhang, Q., Lee, G., and Marszalek, P. E. *Atomic cranks and levers control sugar ring conformations.* J. Phys.: Cond. Matt., **17**, (2005), S1425–S1442

[101] Lee, G., Nowak, W., Jaroniec, J., and Marszalek, P. E. *Molecular Dynamics Simulations of Forced Conformational Transitions in 1,6-Linked Polysaccharides.* Biophys. J., **87**, (2004), 1456–1465

[102] Neelov, I., Adolf, D., Ratner, M., Zhicol, O., and McLeish, T. *Molecular Dynamics Simulation of Dextran Extension at Constant Pulling Speed.* Macromol. Symp., **237**, (2006), 81–89

[103] Rief, M., Fernandez, J. M., and Gaub, H. E. *Elastically Coupled Two-Level systems and a Model for Biopolymer Extensibility.* Phys. Rev. Lett., **81**, (1998), 4764–4767

[104] Wang, R. L. C., Kreuzer, H. J., and Grunze, M. *The interaction of oligo(ethylene oxide) with water: a quantum mechanical study.* Phys. Chem. Chem. Phys., **2**, (2000), 3613–3622

[105] Balamurugan, S., Ista, L. K., Yan, J., López, G. P., Fick, J., Himmelhaus, M., and Grunze, M. *Reversible Protein Adsorption and Bioadhesion on Monolayers Terminated with Mixtures of Oligo(ethylene glycol) and Methyl Groups.* J. Am. Chem. Soc., **127**, (2005), 14548–14549

[106] Hanke, F. and Kreuzer, H. J. *Nonequilibrium theory of polymer stretching based on the Master Equation.* Phys. Rev. E, **72**, (2005), 031805

[107] Lee, D. U., Kidwell, D. A., and Colton, R. J. *Sensing Discrete Streptavidin-Biotin Interactions with Atomic Force Microscopy.* Langmuir, **10**, (1994), 354–357

[108] Moy, V. T., Florin, E.-L., and Gaub, H. E. *Intermolecular Forces and Energies Between Ligands and Receptors.* Science, **266**, (1994), 257

[109] Yan, J., Skoko, D., and Marko, J. F. *Near-field-magnetic-tweezer manipulation of single DNA molecules.* Phys. Rev. E, **70**, (2004), 011905

[110] Yan, J. and Marko, J. F. *Effects of DNA-distorting proteins on DNA elastic response.* Phys. Rev. E, **68**, (2003), 011905

[111] Bustamante, C., Chemla, Y. R., Forde, N. R., and Izhaky, D. *Mechanical Processes in Biochemistry.* Annu. Rev. Biochem., **73**, (2004), 705–748

[112] Kreuzer, H. J., Wang, R. L. C., and Grunze, M. *Effect of stretching on the molecular conformation of oligo (ethylene oxide): a theoretical study.* New J. Phys., **1**, (1999), 21.1–21.16

[113] Lai, P.-Y., Sheng, Y.-J., and Tsao, H.-K. *Releasing a stretched polymer chain: scaling and Monte Carlo studies.* Physica A, **254**, (1998), 280

[114] Hatfield, J. W. and Quake, S. R. *Dynamic Properties of an Extended Polymer in Solution.* Phys. Rev. Lett., **82**, (1999), 3548–3551

[115] Zhuang, X. and Rief, M. *Single-molecule folding.* Curr. Opin. in Struct. Biol., **13**, (2003), 88–97

[116] Manneville, S., Cluzel, P., Viovy, J.-L., Chatenay, D., and Caron, F. *Evidence for the universal scaling behaviour of a freely relaxing DNA molecule.* Europhys. Lett., **36**, (1996), 413–418

[117] Ball, K. D. and Berry, R. S. *Realistic master equation modeling of relaxation on complete energy surfaces: Kinetic results.* J. Chem. Phys., **109**, (1998), 8557

[118] Levy, Y., Jortner, J., and Becker, O. M. *Dynamics of hierarchical folding on energy landscapes of hexapeptides.* J. Chem. Phys., **115**, (2001), 10533

[119] Levy, Y., Jortner, J., and Becker, O. M. *Solvent effects on the energy landscapes and folding kinetics of polyalanine.* Proc. Natl. Acad. Sci. USA, **98**, (2001), 2188

[120] Jarzynski, C. *Nonequilibrium Equality for Free Energy Differences.* Phys. Rev. Lett., **78**, (1997), 2690–2693

[121] Jarzynski, C. *Equilibrium free-energy differences from nonequilibrium measurements: A master-equation approach.* Phys. Rev. E, **56**, (1997), 5018–5035

[122] Braun, O., Hanke, A., and Seifert, U. *Probing Molecular Free Energy Landscapes by Periodic Loading.* Phys. Rev. Lett., **93**, (2004), 158105

[123] Brochard-Wyart, F. *Deformations of One Tethered Chain in Strong Flows.* Europhys. Lett., **23**, (1993), 105

[124] Brochard-Wyart, F., Hervet, H., and Pincus, P. *Unwinding of Polymer Chains under Forces or Flows.* Europhys. Lett., **26**, (1994), 511

[125] Brochard-Wyart, F. *Polymer Chains under Strong Flows: Stems and Flowers.* Europhys. Lett., **30**, (1995), 387

[126] Friedsam, C., del Campo Bécares, A., Jonas, U., Seitz, M., and Gaub, H. E. *Adsorption of polyacrylic acid on self-assembled monolayers investigated by single-molecule force spectroscopy.* New. J. Phys., **6**, (2004), 9.1–9.16

[127] Kreuzer, H. *Physics and Chemistry under Large External Forces: Making and Breaking Bonds for Nanotechnology.* Chinese J. Phys., **43**, (2005), 249–272

[128] Moyal, J. E. *Stochastic Processes and Statistical Physics.* J. Royal Stat. Soc., Series B, **11**, (1949), 120–210

[129] Frisch, M. J., Trucks, G. W., Schlegel, H. B., Scuseria, G. E., Robb, M. A., Cheeseman, J. R., Montgomery, J. A., Jr., Vreven, T., Kudin, K. N., Burant, J. C., Millam, J. M., Iyengar, S. S., Tomasi, J., Barone, V., Mennucci, B., Cossi, M., Scalmani, G., Rega, N., Petersson, G. A., Nakatsuji, H., Hada, M., Ehara, M., Toyota, K., Fukuda, R., Hasegawa, J., Ishida, M., Nakajima, T., Honda, Y., Kitao, O., Nakai, H., Klene, M., Li, X., Knox, J. E., Hratchian, H. P., Cross, J. B., Bakken, V., Adamo, C., Jaramillo, J., Gomperts, R., Stratmann, R. E., Yazyev, O., Austin, A. J., Cammi, R., Pomelli, C., Ochterski, J. W., Ayala, P. Y., Morokuma, K., Voth, G. A., Salvador, P., Dannenberg, J. J., Zakrzewski, V. G., Dapprich, S., Daniels, A. D., Strain, M. C., Farkas, O., Malick, D. K., Rabuck, A. D., Raghavachari, K., Foresman, J. B., Ortiz, J. V., Cui, Q., Baboul, A. G., Clifford, S., Cioslowski, J., Stefanov, B. B., Liu, G., Liashenko, A., Piskorz, P., Komaromi, I., Martin, R. L., Fox, D. J., Keith, T., Al-Laham, M. A., Peng, C. Y., Nanayakkara, A., Challacombe, M., Gill, P. M. W., Johnson, B., Chen, W., Wong, M. W., Gonzalez, C., and Pople, J. A. *Gaussian 03.* Gaussian, Inc., Wallingford, CT, 2004

[130] Momany, F. A., Appell, M., Willetta, J. L., and Bosma, W. B. *B3LYP/6-311++G** geometry-optimization study of pentahydrates of α- and β-D-glucopyranose.* Carbohydrate Res., **340**, (2005), 1638–1655